Summer 2008

Microtextures of Cyanobacterial Mats in Siliciclastic Sedimentary Environments (Modern & Ancient): Applications to the Search for Life on Mars

Dina M. Bower
Old Dominion University

MICROTEXTURES OF CYANOBACTERIAL MATS IN SILICICLASTIC SEDIMENTARY ENVIRONMENTS (MODERN & ANCIENT): APPLICATIONS TO THE SEARCH FOR LIFE ON MARS

by

Dina M. Bower
B.S. May 2003, Richard Stockton College of New Jersey
B.A. May 2003, Richard Stockton College of New Jersey

A Dissertation Submitted to the Faculty of
Old Dominion University in Partial Fulfillment of the
Requirement for the Degree of

DOCTOR OF PHILOSOPHY

OCEAN, EARTH & ATMOSPHERIC SCIENCES

OLD DOMINION UNIVERSITY
August 2008

Approved by:

_____
Nora Noffke (Director)

_____
Donald Swift (Member)

_____
Desmond Cook (Member)

_____
Robert M. Hazen (Member)

ABSTRACT

MICROTEXTURES OF CYANOBACTERIAL MATS IN SILICICLASTIC SEDIMENTARY ENVIRONMENTS (MODERN AND ANCIENT): APPLICATIONS TO NASA'S SEARCH FOR LIFE ON MARS

Dina M. Bower
Old Dominion University, 2008
Director: Dr. Nora Noffke

The current Mars Exploration Rover Program (MER) is one of NASA's most successful missions. The aim of the MER is to explore for possible life on the surface of Mars. My thesis developed new methods of how to detect and to identify microbial mats in siliciclastic sediments (modern and ancient), and to make recommendations on the applicability of MISS as biosignatures. Predominantly, I employed instrumentation portable by future rovers. To search for life on other planets, we need to have information on how this life might look. Most astrobiological studies therefore focus on Earthly analogues of life and its habitats. 'Microbially induced sedimentary structures (MISS)' are formed by benthic cyanobacteria in shallow-marine settings by the interaction of the microbiota with physical sediment dynamics. MISS are found exclusively in siliciclastic sedimentary environments, setting them apart from stromatolites that form in chemically controlled settings. Because the MISS occur since the earliest Archean, the structures constitute important biosignatures. It is noteworthy that we can study both modern as well as fossil examples. In order to compare fossil and modern MISS, I used rock material from the 2.9 Ga old Archean Pongola and Witwatersrand Supergroups, South Africa, that record former tidal and shelf settings. I also investigated modern examples on

Fishermans Island, located on the coast of Virginia at the mouth of the Chesapeake Bay. To describe and to quantify various microtextures such as bacterial filaments, extracellular polymeric substances, mat fabrics, etc., I coupled morphometric and geochemical analyses. Optical microscopy and confocal scanning laser microscopy (CSLM) revealed that the morphology and structure of the microtextures of both Archean and modern material are very similar. Raman spectroscopy and electron microprobe analyses on the fossil material indicate their mineralogical and elemental composition. I distinguished alternating bands of iron hydroxides, titanium oxides, and carbon, as well as mica with striae of titanium oxides and carbon, that reflect the mineralization of the organic components of ancient microbial mat fabrics. These microfossils are the result of *in situ* biomineralization of organic material right after burial during diagenesis and also possibly during recrystallization in the course of post-diagenetic and tectonic overprinting of the host rock. Carbon isotope analyses on the fossil filament-like textures show δ13C values between -22.0-24.2+/-0.5%, typical for preserved organic matter. The morphological and geochemical results, support the presence of cyanobacteria in rocks of at least 2.9 Ga age, and provide Earthly analogs for use on Mars.

This thesis is dedicated to my amazing family for always encouraging me to be who I am and for supporting me through all of my many transformations. This is also dedicated to all the teachers along the way that pushed and inspired me. I want to dedicate this especially to two special undergraduate professors and mentors, Dr. Michael J. Hozik and Dr. Gordan Grguric. Dr. Hozik introduced me to the world of geology with such enthusiasm – I hope I will one day be able to inspire my students in the same way. Dr. Grguric recognized and nurtured the inquistive scientist in me and opened my eyes to the amazing world of chemistry. And to whoever/whatever is beyond human reason or imagination, be it the Source, the Universe, or G-d, I am eternally grateful to have been born into this life with such a wonderful family, friends, and opportunities to grow as a human being on this one planet of many.

ACKNOWLEDGMENTS

I would like to thank the faculty and staff of the Department of Ocean, Earth, and Atmospheric Sciences for their continued support throughout my studies and work. This work would also not have been possible without the support of several esteemed colleagues and faculty of the Geophysical Laboratory, Carnegie Institution of Science, Washington, D.C. I would especially like to thank Andrew Steele, Marilyn Fogel, Chris Hadidiacos, and Robert Hazen. Most of all, I would like to thank Marc Fries, who spent countless hours training me, going over data, and hosting me at the Geophysical Laboratory. This work also could not have been accomplished without the funding from the NASA Exobiology Program and the NASA Mars Fundamental Research Program. Thank you, finally, to Nora Noffke for giving me this exciting opportunity.

TABLE OF CONTENTS

Page

LIST OF TABLES

LIST OF FIGURES

CHAPTER I

INTRODUCTION

1. Significance and Aims

The aim of my doctoral research is to contribute 'microbially induced sedimentary structures (MISS) to the catalogue of biosignatures for the search for early life on Earth and other planets, such as Mars.

Modern and fossil MISS including microbial textures are important biosignatures potentially proving the existence of prokaryotic life in early Earth's history, or on other, Earthlike planets such as Mars. In order to provide NASA with helpful recommendations for life detection using MISS as biosignatures, I tested a great variety of petrological and geochemical methods. I established morphological and geochemical characteristics of modern microbial mats and used those criteria to determine the biogenicity of fossil MISS including microscopic textures. The morphological characteristics include shape, length, and thickness of microbial cells (filaments), their orientation within the mat fabrics, and the distribution of extracellular polymeric substances (EPS). Chemical characteristics include the presence of carbon, carbon isotopic signatures, and hydrous iron oxides with special focus on the fossil textures. The instrumentation I employed can be used by a rover to detect biosignatures on the surface of Mars.

The journal model for this dissertation is *Precambrian Research.*

While Mars and Earth may have shared a similar early planetary history, the chemical equilibria in the atmosphere and lithosphere on Mars did not evolve as it did on Earth. One such difference is the possible instability of carbonates on the Martian surface from UV degradation (Cordoba-Jabonero, 2003) . As such, it is unlikely that carbonate environments conducive to stromatolite formation existed on Mars. It is more likely that biogenic sedimentary structures on Mars would have been formed through the physical interaction between microbes and the sediment, such as the MISS formed in siliciclastic (sandy) substrates on Earth.

Modern siliciclastic tidal flats are often covered by microbial mats constructed by benthic cyanobacteria. These microbial mats cause 'Microbially Induced Sedimentary Structures' ('MISS'). MISS are also preserved in Archean sandstones formed in ancient shallow marine shelf or intertidal environments. Eventhough 1/3 of Archean rocks are sandstones, most paleontological studies on early life have been conducted on precipitated lithologies, such as cherts and carbonates. Carbonates contain stromatolites, which are well known biosedimentary structures that occur throughout geologic history. Thus, MISS are unique. Therefore, my research has filled in an important gap of information that can be applied to understanding not only early life on Earth, but life on Mars as well.

2. Benthic Cyanobacteria : Photoautotrophic and Mobile Prokaryotes

Cyanobacteria are photoautotrophic, and many species can move actively through the sand (Whitton, 1992). What is the taxanomic position of cyanobacteria? The phylogenetic tree of life is divided into three domains, the bacteria and archea (both classified as prokaryotes), and eukaryotes (Fig. 1). Cyanobacteria are prokaryotes. Prokaryotes are single celled microorganisms that lack a membrane bound nucleus (Fig. 2). The genetic information in prokaryotes is contained on single DNA threads that float freely in the cell. In contrast, in eukaryotes, the chromosomes and strands of DNA are surrounded by a membrane in the nucleus. Prokaryotes also lack organelles, such as the mitochondria and endoplasmic reticulum typical for the eukaryotes. Another major difference between prokaryotes and eukaryotes is cell size. The larger eukaryotic cells have an average size of 25 μm, whereas prokaryotic cells have an average size of around 2.5 μm.

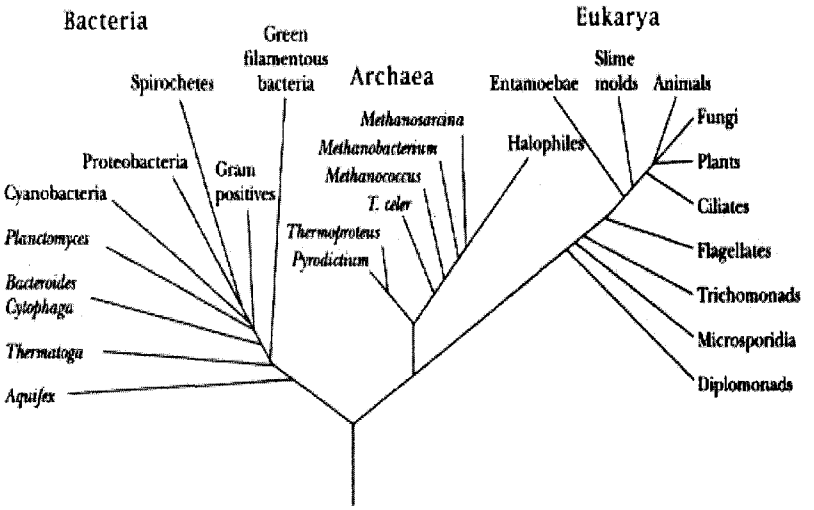

Fig. 1. Phylogenetic tree of life showing branches of unicellular Bacteria and Archea, and the multicellular Eukarya. The Bacteria and Archea are both considered prokaryotes. (image taken from www.bact.wisc.edu)

As a result of their smaller size, prokaryotic cells have a higher surface to volume ratio, which facilitates the transfer of nutrients across the cell membrane. This allows prokaryotic cells to serve as biocatalysts for many chemical reactions and makes them more adaptable to a wide variety of environments. In contrast, eukaryotes must rely on the breakdown of glucose through respiration, and are limited to oxygenic environments.

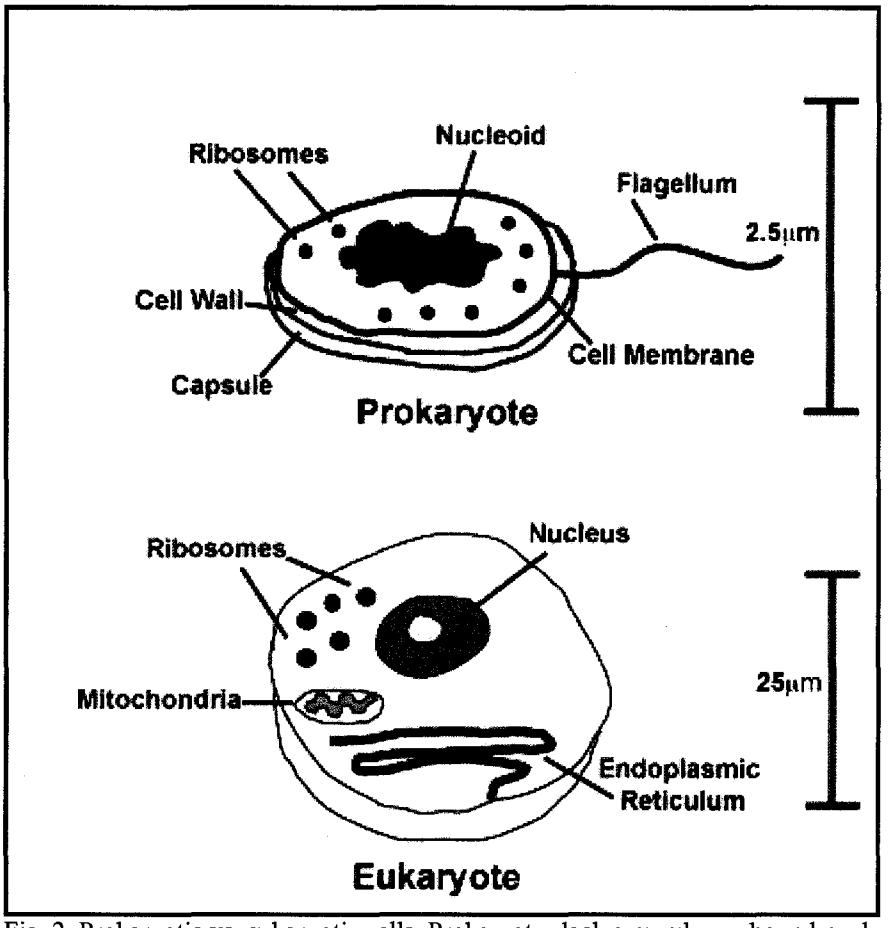

Fig. 2. Prokaryotic vs. eukaryotic cells. Prokaryotes lack a membrane bound nucleus and organelles, such as mitochondria and the endoplasmic reticulum. Those organelles are found in eukaryotes. Prokaryotes are also much smaller than eukaryotes.

The prokaryotes include millions of genetically distinct taxa and are divided into two groups based on sequences of ribosomal RNA: the bacteria (including cyanobacteria) and the archea (Fig. 1). The archea are separated into three groups that use different energy sources: the methanogens, halophiles, and hyperthermophiles. Methanogens are anaerobes (do not require oxygen) that use hydrogen or carbon dioxide in oxygen-poor environments to produce methane. Halophiles are aerobes (require oxygen) that can only exist in salt-rich environments, such as the Dead Sea or evaporite deposits. Hyperthermophiles live in extreme high temperature environments, such as hot springs or hydrothermal vents, and usually utilize elemental sulfur for respiration.

The second category of prokaryotes is the bacteria. Bacteria are divided into several main groups based on DNA sequences (Fig. 1) These groups include spirochetes, green sulfur bacteria, green non-sulfur bacteria, gram positive bacteria, purple bacteria, flavobacteria, bacterioides, thermatogales, and cyanobacteria. Just as in the Archea, each bacterial group differs by metabolic abilities. One of the characteristics that distinguishes bacteria from archea is bacteria have cell walls that consist of either peptidoglycan (polymers of sugars and polypeptides), while the cell walls of the archea contain a variety of proteins, glycoproteins, and polysaccharides, but no peptidoglycan.

Based on genetic sequencing, prokaryotes are believed to be the ancestors of eukaryotes. Eukaryotes likely evolved from a symbiotic relationship between prokaryotes. Although eukaryotes are higher on the evolutionary ladder, prokaryotes are more widespread and

are found in every niche and habitat on Earth. Prokaryotes can be divided into primary producers and consumers (Ormerod, 1992). Primary producers use sunlight (photoautotrophs), chemical energy (chemotrophs) or inorganic matter (lithotrophs) to produce energy and organic matter. Consumers break down organic matter to gain energy, because they cannot produce energy of their own. Cyanobacteria are photoautotrophs.

Cyanobacteria are among the earliest life forms on Earth (Horneck, 2000; Canfield, 2005; Olson, 2006). The name is cyanobacteria is derived from the Greek word "kyanos", meaning "blue". Cyanobacteria are often mistakenly called blue-green algae because of this blue-green pigmentation, as well as because of their large size. Cyanobacteria are a morphologically diverse group of microorganisms that can occur as solitary forms or in colonies. There are two main morphotypes: coccoid and filamentous (Fig. 3). Coccoid species generally consist of round cells ranging from 0.4μm to over 40μm in diameter, and often occur in clusters (Whitton and Potts, 2000). Filamentous species consist of trichomes that occur individually or in bundles, with cell diameters often up to 100μm (Whitton and Potts, 2000).

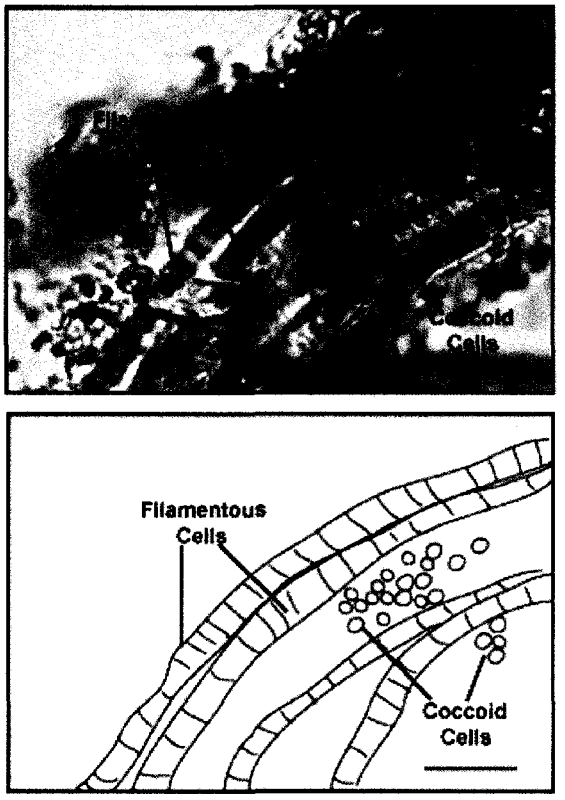

Fig. 3. The two main morphologies of cyanobacteria. They include coccoid and filamentous taxa, scale = 100μm.

Cyanobacteria thrive in a wide variety of aquatic habitats as benthos or plankton (Dvornyk and Nevo, 2003). In benthic environments, such as hypersaline lagoons, hot springs, deserts, and tidal flats, cyanobacteria construct microbial mats. (The characteristics that make cyanobacteria adaptable will be discussed here. However, a discussion of microbial mats can be found in a section below). Cyanobacteria can be found in deserts and tidal flats due to their unique ability to tolerate periods of dessication. Cyanobacteria produce organic solutes during periods of low moisture or enter a dormant state during periods of no moisture. Planktonic and benthic cyanobacteria also produce organic solutes within the cell to tolerate extreme changes in salinity. This

ability to regulate salts within the cell allows many cyanobacteria to live in brines and sabkhas. Cyanobacteria also have the ability to withstand higher levels of solar radiation by producing amino acid derivatives that serve as sunscreens or by having pigmented sheaths to shield the cells from damaging radiation. One example is the UV shielding pigment scytonemin, which is found in the sheaths of benthic cyanobacteria.

Nitrogen fixation is the reduction of atmospheric dinitrogen to a useable form of nitrogen, such as ammonia. Most nitrogen fixation occurs in environments that are oxygen deficient, because the enzyme (nitrogenase) is inhibited by oxygen. However, many species of cyanobacteria are adapted to fix nitrogen in oxygen-rich environments as well (Lundgren and Falkowski, 2003). Heterocystous species of cyanobacteria have specialized, oxygen-free cells called heterocysts that contain the enzyme nitrogenase. It is within these anoxic heterocysts that nitrogen fixation takes place even if the surrounding environment is oxygen-rich. An example of a heterocystous cyanobacterium is the planktonic filamentous species *Anabaena*, which is commonly found in the open ocean. Non-heterocystous cyanobacteria do not have heterocysts, but many can still fix nitrogen in oxic environments in the presence of light . Examples include *Microcoleus chtonoplastes*, a filamentous species commonly found in microbial mats and *Trichodesmium* sp., a filamentous species found in the open ocean (Sroga, 1997).

Photoautotrophic prokaryotes, such as cyanobacteria use solar energy for growth and the production of chemical energy (Bryant and Frigaard, 2006). This important process of the conversion of carbon dioxide into energy using sunlight is termed photosynthesis. There

are two types of photosynthesis, anoxygenic and oxygenic. Anoxygenic photosynthesis is carried out by purple and green bacteria, as well as some cyanobacteria. Sources such as dihydrogen or hydrogen sulfide are used in this process to produce energy without the production of oxygen. During oxygenic photosynthesis microbes use carbon dioxide and water to produce energy along with oxygen. Cyanobacteria need high energetic UV light to use oxygenic photosynthesis.

Prokaryotic cells are surrounded by a bilipid membrane that consists of fatty acids, with a hydrophobic (water repelling) inner lining and hydrophilic (water attracting) outer lining (Fig. 9). The bilipid membrane of phototrophic cells contains antenna-like structures that harvest solar energy. This energy is then directed to complex protein-rich molecules called bacteriochlorophylls (Bchl) that serve as reaction centers for photosynthesis. Each bacteriochlorophyll has the same basic molecular structure. However, slight differences in bonding result in different absorption ranges. For example, Bchl a absorbs light in the 375, 590, 800-810, and 830-890 ranges, whereas Bchl b absorbs light in the 400, 605, 835-850, and 1015-1035 ranges. The main structural difference between the two is the methyl group of Bchl a is replaced by CHO in Bchl b. The blue-green color characteristic of many cyanobacteria is from the green and blue photosynthetic pigments, BChl a and phycocyanin. These pigments allow cyanobacteria absorb a wider range of wavelengths than other phototrophs (Quesada et al., 1999).

3. Biofilms: Single Celled Organisms and Extracellular Polymeric Substances

Under the light microscope, cyanobacteria are surrounded by a clear, slimey substance termed extracellular polymeric substances (EPS) (Fig. 4). Extracellular polymeric substances are adhesive mucilages secreted by microorganisms as a byproduct of cellular growth (Starkey et al., 2004). As carbon is metabolized during the growth of a microbial cell, EPS is produced. Some microbes also produce EPS in response to stress, such as starvation, changes in temperature, or oxygen availability. EPS can occur as structured capsules around microbial cells or as an expansive slime surrounding many cells.

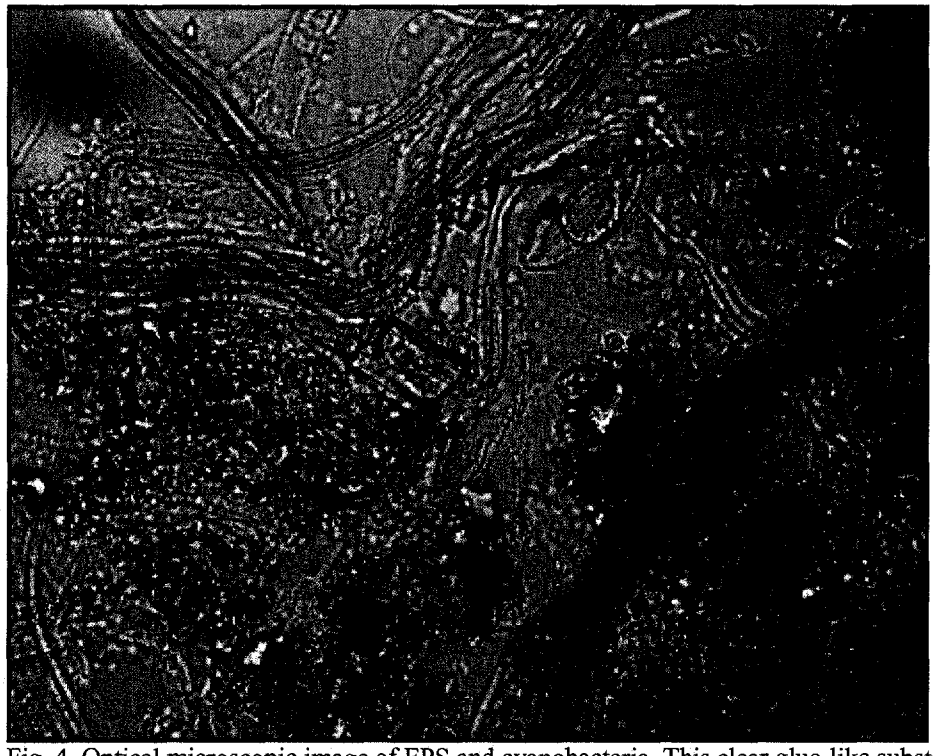

Fig. 4. Optical microscopic image of EPS and cyanobacteria. This clear glue-like substance is secreted by the microbial cells, forming a protective buffer from the surrounding environment, scale = 500μm.

EPS consist mainly of high molecular weight polysaccharides, as well as amino acids, phosphates, lipids and glycoproteins. The composition and amount of EPS produced can vary depending on microbial species. EPS secreted by cyanobacteria are mainly composed of proteins, uronic acids, and pyruvic acids (Kawaguchi and Decho, 2002).

EPS also function as a barrier between the microbial cells and the surrounding environment (Decho, 1990). This can be as a physical or chemical barrier. As a physical barrier, the EPS protect microbes from grazing, since eukaryotes are not able to graze on microorganisms surrounded by mucilage. EPS act as a sponge, creating a chemical barrier. As a chemical barrier, the EPS protect the microbes from environmental fluctuations that could interfere with normal cellular growth and metabolism. This is especially important in marine environments where changes in pH, salinity, nutrient availability, UV intensity, or periods of dessication can occur. This chemical barrier can facilitate the transfer of nutrients or organic matter in from the surrounding environment. Microbes secrete enzymes along with the EPS that break down chemical compounds into useable nutrient forms that are integrated into the microenvironment. The reactive EPS surfaces also keep harmful chemical species out of the microenvironment by binding metals and toxins.

A biofilm is a collection of microbial cells and EPS that accumulate together on a solid surface (Fig. 5). Microorganisms living within a biofilm are protected from environmental changes in the same way that microbes surrounded by EPS are protected.

However, unlike EPS that are usually associated with a specific microorganism, the biofilm forms a micro-layered ecosystem in which many different types of prokaryotic and eukaryotic microorganisms coexist (Decho, 2000a).

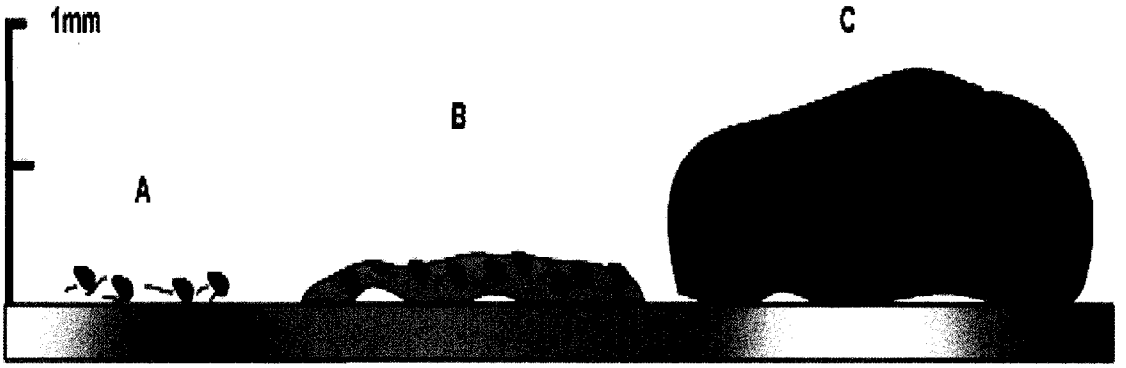

Fig. 5. Biofilms are not the same as microbial mats. (A) A collection of cells colonizes a solid substrate. (B) The cells in the colony secrete EPS, resulting in a biofilm that surrounds the cells. (C) A microbial mat develops from the continued growth of the colonies and continued secretion of EPS. Note the difference in size between the biofilm and microbial mat.

Biofilms can occur on a variety of surfaces, such as rocks, pipes, teeth, intestines, and sand grains (Puredorj-Gage and Stoodley, 2004). The structure of a biofilm can vary between single layers of randomly dispersed cells to multiple layers of organized cell associations. Single film, or planar, biofilm structures are the simplest. These biofilms are typical of those found on teeth or in controlled laboratory settings. Another type is made up of stacks of colonies within columns of EPS. This type is typical in water pipes.

4. Microbial Mats: Stratified Ecosystems in Shallow-Marine Settings

Microbial mats are dense, laterally continuous layers of microbial cells and EPS that form on a solid surface (Stal, 1994). Microbial mats function as a complex biofilm, but are vertically stratified on a millimeter or higher scale (Fig.5) This is in contrast to biofilms, which are vertically stratified on a scale less than a millimeter. The vertical stratification in microbial mats is dictated by the structure of the microbial community and can be divided into layers based on metabolism (Fig.6). The uppermost layers are dominated by oxygenic phototrophs (Wimpenny et al., 2000). Oxygen rich upper layers are also colonized by aerobic heterotrophs. Since oxygen is removed from the sediments during respiration, the lower layers become anoxic. These layers are colonized by anaerobic sulfate reducing and sulfide oxidizing bacteria, such as purple sulfur bacteria.

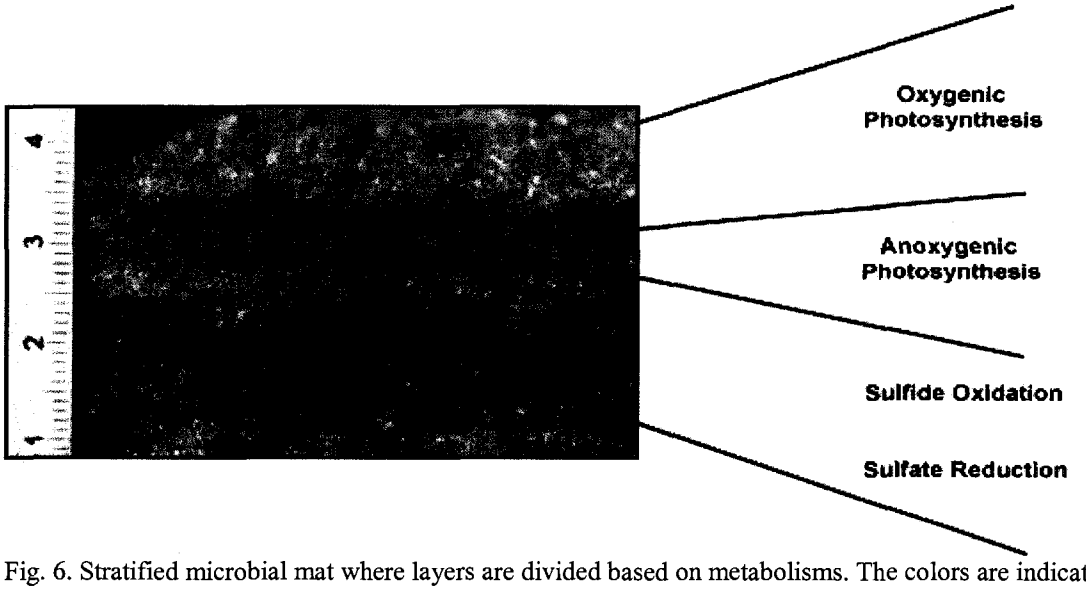

Fig. 6. Stratified microbial mat where layers are divided based on metabolisms. The colors are indicative of microbial pigments: orange = carotenoids, green = photosynthetic pigments of oxygenic phototrophic microbes, pink = photosynthetic pigments of anoxygenic phototrophic microbes, and black is from the production of sulfides. Scale is in centimeters. (Image from www.bact.wisc.edu)

Microbial mats can be found in a wide variety of environments, such as hydrothermal vents, hot springs, Antarctic lakes, and tidal flats. My work focuses on microbial mats in tidal flat environments (Fig.7). These environments are characterized by constant reworking of sediments from wave action and tidal floods. Tidal flats are divided into zones based on topography and tidal influence. The lower intertidal zone is between the low water line and the high water line and is characterized by a steady reworking of sediments. The upper intertidal is characterized by periodic reworking by flood currents. The lower supratidal is characterized by periods of subaerial exposure. (Fig.17).

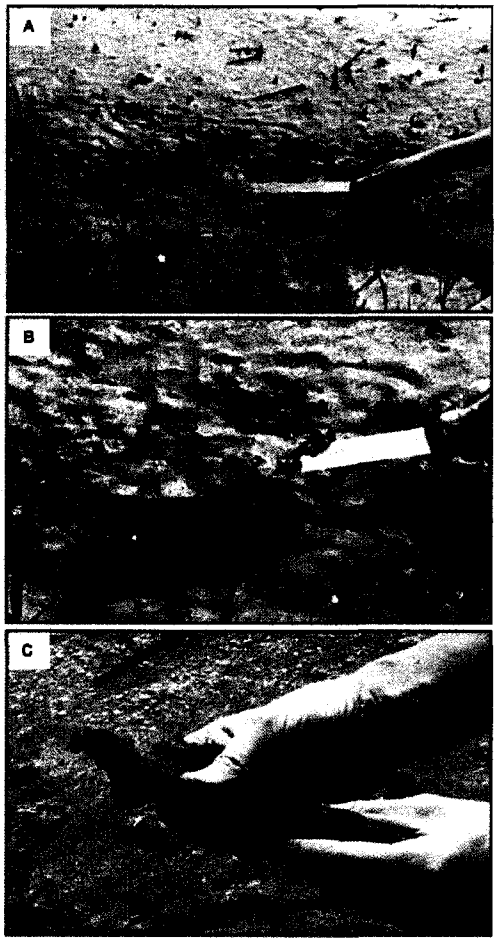

Fig. 7. Microbial mat typical of a modern silciclastic tidal flat. (A) Slicing into a microbial mat that covers the entire tidal flat surface. (B) Piece of a microbial mat removed. (C) A thick, cohesive microbial mat.

Cyanobacteria are the main constructors of microbial mats in tidal flat environments (Noffke et al., 1997; Stal, 1994). The most common mat building cyanobacteria are the filamentous species *Microcoleus chthonplastes* and *Oscillatoria limosa*, as well as the coccoid species *Merismopedia punctata* (Fig. 29). The cells of *M. chthonoplastes* are thin trichomes ensheathed in glycoprotein and are usually bundled. The cells of *O. limosa* are singular thick trichomes that are not ensheathed. The cells *M. punctata* are often found in pillow-like clusters.

The cyanobacteria colonize the tidal flat surface and secrete large amounts of EPS. Once a biofilm is established, the cyanobacteria trap and entrain sand grains. Species such as *M. chthonoplastes* orient themselves upright to baffle and trap sediments. The result is a microbial mat of interwoven trichomes and sand grains, along with communities of heterotrophic bacteria, fungi, and diatoms within an EPS matrix.

A lateral succession of different cyanobacterial populations develops in response to the changes in hydrodynamic conditions with topography. This is termed a biofilm catena (Noffke et al., 2001b). For example, the lower intertidal zone is typically dominated by *M. punctata*. As the water is stirred up, clusters of *M. punctata* attach to sand grains with EPS and remain in suspension in the water above the sandy surface. The clusters then settle back down to the surface once the agitation stops. The upper intertidal is dominated by *O. limosa*, which forms thin temporary mat layers. This cyanobacterium can move rapidly and therefore is well adapted to those intertidal sites of frequent reworking. The

lower supratidal is dominated by *M. chthonoplastes*, which (because of its ubiquitous amounts of EPS) is able to withstand longer periods of desiccation.

5. Microbially Induced Sedimentary Structures: Microbial Trace Fossils

In the shallow marine siliciclastic environments of moderate climate zones, the interaction between the physical dynamics and benthic cyanobacterial populations results in the formation of Microbially Induced Sedimentary Structures (MISS) (Noffke et al., 1997; Noffke, 1998, 1999, 2003). In moderate climate zones, little to no chemical precipitation takes place. Instead, physical sedimentary dynamics, such as tidal erosion and deposition, predominates. This is contrary to the more well-studied stromatolites in shallow marine carbonate environments of tropical climate zones. In carbonate environments, the metabolic activities of cyanobacteria result in the precipitation of minerals and the formation of laminae and stromatolites (Stolz, 2003; Dupraz and Visscher, 2005).

There are 16 main types of MISS specific to siliciclastic sedimentary environments. For example, 'erosional remnants and pockets' result from the partial erosion of a mat covered sedimentary surface (Fig. 8) (Noffke, 1999)."Remnants" are raised areas of sediment that are covered by dense, erosion resistant microbial mats. "Pockets" are deeper surface portions that are not overgrown by protective mats, so erosion takes place.

"Multi-directed ripple marks" result from patchy coverage of ripple marks by microbial mats at different stages of maturity (Fig. 8). The ripple marks covered by mat layers are protected against reworking, while the surrounding area is eroded. Subsequent ripple marks form in the eroded areas with different orientations (Noffke, 1998).

Fig. 8. Microbially induced sedimentary structures (MISS). (A) An "erosional remnant (R) and "pocket" (P) from a modern tidal flat, scale = 4 cm. (B) An "erosional remnant (R) and "pocket" (P) from the 2.9 Ga Pongola Supergroup, South Africa, scale = 10 cm. (C) "Multidirected ripple marks" (RM) on a modern tidal flat, scale = 10 cm. (D) "Multidirected ripple marks" (RM) from the 2.9 Ga Pongola Supergroup, South Africa, scale = 45 cm.

Wrinkle structures ("elephant skin") form in the lower supratidal zone from tufts, pinnacles, and bulges in a microbial mat (Gerdes and Klenke, 2003). These features occur

when bundles of filamentous cyanobacteria stand above the microbial mat to be closer to the sunlight (Gerdes and Klenke, 2003).

Polygons are MISS that result from fluctuating periods of desiccation in the upper supratidal zone (Fig. 25). During times of tidal inundation, a thin microbial mat layer forms on the sediment surface. During times of dryness, when the water does not cover the upper supratidal zone, these mats shrink and form polygonal patterns with crack-like margins. Once the mats become flooded again, they grow and extend over the margins. This pattern continues as the seasonal conditions fluctuate.

Similar abiogenic macrostructures are also common in modern shallow marine environments, as well as preserved in the rock record. Ripple marks and wrinkle structures can be formed through strictly physical processes without any biotic interaction. Ripple marks occur in sandy environments that are affected by the continual movement of waves one the surface. This consistent movement results in the formation of ridges and troughs.

A diagnostic characteristic to delineate MISS from abiogenic sedimentary structures are the filamentous textures associated with MISS (Draganits and Noffke, 2004;Noffke et al., 2006a, b, 2008). Modern MISS contain living material, and below this living mat material are the remnants of recently buried microbial mats. These recent and sub-recent mats are recorded in relief casts (Fig. 24). Relief casts are made from box cores through tidal flat sediments.

Just as they are preserved in recent sediments, MISS are also well preserved in ancient rocks (Noffke et al., 2001a, b, 2002, 2006a,b, 2008; Bouougri and Porada, 2002; Banerjee and Jeevankumar, 2005). Fossil MISS contain filamentous textures, representing fossilized bacterial filaments that underwent lithogenic diagenesis (Fig. 31) (Kazmierczak and Kremer, 2002; Noffke et al., 2002, 2003b, 2006a,b, 2008). As such, the association between MISS and fossil textures can be important in proving the existence of microbes on ancient Earth and on Mars.

6. The Interaction of Microbes with Minerals: A Complex Relationship

Throughout geologic history, microbes have had an intricate relationship with rocks and minerals (Banfield and Hamers, 1997). In aquatic environments, rocks provide substrates for microbial communities to anchor on to, protecting them from currents. Many rocks contain extensive networks of microscopic pores and fissure cracks, providing sites for microbes to grow and flourish. Communities of microbes even exist within the fractures and cracks of rocks deep within the Earth's lithosphere.

The building blocks of rocks are minerals (Nesse, 2000). Minerals are inorganic crystalline solids composed of atoms arranged in a three dimensional lattice (Fig.9). The atoms that make up these lattices are commonly made up of elements most abundant in

the earth's crust, such as silica, oxygen, aluminum, iron, calcium, magnesium, potassium, and sodium.

The crystal lattices that make up all of these minerals are made up of charged chemical species that can readily exchange with ions in solution (Banfield and Hamers, 1997). This makes mineral surfaces highly reactive with their surroundings. Ions in solution can react with the charged mineral surfaces by removing and adding ions to initiate precipitation or induce secondary mineralization. This characteristic is important in the interactions between minerals and microbes.

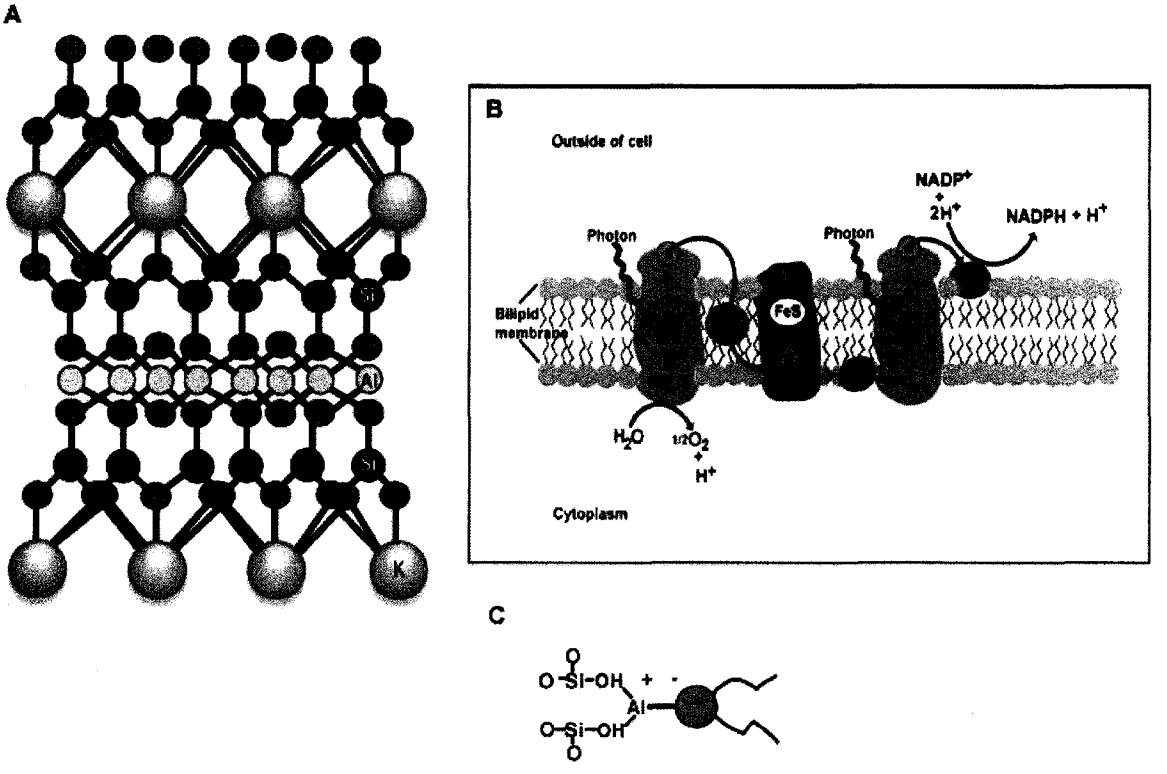

Fig. 9. Mineral and microbial structures. (A) Lattice structure of muscovite, made up of Al, OH, Si, O, and K atoms. (B) Bilipid membrane and photosystems of a photosynthetic microbe. (C) Outer portion of bilipid membrane is negatively charged to react with positively charged ions to precipitate clays on the surface of the cell.

Since microbial cells are also highly reactive, ionic exchange between cell surfaces, ambient fluids, and mineral surfaces occurs readily (Ehrlich, 1990). In the process of removing rock or mineral constituents, microbes also induce the precipitation of minerals (Fortin et al., 1997). The production of minerals by microorganisms is termed biomineralization. Biomineralization can occur within the cell, intracellulary, or outside the cell, extracellularly (Konhauser, 1998). Biomineralization can also either be direct or indirect. Direct biomineralization involves the precipitation of minerals resulting from the direct influence of microorganisms during life processes or during the death of a cell. Life processes include the breakdown of organic matter in respiration. During respiration in aqueous systems, bacteria pump protons into the microenvironment. These protons activate the cellular surfaces, creating binding sites for ions. Indirect biomineralization is the result of mineral precipitation on cellular or extracellular material without the direct influence of a living organism.

7. The Fossil Record of Microbiota: The Biogenicity of Microfossils

The biogenicity of microfossils means the degree of certainity we can identify a feature in the rock as fossil of a microorganisms. Fossils of complete cells are rarely ever found, so it is necessary to gather many lines of evidences to make conclusions on biologic origins. Following the death and burial of microbes, that same matrix-like structure of EPS that

facilitates chemical reactions and the binding of metals serves as a template for mineral precipitation by creating a large surface area where chemical reactions can take place. These materials act much like rock or crystallized mineral surfaces by providing charged species for ionic exchange with fluids (Strevett and Chen, 2003). Cell walls and EPS buried in the sediment can act as sites of mineral nucleation and mineral replacement of organic material (Schultze-Lam et al., 1996; Hofmann and Farmer, 2000; Al-Hanbali et al., 2001; Westall et al., 2001).

Despite the phenomenom of biomineralization, microfossils of mat forming organisms from the early Archaean and Proterozoic are rare. The compelling morphological evidence for the existence of ancient microbial mats as mineralized cellular and extracellular structures and fossil textures is still under debate (Golubic and Seong-Joo, 1999; Westall et al., 2001; Brasier et al., 2002; 2005; 2006; Schopf et al., 2002; Altermann and Kazmierczak, 2003; Whitfield, 2004). One problem is the nature of carbon, which constitutes the bulk of organic matter. Carbon is highly reactive, so over geologic time scales most of the original carbon associated with bacterial textures will not remain in a host rock. Another problem is the loss of distinctive cellular features as a result of diagenesis, such as loss of segments or cell walls.

With such a low preservation potential and high degree of controversy with the issue of fossil origin, it is necessary to obtain as many lines of evidence as possible to prove biogenicity. A feature preserved in a rock is biogenic if it is of biological origin. This is in contrast to 'something' that is abiogenic, or of an abiological origin. The difficulty in

proving biogenicity is that often abiogenic signatures mimic biogenic ones. For example, in modern geothermal sinters, filamentous microbes become encrusted in silica and the general morphological features are preserved (Jones et al., 2001). However, the taxonomic features are obliterated during the silification process. To make matters more difficult, abiogenic filamentous silicified structures that look like biogenic filaments have been synthesized in laboratory settings (Garcia-Ruiz et al., 2003). In another example, isotopic carbon signatures or kerogen can be derived from microbes (Schidlowski, 2001). Isotopic carbon signatures indicative of life can also be similar to those produced by volcanic activity, which can commonly be observed in hydrothermally produced veins (Gee, 2002). These abiogenic veins look like biogenic fossil textures in chert, but the difference is not apparent based on morphology alone. Kerogen, an organic end product, can transform into graphite under high pressure and temperature. However, it is often difficult to distinguish graphitic kerogen from disordered graphite (De Gregorio and Sharp, 2003). Therefore, to prove biogenicity, several lines of evidence that include carbon isotopes, geochemical signatures, and morphological characteristics of sedimentary structures and textures are used.

8. The Archean: Early Earth and the Dawn of Life

The Archean Eon spanned 1.5 billion years, from 3.8 Ga to 2.3 Ga, and is divided into the Eoarchean (3.8 Ga to 3.6 Ga), Paleoarchean (3.6 Ga to 3.2 Ga), Mesoarchean (3.2 Ga to 2.8 Ga) and Neoarchean (2.8 Ga to 2.5 Ga) (Fig. 10). The Archean was a time in planetary history when the Earth's geosphere, atmosphere, and hydrosphere were each

still developing into an integrated system conducive to life (Bleeker, 2002). Yet, despite inhospitable conditions, early life forms such as cyanobacteria began to appear (Canfield et al., 2000; Ericksson et al., 2004; Ohmoto, 2004).

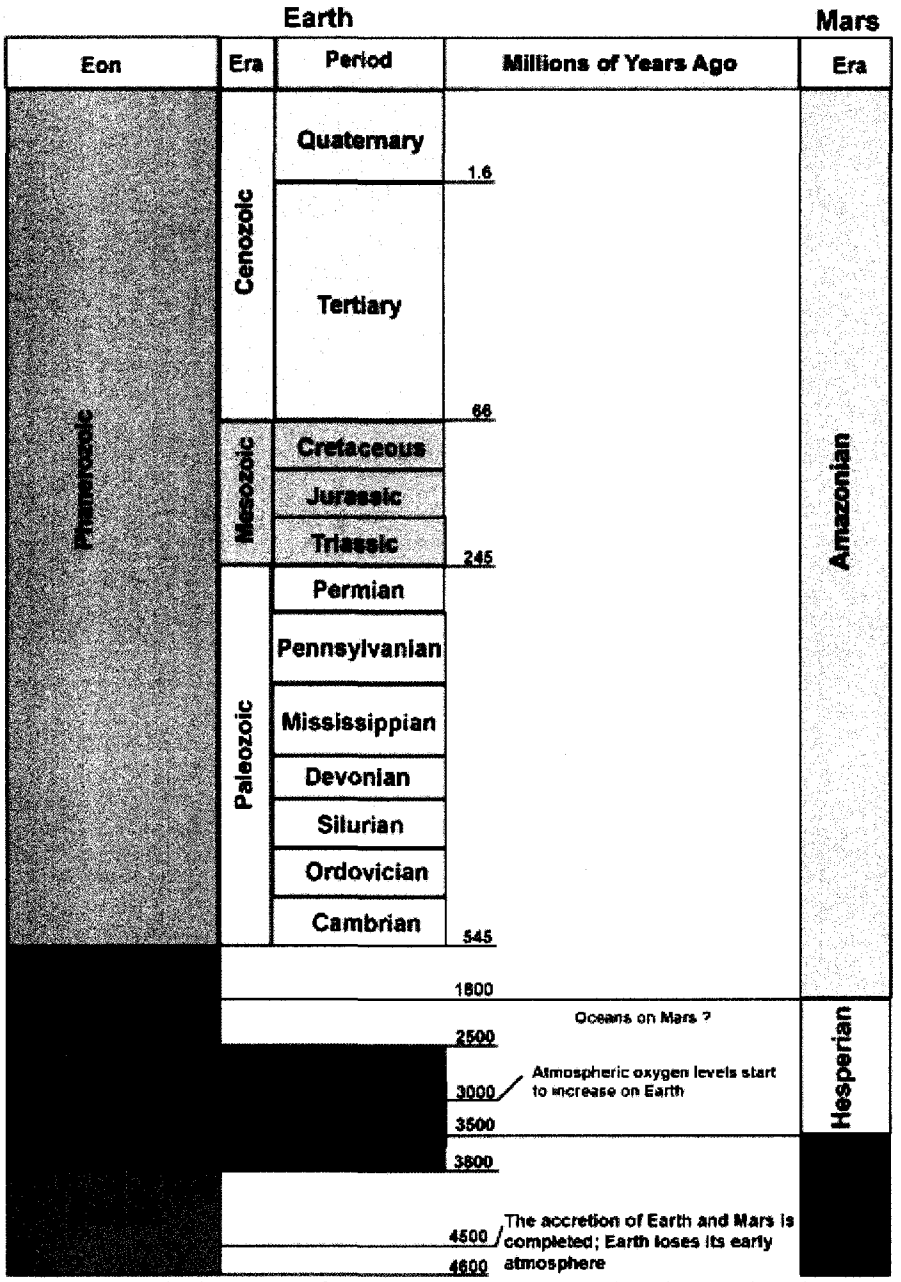

Fig.10. Geologic time scale of Earth and Mars. Both Earth and Mars shared early geologic histories, but probably diverged sometime during the Precambrian.

During much of the early Archean, the Earth was subjected to destructive impacts, radiogenic heat production, active volcanism, and the growth of continents resulting in a highly dynamic regime much different than that of post-Archean Earth (Bleeker, 2002). Before 3.2 Ga, only 5% to 10% of the Earth's crust was continental, resulting in the predominance of oceanic and island arc sedimentation (Lowe, 1992). The ocean basins were still forming, and seas were predominantly shallow. The concentrations of oxygen, carbon, hydrogen, sulfur, and iron species in the Earth's early atmosphere and oceans are still under debate. (Holland, 2002; Ohmoto, 2004; Canfield, 2005). Where possible, I will present both sides.

According to one group of scientists, the Eoarchean into the early Mesoarchean (3.8- 2.8) was characterized by atmospheric O_2 concentrations of about 10^{-8}ppm, CO_2 concentrations greater than 1000ppm, and H_2 and CH_4 concentrations of close to 1000ppm (Catling et al., 2001; Ohmoto, 2004). In the ocean, free Fe^{2+} oceanic concentrations were about 0.1nM, sulfide concentrations (from volcanic H_2S) were about 0.01nM, and SO_4 concentrations were about 0.4nM (Holland, 2002;Canfield, 2005; Kasting, 2005). In these models, only the photic zone (first 100-200 m) of the ocean was oxic, and everything below was an anoxic, reducing environment (Habicht et al., 2002; Huston and Logan, 2004; Strauss, 2004). Also, the reducing nature of the atmosphere would have allowed biologically detrimental UV-B and UV-C solar radiation to reach the Earth's surface (Canfield, 1999; Ronto et al., 2003). Earth's atmosphere remained unchanged until around 3.0 Ga, when oxygen levels started to increase, and it wasn't

until about 2 Ga that the composition of the Earth's atmosphere began to mimic modern conditions (Holland, 2002; Canfield, 2005; Kasting, 2005). Similarly, oceanic concentrations of SO_4, H_2S, and Fe^{+2} did not reach modern levels until close to 700 Ma (Habicht et al., 2002; Canfield, 2005). Much of the rise in atmospheric oxygen levels during the Mesoarchean is attributed to the evolution of oxygenic photosynthesis (Canfield et al., 2000).

In contrast, other studies indicate that as early as the Eoarchean, the atmosphere had about 1ppm of CH_4 and H_2, close to 10% oxygen, and a range of CO_2 concentrations between 5% and 1000%, while the ocean had only about 0.001nM Fe and H_2S concentrations, and a range of 10mM to about 30mM of SO_4 (Dimroth and Lichtblau, 1978; Lasaga and Ohmoto, 2002; Ohmoto, 2004). These values are the same as those for the modern Earth, with the exception of modern CO_2, which is closer to 300ppm. These models suggest a completely oxic ocean with the exception of a few semi-enclosed anoxic basins with little to no change throughout the Archean (Ohmoto, 2004).

At the start of the Mesoarchean (3.2 Ga), shallow marine environments began developing on the edges of stable continents (De Wit et al., 1992; Eriksson, 1994). With the weathering of continental rocks providing nutrients, such as phosphate, and plenty of solar energy, these quiet aquatic environments would have been advantageous for lifeforms, such as photosynthetic cyanobacteria to begin their evolution (Olson, 2006). If the "low to no atmospheric oxygen" group is correct, it is possible that anoxygenic photosynthetic or facultative aerobic cyanobacteria were the first to colonize the early

Earth. If the "oxygen-rich atmosphere" group is correct, than the conditions would have been right for the oxygenic photosynthesizers to flourish. In either case, newly forming microcommunities would have benefited from the establishment of microbial mats, and microbes, such as filamentous cyanobacteria would have thrived during the Mesoarchean (Horneck, 2000; Olson, 2006).

Virtually all traces of early Archean rocks have been erased through tectonism and recycling (Bleeker, 2002). What remains are several small exposures of cratons. These include the Pilbara craton of northwestern Australia, the Nain craton of western Greenland, the Slave craton of Canada, and the Kaapvaal craton of southern Africa (De Wit et al., 1992; Bleeker, 2002). These cratons and overlying sedimentary rocks provide limited clues to the environmental conditions and life forms that existed throughout the Archean (Ericksson et al., 1998). This thesis focuses on the siliciclastic sedimentary rocks of the 2.9 Ga Pongola Supergroup, South Africa (Fig. 15).

10. Mars: Planetary History, Missions, and the Search for Life

Martian geologic history is divided into three main subdivisions, the Noachian from 4.5 Ga - 3.5 Ga, the Hesperian from 3.5 Ga – 1.8 Ga, and the Amazonian from 1.8 Ga – present (Fig. 10). Mars formed the same time as Earth, and the early geologic history of

Mars may have been similar to Earth's (Brack, 1996; Malin and Edgett, 2000). Morphologic features and geochemical signatures indicate similar geologic processes, such as plate tectonics and volcanism (Cabrol et al., 2001; Lindsay and Brasier, 2002; Cordoba-Jabonero et al., 2003). Erosional features, such as fluvial networks, on the Martian surface suggest that prior to 3.5 Ga ago, the martian climate was probably warm and temperate, making it conducive to the existence of water (Horneck, 2000; Cabrol et al., 2001; Morrison, 2001; Ronto et al., 2003; Doran et al., 2004). Studies of Martian craters show there may have been a shallow global ocean during the Late Hesperian/Earl Amazonian (Boyce et al., 2005). There is further evidence supporting a warmer Martian paleoclimate based on models using solar luminosity, silicate weathering rates, global energy balance, CO_2 partial pressures, mean global surface temperatures, and biological productivity (Franck et al., 2000).

While there is evidence of initial similarities between early Mars and Earth, the enivronment was probably still different in some respects. The early Proterozoic Earth experienced and increase in ozone levels, decreasing exposure to harmful UV radiation. On Mars, however, UV fluxes continued to increase (Cockell, 2000). Detailed CO_2 models have indicated polar ice caps that are too large and low partial pressures of CO_2 that reflect hazardous UV conditions and an environment inhospitable for life (Cordoba-Jabonero et al., 2003). However, the prevalence of volcanic landforms suggests the possiblity of the release of SO_2 gases from eruptions. SO_2 is one of the main volatile volcanic gases and could absorb radiation in the same wavelength range that ozone does. There is also the possibility that just a few millimeters of martian dust could provide a

shield against damaging wavelengths, allowing some forms of life to exist (Cockell and Raven, 2004).

So, while it is unlikely any forms of life exist on Mars at the present time, conditions 3.5 – 1.7Ga could have supported microbes (McKay, 1998; Horneck, 2000). Cyanobacteria are good candidates as inhabitants on early Mars for several reasons. They are known as the main primary producers of organic matter on early Earth, and were probably directly responsible for the oxygenation of early Earth's anoxic atmosphere (Golubic et al., 2000). Cyanobacteria have a ubiquitous distribution on Earth and can be found in a wide range of environments, including the open ocean, tidal flats, hydrothermal vents, hot springs, and polar environments (Canfield, 1999; Hofmann and Farmer, 2000; Pierson and Parenteau, 2000; Noffke, 2003; De los Rios et al., 2004).

Why do we search for MISS on Mars? MISS on Earth are macroscopic indicators of life that are found throughout the geologic record (Noffke et al., 2003b,2006a, 2008; Noffke, 2007). The assumption is that similar structures could be on Mars as well. On the surface of Mars, geological surveys are conducted by a rover equipped with panoramic and multi-spectral imagers to detect sedimentary structures and textures of potential biological origin (Bell et al., 2004; Cook, 2005; Griffiths et al., 2005; Erickson et al., 2007) (Fig 11). Recent images taken by the rover Spirit show sedimentary features such as ripple marks that can be recognized from a distance (Fig 12a). A closer view of the ripple marked region indeed reveal well-developed ripple marks next to a crust-like

material (Fig 12b). Upon locating a ripple marked region, a rover equipped with a microscopic imager got an even closer view of the features (Fig 13).

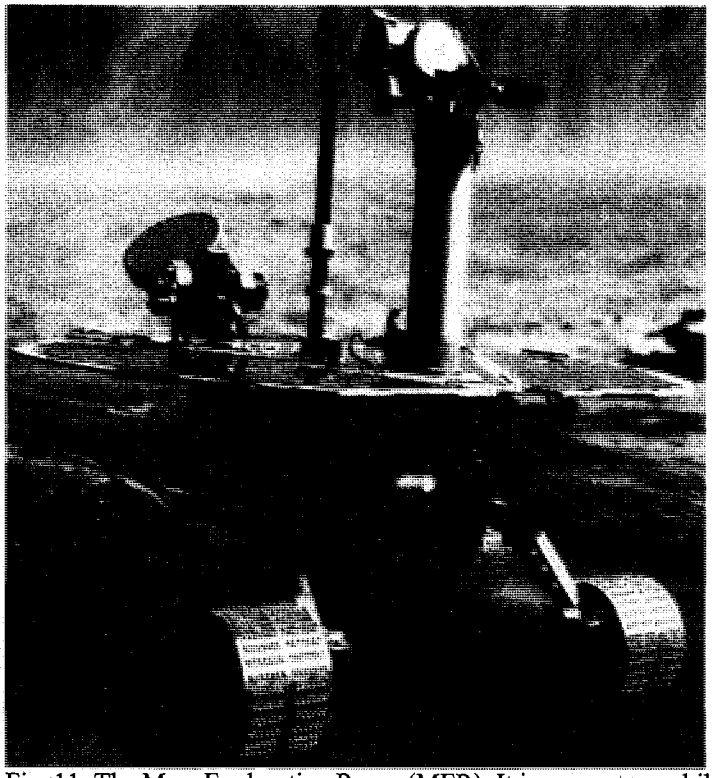

Fig. 11. The Mars Exploration Rover (MER). It is a remote, mobile laboratory equipped with cameras, microscopic imagers, and spectroscopic analyzers to detect signs of life on the surface of Mars. (taken from http://marsrover.jpl.nasa.gov/gallery/)

The Mars rover can also be equipped with instruments such as a miniaturized Raman spectrometer coupled with a confocal microscope for upcoming missons (Edwards et al., 2003; Bishop et al., 2004; Sharma et al., 2006; Sharma, 2007). With such equipment the rover can obtain mineralogical and molecular information to compare with Earthly analogs of biogenic minerals or compounds (Edwards et al., 2003, 2005; Sharma et al., 2006).

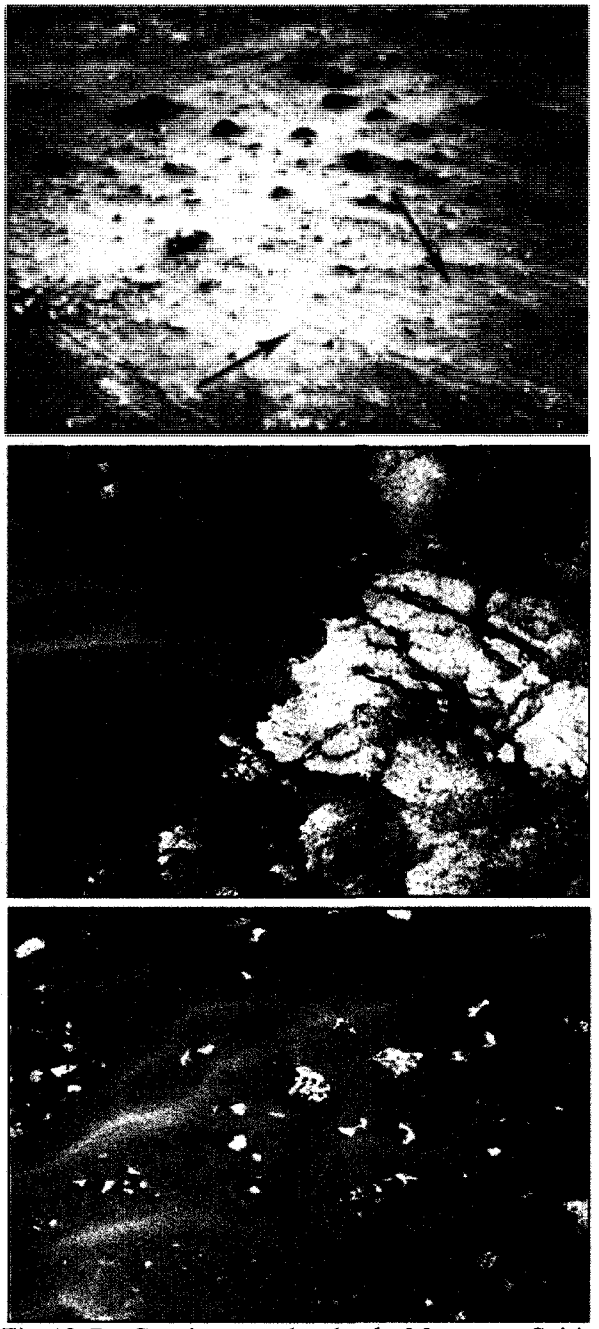

Fig. 12. PanCam images taken by the Mars rover Spirit. (A) Overview image of the Martian surface where ripple marks can be seen (arrows). (B) Arrow points to a ripple marked surface (C) Arrow points to a closer view of a ripple marked surface. (taken from http://marsrover.nasa.gov/gallery/press/spirit/)

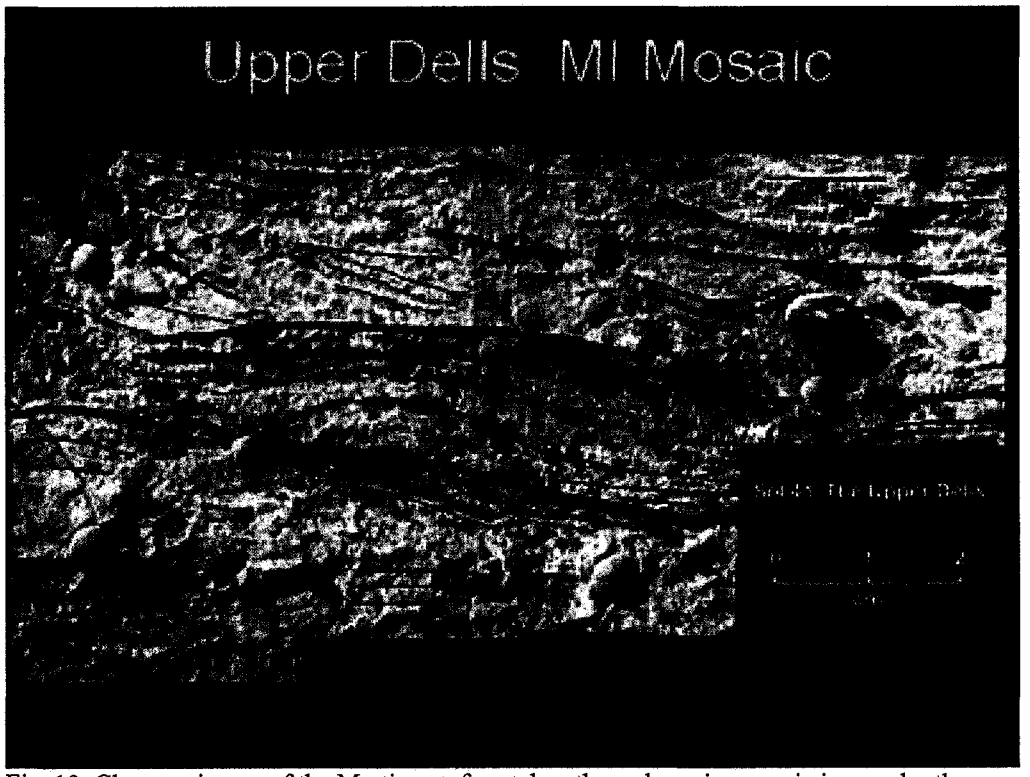

Fig. 13. Close-up image of the Martian surface taken through a microscopic imager by the rover Spirit. Note the laminae that are similar to what is seen in the rocks from the 2.9 Ga Pongola Supergroup, South Africa, Earth. (taken from http://marsrover.nasa.gov/gallery/press/spirit/)

CHAPTER II

STUDY AREAS

1. Modern Tidal Settings: Fishermans Island, Virginia

Geologists are often faced with the challenge of explaining the origin of structures preserved in rocks. This becomes even more difficult, if we find fossils of tiny bacterial cells. These fossils are difficult to detect, often distorted by diagenetic processes, altered by tectonics or metamorphosis, or simply nearly dissolved. Especially the very old rocks of Archean age experienced many changes, and for any texture or structure resembling a "microfossil" the question of its biogenicity, its true biological origin, rises. In order to provide a more complete explanation of the origin of possible biogenic structures, such as MISS, it is necessary to compile a catalogue of criteria of identification from similar structures formed by living microbiota. The reason is that today, in the modern environment, we can study processes, and observe their manifestation as structures or textures. This information allows us to determine the origin of similar features that we can observe in the fossil sediment. To investigate modern analogues of microbial mats and MISS, I studied the tidal flats of Fishermans Island every few months from September 2003 to September 2004.

Fishermans Island is a barrier island located off the coast of Virginia, USA (Fig. 14). It comprises a siliciclastic tidal flat. The island is situated in the moderate to subtropical climate zone with average seasonal temperatures ranging between 1 degree C in the

winter and 24 degrees C in the summer. Average annual wind speed is close to 11mph generally out of the ENE. The average regional rainfall is approximately 45.7" per year, and the mean tidal range is around 1 m. The tidal flats are overgrown by microbial mats during the summer months (May to September).

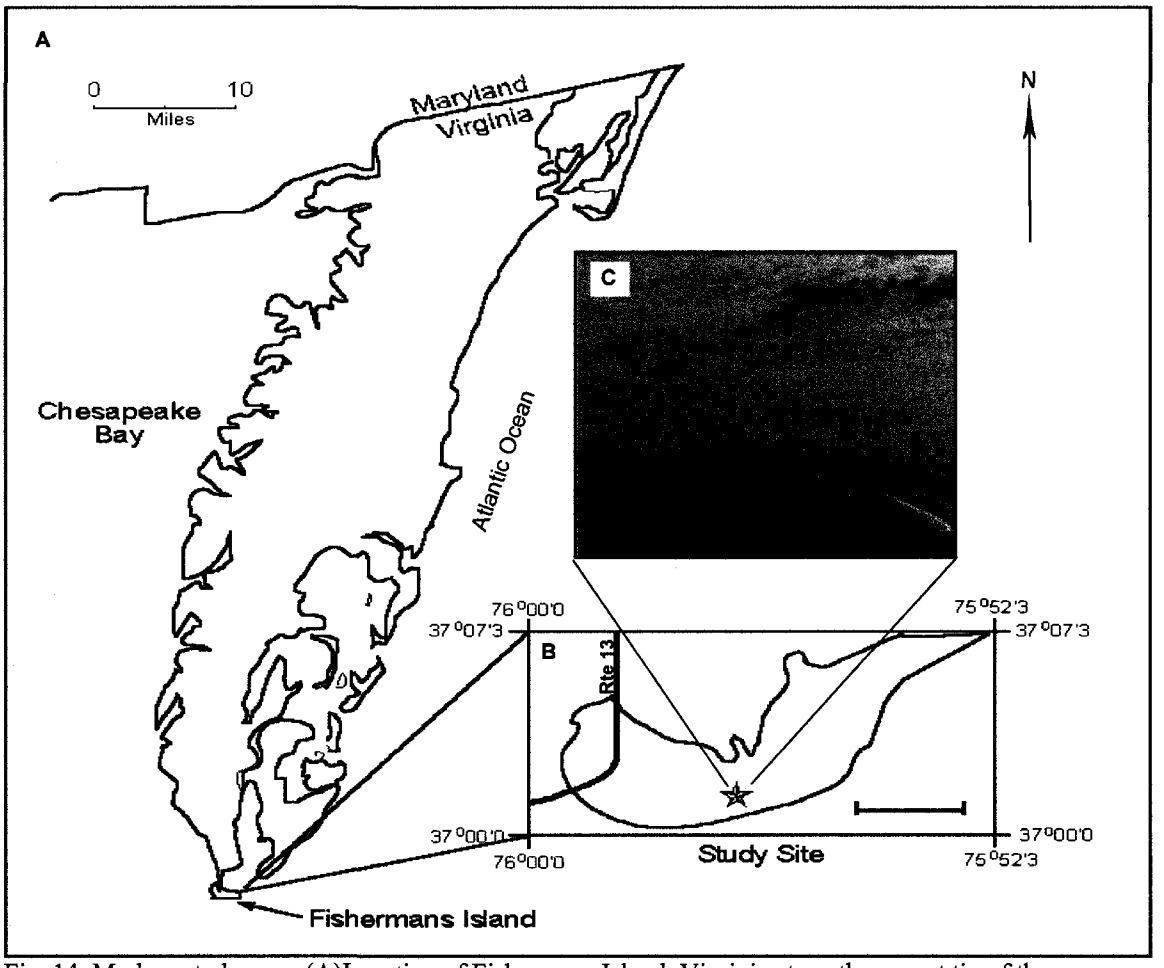

Fig. 14. Modern study area. (A)Location of Fishermans Island, Virginia at southernmost tip of the peninsula at the mouth of the Chesapeake Bay. (B) Close-up of study site location relative to Rte 13. (C) Overview photo of tidal flats on Fishermans Island.

2. Ancient Tidal Settings: Wit Mfolozi River Gorge, South Africa

The Pongola Supergroup is part of the late Archean Witwatersrand Basin in South Africa. It unconformably rests on the pre-3.0 Ga Ancient Gneiss complex and granite-greenstone basement of the Kaapvaal craton (De Beer and Eglington, 1991). The Witwatersrand Basin is part of a retroarc foreland system that formed in response to crustal thickening along the Kaapvaal Craton (Catuneanu, 2001; Ericksson et al., 2005b).

The sediments of the Pongola Supergroup were deposited in the back-bulge basin, starting with a short period of volcanism that produced the mainly igneous Nsuze Group around 3.0 Ga (Ericksson et al., 2005a). Following the uplift and peneplaning of Nsuze rocks between 2.8 and 2.9 Ma, the predominantly sedimentary Mozaan Group was deposited. The Witwatersrand Basin underwent periods of low-grade regional metamorphism as a result of continued tectonism and the collision of the Zimbabwe and Kaapvaal Cratons towards the end of the Archean and into the Paleoproterozoic.
The Mozaan Group reflects deposition on a stable cratonic setting and a shallow-marine shelf (Gold and Von Veh, 1995). These deposits underwent lower greenschist facies metamorphism. Several formations make up the Mozaan Group. For the purpose of my work, two units in the Mozaan Group are of importance: the Sinqueni Formation at the base, overlain by the 1500 m thick Ntombe Formation (Fig. 16). Outcrops of these successions are found in the southeastern margin of the Kaapvaal craton (Fig. 15).

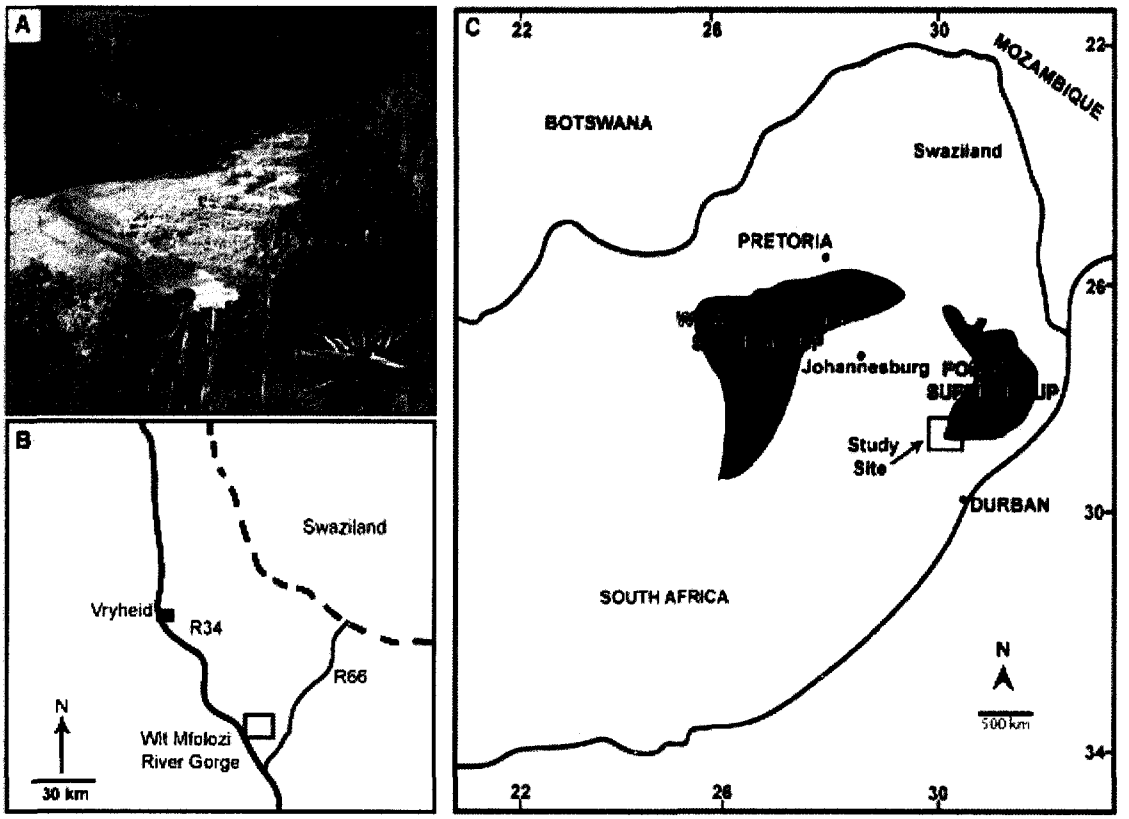

Fig. 15. Study area in South Africa. (A) Wit Mfolozi River Gorge. (B) Main roads and location of study site. (C) Location of study site and relationship between the Pongola and Witwatersrand Supergroups.

The Sinqueni Formation

The 600 m thick Sinqueni Formation is divided into three units, the 330m thick basal quartzite Dipka member, overlain by the 80 m thick shale Ijzermijn member, and the quartzite Kwaaimam member at the top (Fig. 16). The Ijzermijn member also contains a 5m thick banded iron formation. The Dipka member reflects a current-dominated marine shelf facies. The Ijzermijn member reflects a muddy shelf environment. The Kwaaimam member reflects a current-dominated marine shelf, as well as a tide-dominated shelf.

The Ntombe Formation

The 1500 m thick Ntombe Formation consists of alternating siltstone and shale with fine-grained quartzites (Fig. 16). This formation reflects a storm-dominated shelf sand facies. The Ntombe Formation also contains the Mhlathuze member, a laminated shale and iron stone unit at the base, and is capped by the Scotts Hill member, an iron formation.

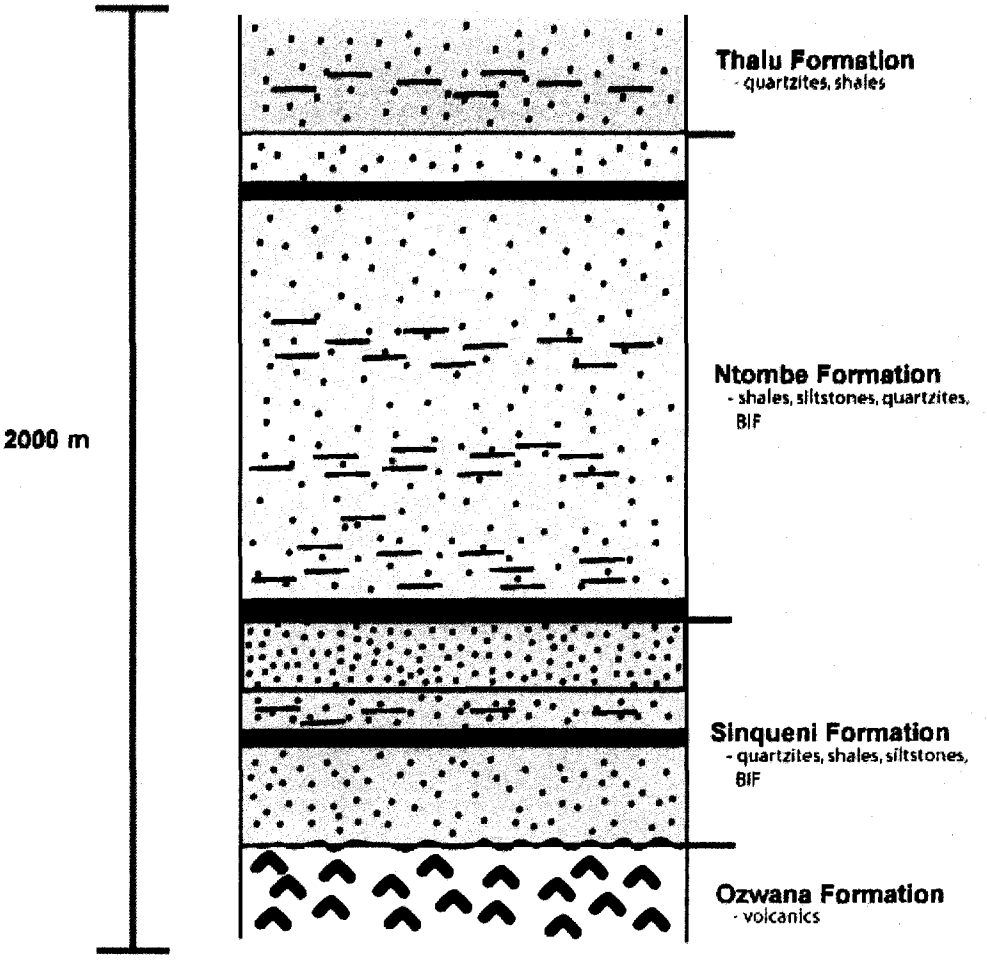

Fig.16. Stratigraphic column of 2.9 Ga Mozaan Group. The 600 m thick Sinqueni Formation consists of quartzites interbedded with shales and siltstones and contains one banded iron formation units and unconformably lies on the volcanic rocks of the Ozwana Formation. The 1500 m thick Ntombe Formation consists of quartzites interbedded with shales and siltstones and has two banded iron formation units.

The Brixton Formation

The Witwatersrand Supergroup is a correlative of the Pongola Supergroup, and is likely the other half of the orginal Pongola-Witwatersrand ocean basin (Gutzmer et al., 1999)(Fig. 15). The 800 m thick 2.98 Ga Brixton Formation of the Witwatersrand Supergroup is composed of alternating sandstones, siltstones, quartzites, and shales. This formation reflects a storm-dominated shelf sand facies. Previously collected and analyzed samples from the Brixton Formation were also used for comparison.

The Pongola Supergroup outcrop is located in the White Umfolozi River Gorge at 31°15' E and 28°10' S, in Kwazulu-Natal, about 70 km south of Vryheid (Fig. 15). Here, the Sinqueni Formation is exposed. It is a succession that records an ancient siliciclastic tidal flat comparable to that of the modern Fishermans Island. As part of a party conducting a geological survey, along a 46m stratigraphic section, I identified and numbered rock beds that contained MISS (Fig. 25) (Noffke et al, 2008). I identified quartz-rich sandstones with ripple marks, desiccation cracks, current lineation, and flaser bedding – all indicative for tidal settings. Abundant cross-stratification is caused by strong currents in the always subaquateous subtidal. Mud- and siltstone are present, but do not make more than 15 to 20 % of the overall rock succession. The dominating fine sandstones are composed of 65 % quartz, 10% mica (muscovite and chlorite), 20 % feldspar, as well as associatory minerals such as heavy minerals (rutile, etc).

CHAPTER III

METHODS

1. Field Work: Descriptive Observations and Quantitative Measurements

1.1 Survey on Modern Microbial Mats, Sampling of Sediment Cores

To understand the distribution of microbial mats across the intertidal zone, I took a 24 meter transect from the low water line to the high water line of the tidal flats (Fig. 17). The lower supratidal zone extends about 12 meters from the low water line and is characterized by biweekly inundation of water. The upper supratidal zone spans from about 12 meters up to the high water line and is not influenced by marine water except during severe storms.

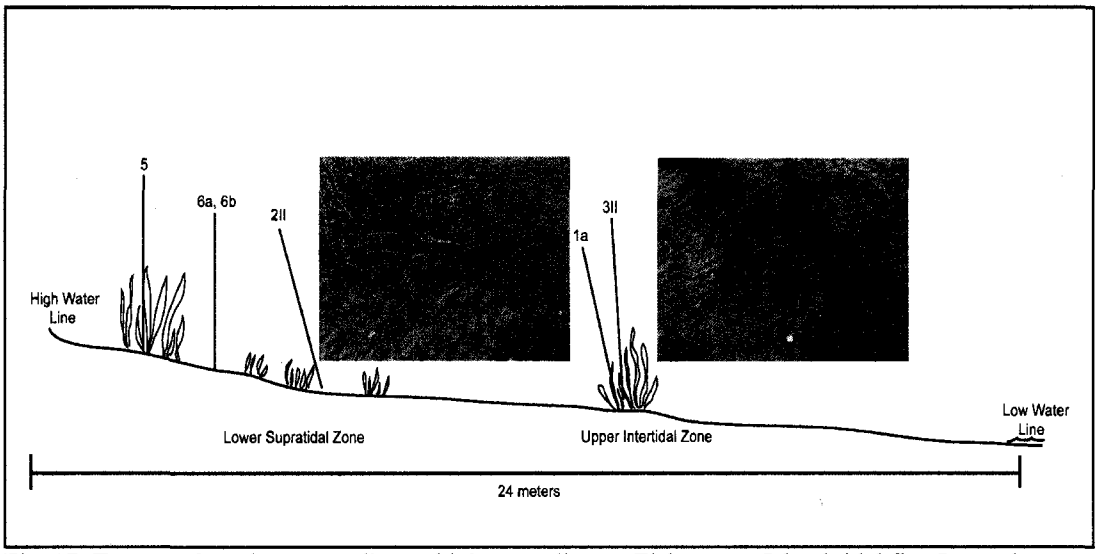

Fig. 17. Transect from low water line to high water line on Fishermans Island tidal flat. Inset photos show locations of erosional remnants and pockets in the lower supratidal zone and multidirected ripple marks in the upper intertidal zone, scales = 5 cm. Petri dish sampling locations indicated by numbered sections.

I investigated the distribution of the microbial mats on the tidal flats, as well as the types of MISS. I also documented the types of plants and invertebrates associated with the mats. The occurrences of the microbial mats are documented on a map (Fig. 17).

In order to examine the general characteristics of microbial mats and mat fabrics in the laboratory, I collected samples of mat-overgrown sediments by pressing 150 x15 millimeter petri dishes into the mat surfaces. The petri dishes held samples of mat layers with about 2 cm of the underlying sediment, making grain size analysis possible within and directly below the mat layer (Fig #). To maintain live specimens, I kept mat samples in an incubator under a 12 hour light cycle and a temperature close to 20°C to achieve near ambient night/day conditions comparable to those on Fishermans Island.

The depositional surfaces of a tidal flat do not reveal intrasedimentary structures or textures. Therefore it is necessary to apply a technique called relief casting to make the internal structures visible. Relief casts are artificially hardened sediment cores that display intrasedimentary structures in three dimensions. To document internal MISS in three dimensions and to see recently buried microbial mat layers in relief casts, I first took box cores along the same 24 meter transect, from the water line to the upper supratidal zone (Fig. 17). I employed 25 x 18 x 7 cm metal boxes that are made up of a bottom and top piece. First, the bottom piece was pressed into the sediments until uppermost edge was level with the surface (Fig. 18). The top piece was then attached.

Using a shovel, the core was pried out of the sand (Fig. 18). Then the core was closed, and the box was transported to the laboratory to make a relief cast (see laboratory methods) (Fig. 18).

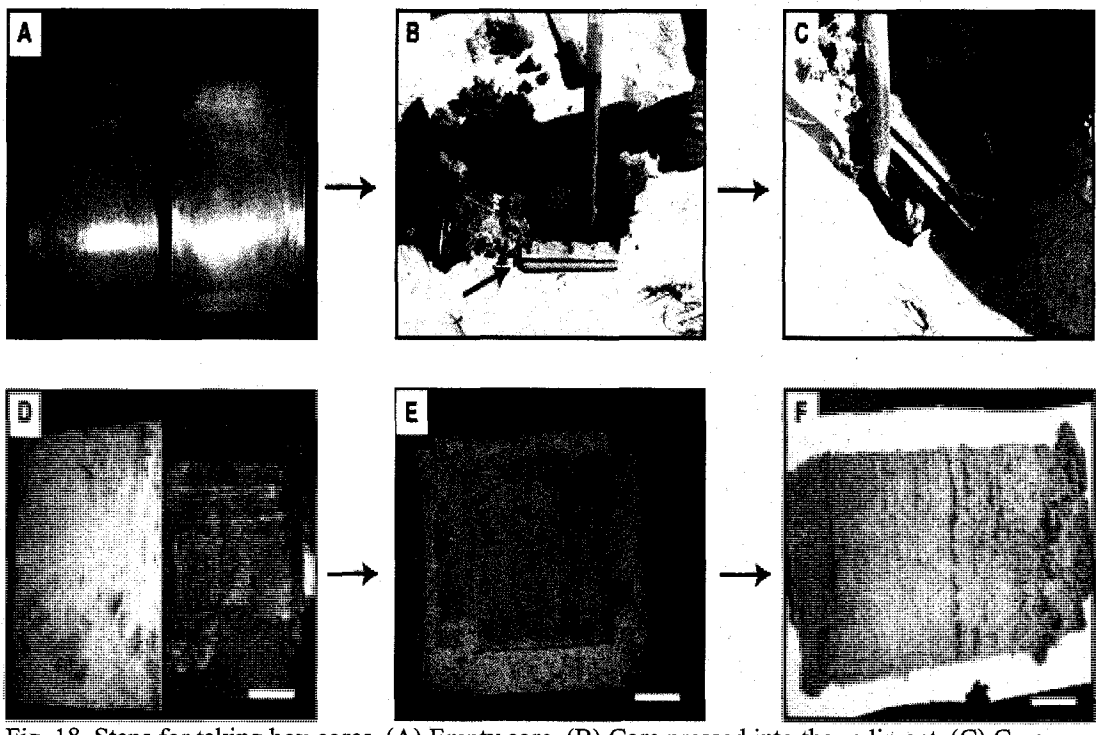

Fig. 18. Steps for taking box cores. (A) Empty core. (B) Core pressed into the sediment. (C) Core pried out with shovel. (D) Lid removed from core. (E) Core after first drying before hardening. Araldit hardener poured onto core (F) End product is a relief cast.

1.2. Geological Survey on Ancient Microbial Mats, Collection of Rock Samples

In preparation for my field studies in South Africa, it was necessary to learn how to recognize MISS in rocks. To train my eye to see the MISS, I made detailed sketches of several samples of sandstones previously collected from the Brixton Formation (Fig. 19).

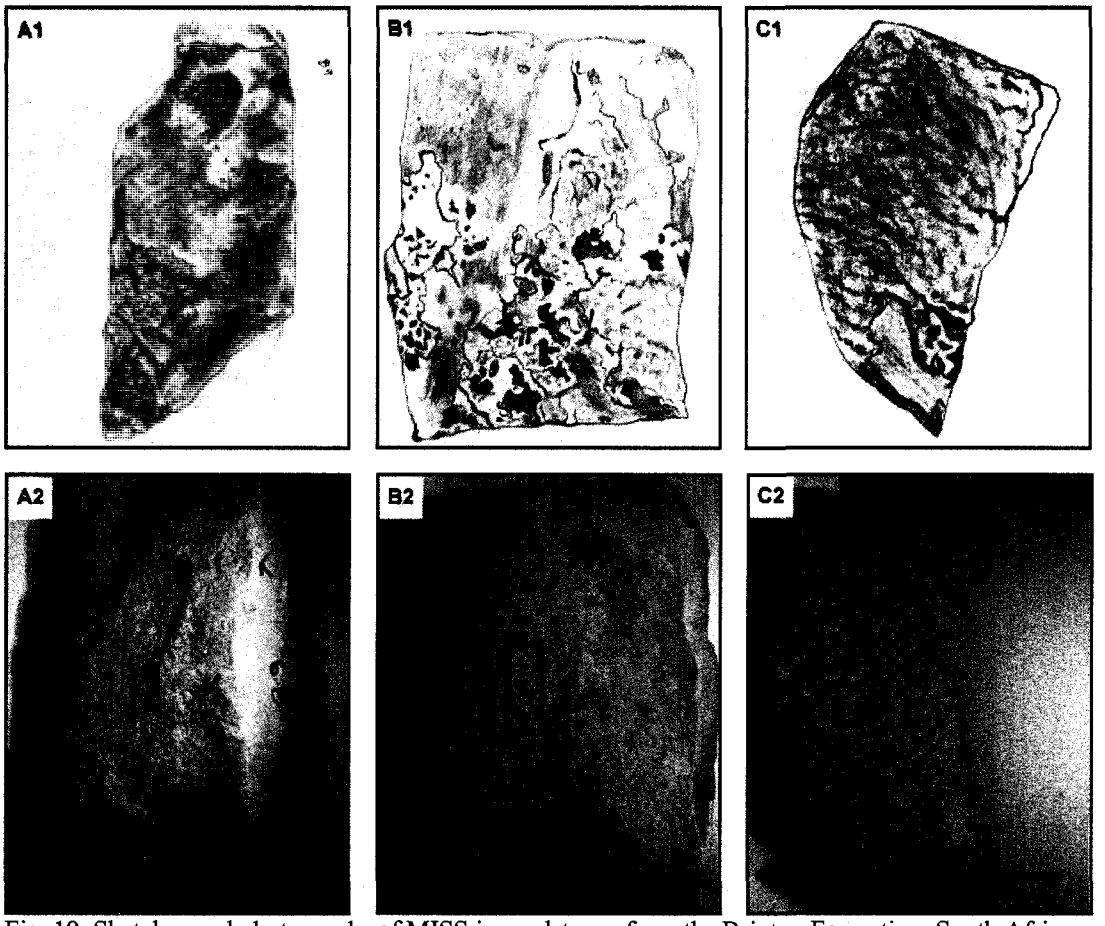

Fig. 19. Sketches and photographs of MISS in sandstones from the Brixton Formation, South Africa. (A1) Sketch of erosional remnants and pockets and (A2) corresponding photo, scale = 6 cm. (B1) Sketch of a microbial mat layer and (B2) corresponding photo, scale = 4 cm. (C1) Sketch of wrinkle structures and (C2) corresponding photo, scale = 8 cm.

In order to compare the fossil MISS with microbial mats and their structures in modern tidal flat environments, I photographed each rock bed to document the various types of MISS (Fig. 20). Our survey showed that the ancient microbial mat facies correlated with the ancient tidal zones: thin microbial mats occur in the intertidal areas, whereas thick, carpet-like microbial mats developed in the supratidal area. This distribution we find today in the modern tidal flats as well.

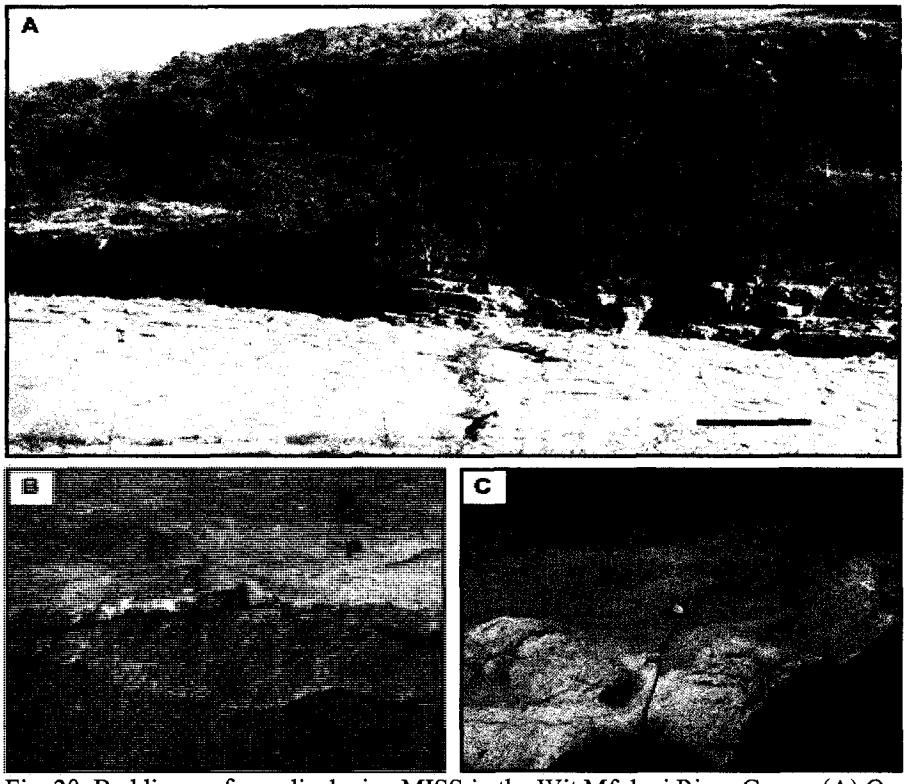

Fig. 20. Bedding surfaces displaying MISS in the Wit Mfolozi River Gorge. (A) Overview of ripple marked sandstone surface, scale = 1 m. (B) Close-up of the edge of an outcrop with erosional remnants (R) and pockets (P), scale = 4 cm. (C) Outcrop of polygons (Py), scale = 5 cm.

Whereas on Earth, we can walk either on modern tidal flats or on ancient bedding planes and search for microbial mats or MISS, on Mars and other planets we have to employ remote sensing techniques. However, microbial mats and MISS cannot be detected easily, and can appear completely different with the change of the sediment or sedimentary rock. Similarly, varying illumination on the rock's surface can affect the visibility of MISS. This may sound insignificant, but indeed it was our indication on this problem, which assisted JPL to gain better images of surface structures from Mars using the rover cameras. To record the effects of light angle and intensity on the visibility of MISS, I took photographs of MISS at different times of the day, and in different weather conditions (sunshine, overcast, etc.).

In order to sample, I carefully removed MISS-containing rock slabs by chisel and hammer (Fig. 21). Each rock sample was marked with a number corresponding to the rock bed from which it came. The surfaces of the samples were indicated by arrows to show which way was up (Fig. 21). After our return to Johannesburg, the samples were all shipped in large metal canisters from South Africa to the United States for laboratory analysis.

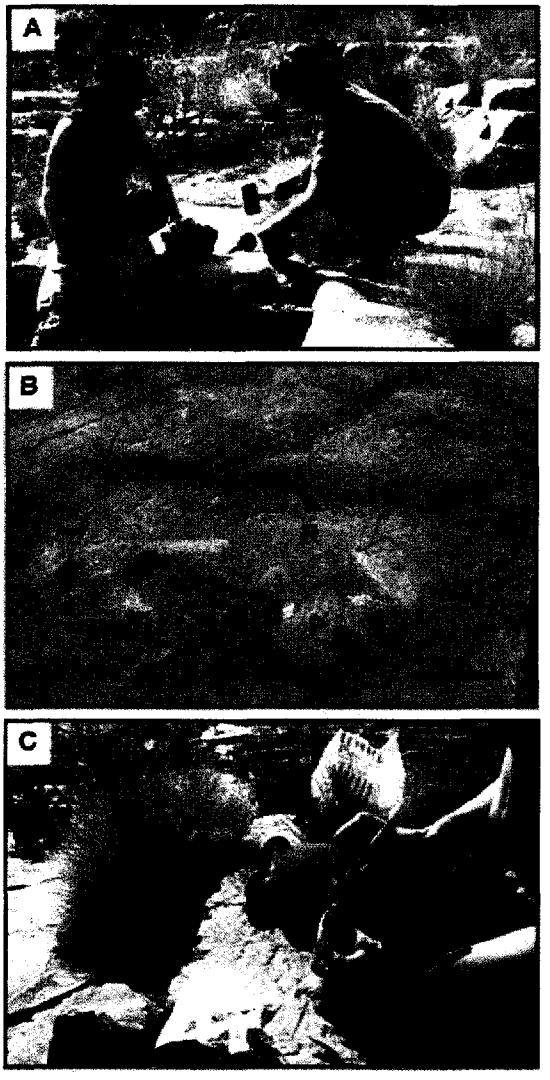

Fig. 21. Collecting samples in the Wit Mfolozi River Gorge. (A) Rocks were taken by hammer and chisel from rock beds containing MISS. (B) Arrows point to pieces of an ancient microbial mat chipped from an outcrop containing erosional remnants (R) and pockets (P), scale = 5 cm. (C) Individual pieces were labeled with arrows indicating the uppermost surface where the MISS are preserved.

2. Analytical Laboratory Methods

2. 1. Relief Casts

To examine the internal sedimentary structures of microbial mats in the tidal flat sediments, I made relief casts from the box cores taken from Fishermans Island. The box cores were left out to dry at room temperature for 24 hours. Once the cores were dried, I cut them to form a planar surface with the edges slightly higher than the middle (Fig. 18). I then dried the samples further in an oven for 24 hours at 105 degrees Celsius. Before removing the samples from the oven I made a 1:1 mixture of Araldite F epoxy resin and hardener. While the samples were still hot, I poured a total of about 250 grams of the mixture on each box core sample. The saturated samples were then dried in the oven for 2-3 hours at 80 degrees Celsius to remove any gas bubbles in the resin. Once this was done, the samples were baked for 24 hours at 120 degrees Celsius. After 24 hours, the samples were taken out to cool. Once cooled, samples were rinsed with tap water and then left to dry at room temperature (Reineck, 1970).

2. 2. Identification of Macrostructures

With the possibility of the occurrence of MISS in Martian rocks, it is necessary to establish a method for the visual detection of macroscopic MISS. MISS, such as multi-directed ripple marks and erosional remants and pockets can be found in both modern and ancient sandy tidal flats. On the surface of Mars, geological surveys are conducted by a rover equipped with panoramic and multi-spectral imagers to detect sedimentary structures and textures of potential biological origin (Bell et al., 2004; Griffiths et al,

2005). With this in mind, I set up experiments in the laboratory based on my field observations to enhance the detection of MISS using a light source.

I used a Canon ZR200 and a Sony DSC-F707 Cyber-shot digital camera to photograph the MISS samples. The rock samples were placed on a white background. The surfaces were illuminated with a focused beam of light from a Nikon MKII 150 Watt fiber optic lamp (Fig. 22). I conducted the experiments in a totally dark room.

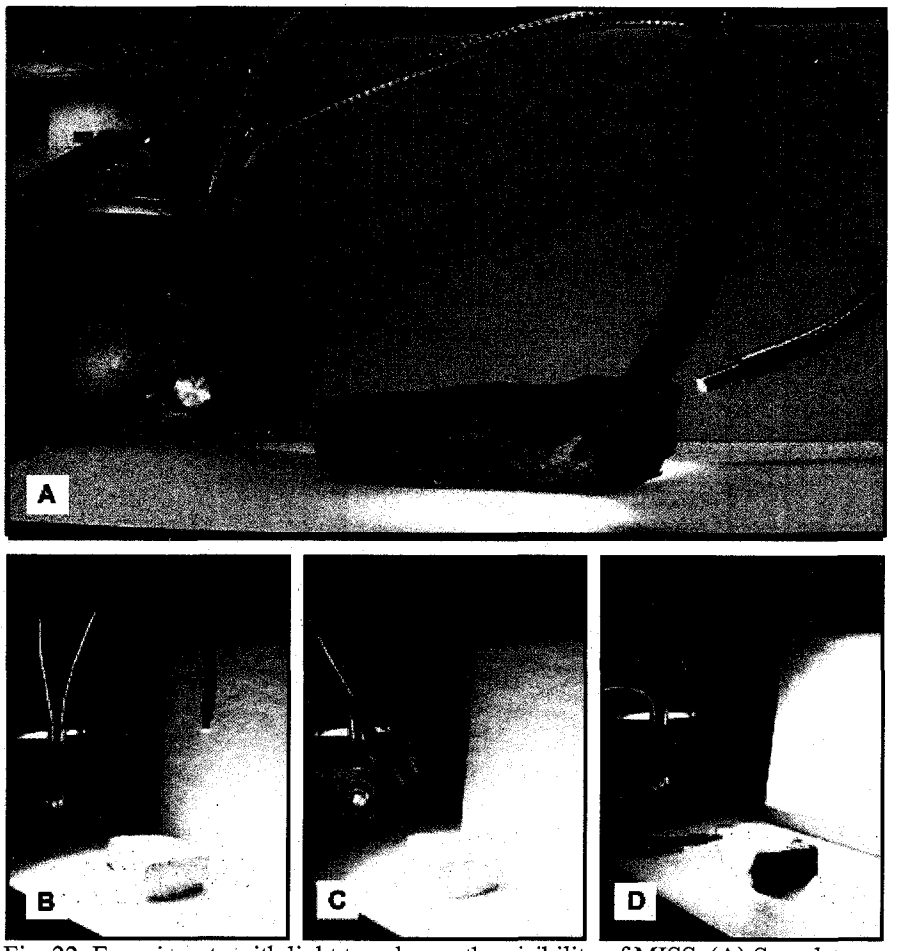

Fig. 22. Experiments with light to enhance the visibility of MISS. (A) Samples were set up on a white background, and the lamp positioned to illuminate the MISS. (B) Lamp positioned to directly illuminate sample surface from above (B). (C) Lamp positioned to illuminate the sample surface at an angle. (D) Lamp positioned to illuminate parallel to sample surface.

I manipulated the angle of lamp and took photographs of the MISS with the camera at a fixed position. The first lamp placement was set perpendicular to the rock surface (Fig. 22). Subsequent placements were set at 15 degree increments, with the final lamp position placed parallel to the rock surface (Fig. 22).

2. 3. Optical Microscopy

To establish a set of criteria for the identification of mat textures in the Archean rock material, I examined the internal textures of modern microbial mats with optical microscopy. General characteristics of the microbial mats and mat fabrics were determined by looking at the petri dish samples under an Olympus SZX12 stereomicroscope (Fig. 27). I focused on filaments, mat fabrics ("networks" composed of filaments), thickness of mat layers, EPS content, and sand grains incorporated in the mat fabrics. (Table #). Ten sets of subsamples from each petri dish were examined. First, pieces of microbial mats were removed from the petri dishes and placed on separate watch glasses. This provided a view into relatively undisturbed mat fabrics, so that the physical characteristics of the microbial filaments could be observed under low magnifications. Sand grains from within the mat layer and at five 1 cm increments directly below the mat layer were measured using standard sedimentological techniques for measuring sorting, grain size, and roundness (Tucker, 1988).

In order to investigate the textures under higher magnification, I made slides of modern microbial mats. The petri dish samples were sliced vertically to obtain a 1x1 cm piece of mat. The slices were placed with a few drops of water to retain moisture on glass slides with a cover slip. None of the mat samples were chemically fixed or preserved. The benefit of using unfixed thin sections, is that the specific details of microbial species in the microbial mat are not obscured by dehydration, baking, and oxidation during fixation. The slides were examined using an Olympus BX51 microscope.

In order to closely examine the microtextures associated with the fossil MISS it was necessary to make thin-sections of the rocks. The arrows on each rock sample indicated the upper bedding plane, so I was able to make vertical cuts through the rocks, and the ancient mat layers. Thin and thick sections were made (Fig. 23).

Large rock pieces up to 10 cm in thickness were cut using a Target Portasaw fitted with a 13.5" diamond blade (Fig.23) Medium pieces up to 5 cm in thickness were cut using a Craftool saw fitted with a 6.5" Raytech Green Blazer blade. Smaller pieces less than 5 cm in thickness were cut using a Raytech ALP10S saw fitted with a 10.5" Raytech Green Blazer blade. No oil was used to clean or lubricate the blades to avoid contamination of the samples. The reason is that oil contains hydrocarbons that can interfere with geochemical analyses on ancient organic matter (carbon).

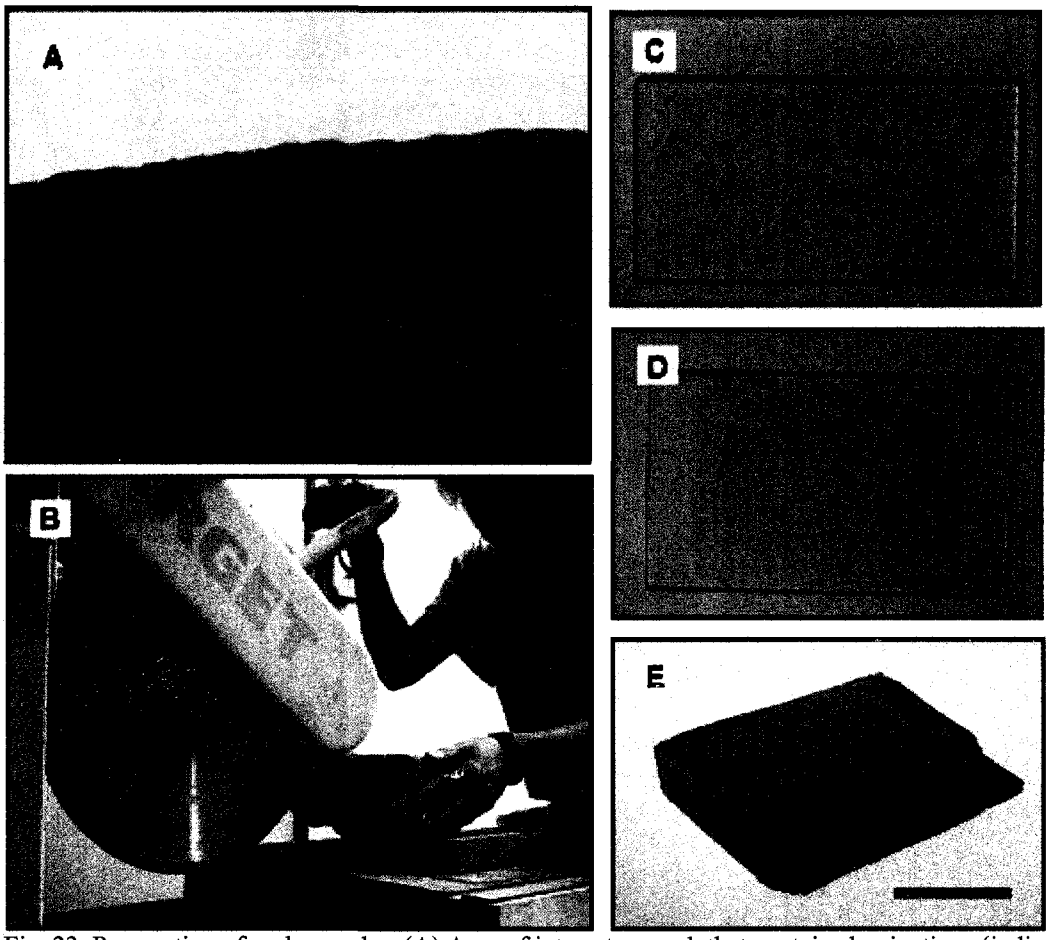

Fig. 23. Preparation of rock samples. (A) Area of interest on rock that contains laminations (indicated by arrow) and MISS, scale = 1.5 cm. (B) Rocks were cut using diamond blade rock saws. (C) 45μm thin section from Sinqueni Formation sandstone, scale = .75cm. (D) 30μm thin section from Ntombe Formation sandstone, scale = 2 cm (D). (E) Thick section from Sinqueni Formation sandstone, scale = 3 cm.

I prepared rock slices of about size 1cm in thickness and $3cm^2$ in surface area to make thin and thick sections for microscope analysis (Fig. 23). Optimal light penetration of the thin section occurs within the thickness range of 5μm to 45μm. To make my thin sections within this precise range, some of the cut samples were sent out to Spectrum Petrographics, Inc, in Vancouver, BC, a company that performs sectioning and petrographic analytical services.

I also prepared thick sections by polishing some of the cut samples on a Buehler Ltd polisher with a slurry of alumina powder and water (Fig. 23). I used sandpaper grits from hardest to lightest, 240, 320, 400, and 600 until the saw marks were no longer visible on the polished surface. Thick sections are generally from 1mm to 2cm in thickness and used for surficial analyses that do not involve light transmission through the sample.

Previously prepared thin sections from the 2.9 Ga Mesoarchean Ntombe Formation, Pongola Supergroup and Brixton Formation, Witwatersrand Supergroup, South Africa, were also used in this study. Using optical microscopy, I documented the dimensions, orientations and morphological characteristics of the fossil textures in the Sinqueni, Ntombe, and Brixton Formations for comparisons with modern cyanobacteria and microbial mat fabrics. To do this, thin sections of the Mesoarchean samples were examined using an Olympus BX51 system microscope and Olympus SZX12 stereomicroscope. Photographs of the microtextures were taken with an Olympus Q-color 3 digital camera, and images were edited using Olympus Microsuite software.

The Olympus BX51 was also used to examine the mineralogy of the Mesoarchean samples. Point counts of the minerals in the thin sections determined the basic mineral compositions for comparison to the modern samples.

2. 4. Confocal Scanning Laser Microscopy (CSLM)

Confocal scanning laser microscopy (CSLM) is a non-destructive imaging technique that takes serial sections of a sample and reconstructs textures in three dimensions (Petford, et al., 1999). Optical sections of a sample are obtained at different depths where only a pinhole of laser light penetrates the sample (Menendez et al., 2001). Reflected or fluorescent light is collected by the objective lens where it is refracted to a second pinhole aperture, rejecting any out of focus light (Aplin et al., 1999). To acquire three dimensional images, scans are made through the z-plane in serial sections. With CSLM, samples can be imaged in three dimensions, as opposed to conventional two dimensional microscopy. CSLM techniques provide a way to observe the internal textures of living microbial mats without disturbing the original microstructure (Pierson and Parenteau, 2000).

As discussed in the introduction, microbial mat textures are replaced by minerals during the fossilization process. Mineral replacement creates textures of similar size and shape to the original biogenic microstructures, such as microbial filaments, rods, or coccoids (Ferris et al., 1986; Schultze-Lam et al., 1996; Hofmann and Farmer, 2000; Noffke, 2000; Noffke et al., 2003a). Two dimensional morphologies of microtextures can be investigated through basic microscopy, but three-dimensional views of microtextures provide more conclusive information on filaments, mat fabrics, situations of EPS, etc. These characteristics are important for the evaluation of biogenicity of textures. For

example, fossilized filamentous microbes are preserved with tubular filaments of a constant diameter, in contrast to abiogenic tubular microstructures of inconstant diameters (Hofmann and Farmer, 2000).

I cut 1-2 mm thick cross-sectional pieces through living microbial mats collected from the tidal flats of Fishermans Island, Virginia to make slides. Each piece was placed on a glass slide with one or two drops of water. Pillars of petroleum jelly were placed at corners surrounding the mat piece, and a cover slip was pressed down until touching the sample (Pierson and Parenteau, 2000). To investigate the microtextures in the Mesoarchean samples, I used thin sections from the Ntombe Formation.

To make comparisons between the modern and Mesoarchean samples, the fabrics of microbial mats, filaments, EPS, and void spaces were described and quantified in three dimensions by CSLM. The filaments were defined by their tubular shapes. The void spaces were assigned to empty pockets within the mat fabrics that did not contain filaments, sand grains, or EPS. The EPS encompassed the dense, organic rich areas within the mat fabrics. Using a grid system of 1 mm x 1 mm that I moved systematically across a sample, I quantified the percentage of filaments, void spaces, and EPS for both the modern and Mesoarchean samples.

I examined the modern and ancient samples using Olympus BX51 and BX61 epifluorescent microscopes equipped with a krypton-argon laser with excitation

wavelength of 488 nm and emission filter >515 nm. I used 20x, 40x, 60x LucPlan FL, and 100x LM Plan FL objective lenses and observed the samples under BF transmitted light and FITC or TRITC (rhodamine dye) cubes. I used Fluoview 3.3 CSLM software to obtain images and make measurements of textures. Fluorescent stains were not applied to the samples, because in situ staining of rock samples on the surface of Mars would likely not be possible (Decho and Kawaguchi, 1999; Bower and Noffke, 2004).

2. 5. Electron Microprobe Analysis

Since a great debate exists over proving the biogenicity of microtextures, it is necessary to use as many lines of evidence as possible. I did Electron Microprobe analyses on thin sections of the Mesoarchean samples to compare the results with those obtained through Raman spectroscopic analysis. This way, the composition of the microtextures could be confirmed by a second test. Electron microprobe uses a focused electron beam to irradiate fixed spots of a sample within the range of 0.2 and 20.0μm. This excites the electrons in the sample to produce fluorescent x-rays that are specific to a given element. A detector captures the x-rays to identify the components (Reed, 2005).

Following the procedures of Boyce et al. (2001), I coated the thin sections from the Sinqueni and Ntombe Formations with aluminum. Aluminum is a good conductor and does not easily absorb electrons. Carbon coatings, which are typically used for electron

microprobe samples were not used. The carbon would mask any original and possible biological carbon in the samples, or even lead to wrong interpretations of presence of carbon.

Under the guidance of Chris Hadidiacos at the Geophysical Laboratory of the Carnegie Institution, Washington, D.C., I used a JEOL 8900 electron microprobe with five wavelength-dispersive spectrometers and an energy-dispersive spectrometer. Scans were done at 15 kV with a beam current of 300 nA. For the Ntombe Formation sample I did overnight scans for elements C, O, Fe, Ca, Si, S, Cr, and Mg on laminae at magnifications between 850x and 1500x. C, O, Fe, Si, and Mg were chosen, because the Raman analyses showed that the micotextures are made up of compounds containing these elements. Ca, S, and Cr were chosen, because these elements are commonly used in biological processes (Fenchel et al., 2000). For the Sinqueni Formation samples I did overnight scans for elements C, O, Ti, Fe, S, Zn, K, Si, P, Mg, Cr, Mn, and Ba on laminae at magnifications between 750x and 1000x. C, O, Fe, Ti, Si, K, Ba, and Mg were chosen, because the Raman analyses showed that the micotextures are made up of compounds containing these elements. Zn, S, Mn, P, and Cr were chosen, because these elements are commonly used in biological processes or incorporated into biomolecules (Libes, 1992; Stone, 1997). From these data, maps showing elemental compositions were created. I also used energy dispersive spectroscopy (EDS) on microbial textures, and the surrounding material to obtain qualitative information of elemental abundances in the samples.

2 .6. Micro Raman Spectroscopy (RAMAN)

Raman spectroscopy is a non-destructive technique used for the characterization of minerals and the identification of biomolecules (Wang et al., 1998; Popp et al., 2002; Bishop et al., 2003; Sharma et al., 2003; Stopar et al., 2005). Biogenic minerals and biomolecules are biosignatures that in concert with morphological textures strongly support biogeneicity of a fossil in question. Rock samples are scanned using a laser of a specific wavelength, such as near infrared Nd^{+} YAG laser at 1064nm or He:Ne laser at 633 nm (Popp et al., 2002; Edwards et al., 2005). As the spectra of materials are measured, the laser light is monochromatically scattered as it interacts with the molecular vibrations of the chemical compounds of a sample (Wynn-Williams and Edwards, 2000). Each chemical compound such as Fe, C, etc or cellular compounds has its own unique Raman spectrum (Table 2) (Wang et al., 1998;Wynn-Williams et al., 1999; Sharma et al., 2005).

Mineral phases of rock forming minerals, accessory minerals, and diagenetically altered minerals can be identified using Raman spectroscopy as well (Wang et al., 1998). Raman spectroscopy can also reveal their spatial distribution in a sample (Popp et al., 2002; Schopf et al., 2002). This documentation of minerals and their spatial distribution is a great benefit when determining the possible origin of fossil-like textures in rocks.

Raman techniques have the advantage that samples do not require much preparation, and that in situ measurements can be done . This means that Raman is an excellent tool for the identification of possible fossils in rocks on the surface of Mars (Haskin et al., 1997; Stopar et al., 2005). Currently NASA technicians are developing a miniaturized Raman spectrometer coupled with a confocal microscope, which can be transported by a mobile rover (Edwards et al., 2003; Bishop et al., 2004). For our study, a rover could identify a possible MISS on the Mars surface, and could scan the rock surface for specific chemical biosignatures.

To determine the best locations for Raman measurements in a thin-section, I specifically identified specific well-visible mat textures by optical microscopy. Raman spectra were collected from the Ntombe and Sinqueni samples and one modern microbial mat sample using a WITEC Digital Pulse scanning near-field optical microscope (AlphaSNOM) with Scan Control Spectroscopy Plus at the Geophysical Laboratory, Carnegie Institution in Washington, D.C. (guidance provided by Marc Fries and Andrew Steele). The Raman scans were done across microtextures in the thin sections using a frequency-doubled YAG laser with wavelength 532nm. The laser was focused through a 25μm diameter fiber and a 20x ocular lens. The average scan speed was 4-6s dwell time per pixel at 78 kW cm^{-2} (Fries and Steele, 2005). Scans were conducted for different lengths of time, from short spot scans of 1 minute lengths to long 9hr scans. The scan times, dwell times, and scan areas were adjusted depending on the target region in the sample.

Using WITeC 1.84 software, I analyzed the spectra generated by elemental constituents in the samples. I created virtual maps of each sample showing the spatial elemental and mineral composition of the microstructures from the data collected. I also collected and organized a list of relevant minerals and their Raman spectra for use in data interpretation (Table 1).

Mineral	**Chemical Formula**	**Raman Spectra**
Quartz	SiO_2	201/263/354/394/465/693/795
Milky Quartz	SiO_2	128/207/464
Carbon-G	C	1580-1610
Carbon-D	C	1350
C=C	C=C	1006/1157/1525
C-H Stretch	CH	2500-3000
O-H Stretch	OH	3000, 3400
OH-deformation	OH	1650
OH-libration	OH	725
Si-O-Si	Si-O-Si	600, 705
Anatase	TiO_2	144/197/399/513/639
Biotite	$K(Mg,Fe^{2}+)_3[AlSi_3O_{10}(OH,F)_2$	550/670-700
Chlorite	$(Mg,Fe,Al)_3(OH)_6[(Mg,Fe,Al)_3\{(Si,Al)_4O_{10}\}(OH)_2]$	350/550/670-700/800-1150
Goethite	α - FeOOH	245/302/386-390/478/547/681/998/1110/1299/3095
Hematite	α - Fe_2O_3	214/225-274/294/405/498/609/1313
Ilmenite	$FeTiO_3$	234/369/682/789
Kaolinite	$Al_2Si_2O_5(OH)_4$	260/3621/3687
Lepidocrocite	γFeOOH	343/379/500
Magnetite	Fe_3O_4	380/667-690
Microcline	$KAlSi_3O_8$	126, 157/265, 285/453, 476, 513
Muscovite	$KAl_2(Si_3Al)O_{10}(OH,F)_2$	260/420/700
Rutile	TiO_2	447/612-618/

Table 1. Reference list of minerals and compounds with Raman spectra. Minerals and compounds listed are typical for siliciclastic sedimentary rocks.

2. 7. Carbon Isotope Analysis

A commonly used proxy used to prove the biogenicity of microfossils is the presence of biological carbon as defined by carbon isotopes. As discussed in the introduction, autotrophic organisms, such as cyanobacteria, fix CO_2. This carbon fixation results in the fractionation of $^{13}C/^{12}C$, with a preference for ^{12}C. Thus, $\delta\ ^{13}C$ values derived from biological processes tend to fall in the range of -10 and -40. Recent data have shown an abiogenic source of negative $\delta\ ^{13}C$ values as well, and there is also much overlap in biogenic values. On its own, carbon isotope analysis may not be completely valid. However, in concert with other types of geochemical methods, carbon isotope analysis provides an extra line of evidence.

To prepare the Mesoarchean samples for analysis, I broke the rocks into small pieces using a hammer and steel plate. The pieces were divided up into i) outer pieces (those in contact with the atmosphere) and ii) inner pieces (those not in contact with the atmosphere). I wore gloves during the sample preparation process to avoid contamination. The pieces of rock were ground into a fine powder using a steel grinder and then with a traditional mortar and pestle. These pieces were put into separate clean and labeled vials. I scooped between 9mg and 15mg of the sample powder into pre-tared steril silver cups. Each cup with sample was folded into a tiny ball and put into a steril capped micro-test tube and labeled. I then cleaned the sample powder using methylene chloride (DCM) to extract any soluble organic contaminants.

To detect the presence of carbon and carbon isotopes, the samples were run on a CHN analyzer at the Geophysical Laboratory of the Carnegie Institution, Washington, D.C. under the guidance of Robert Hazen and Marilyn Fogel. We used a Carlo Erba elemental analyzer interfaced with a Finnigan DeltaPlusXL continuous-flow isotope-ratio mass spectrometer. The samples were run in triplicate.

CHAPTER IV

RESULTS

1. Distribution of Microbial Mats on Fishermans Island

On the tidal flats of Fishermans Island, two microbial mat types were identified along the 24 meter transect (Fig.17). The most prevalent is mat type I, which is characterized by a mat layer of about 1mm thickness. The dominant constructor of mat type I is *O. limosa.* These mats form multidirected ripple marks on the sandy surface in the upper intertidal zone. Mat type II is characterized by a mat layer of close to 2 mm thickness and dominantly constructed by *M. chthonoplastes*. These mats typically form erosional remnants, with "pocket" areas where erosion took place in the lower supratidal zone. The *M. chthonoplastes* dominated type II mats form a cohesive layer interweaving grains of the sediment surface, making it difficult to separate the mat from the underlying sand. This suggests that *M. chthonoplastes* contributes to the strength of a mat (counteracting to tensile forces efficiently) and increases its biostabilization effects. *M. chthonoplastes* secretes large amounts of EPS, enhancing cohesiveness between sand grains and filaments. Earlier studies conducted on Mellum Island in the North Sea have also shown the biostabilization effects of *M. chthonoplastes* dominated microbial mats in general withstanding the erosional forces of currents of velocities of up to 1.60 m per second (Noffke, 1999). The *O. limosa* dominated type I mats are thin and are easily peeled off the sediment surface. However, the mats remain intact after they are removed from the sediment surface. The reason is that the mats do not "grab on to" the sediments below as

strongly as the *M. chthonoplastes* dominated mats do. (This will be further discussed in the optical microscopy results section)

Three plant species occur within the study area : *Spartina alterniflora, Distichlis spicata,* and *Salicornia salicornia. S. alterniflora* (Saltmarsh Corgrass) grows in a tall form in areas of daily tidal flooding and in a short form near the upper tidal limit. This species is ubiquitous, and enriches large amounts of organic material that is covered by bacteria and algae (Lippson, 1997). *D. spicata* (Saltgrass) is a short, wirey grass typically found in salt and brackish marshes (Lippson, 1997). *S. salicornia* (Glasswort) generally grows in dry salt pans (Lippson, 1997). On Fishermans Island, the microbial mats were growing mostly around *S. alterniflora* and *D. spicata.* (Details involving the association between the plants and microbial mats were not examined in this study).

Two common macroorganisms inhabit the areas covered by microbial mats on Fishermans Island. One is *Ocypode quadrata* (Ghost Crab), a crab species that inhabits the upper intertidal zone (Lippson, 1997). The other macroorganism is a snail species, *Littorina irrorata* These thick-shelled snails, that are known to graze on algae, plant detritus, and bacteria (Lippson, 1997).

The 18 relief casts that I made from the sediment cores reveal that several generations of microbial mats had developed on Fishermans Island over time (Fig. 24). The size of the relief casts are about 23 x 18cm. The surface layers representing the most recently living mats atop the tidal sands are about 1mm thick. The sub-recent microbial mats buried in

the sandy layers underneath are about 2-3 cm below the surface, and are sometimes stacked to piles of 9 cm filling the upper half of the relief casts. All of these mat layers are parallel to the surface. The thicknesses of these relict mats are also around 1mm. Within the upper 9 cm of the relief casts, the preserved mat layers in general are spaced 1 mm.

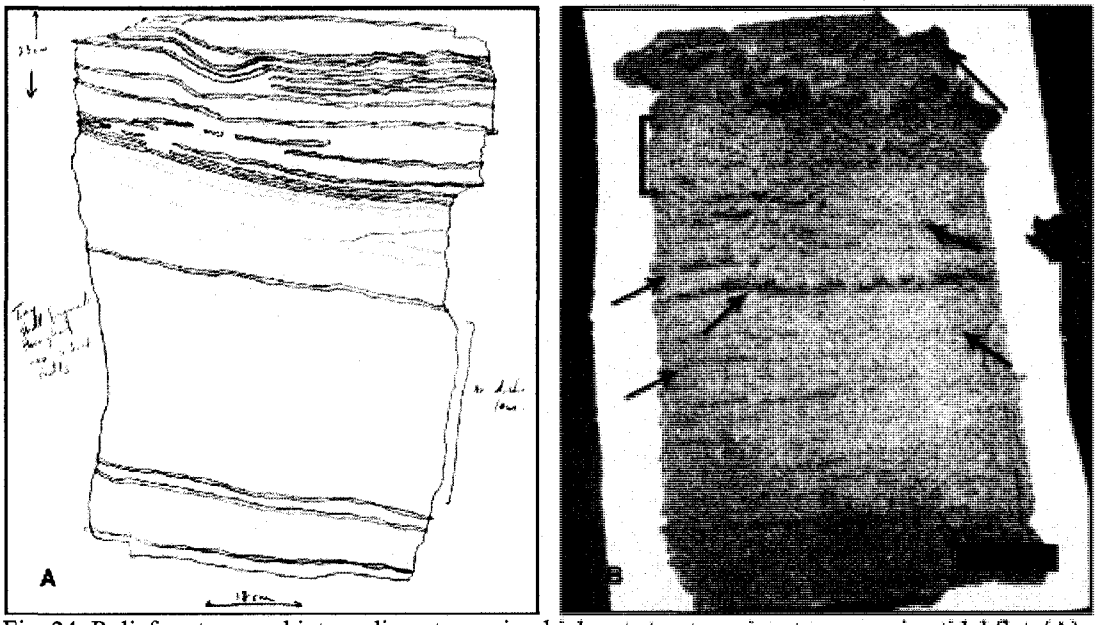

Fig. 24. Relief casts record intrasedimentary microbial mat structures in a transgressive tidal flat. (A) Sketch of relief cast from Fishermans Island showing regular spacing of mat layers of about 1mm close to the surface, followed beneath by irregularly spaced mat layers. (B) Photo of relief cast with arrows indicating mat layers. Bracketed area shows a region where gas bubbles accumulated in consequence of the decay of a mat layer underneath, scale = 5cm.

It appears that the upper portions of the relief casts record the lower supratidal zone with thick microbial mats of *M. chthonoplastes* type forming stacks of prominent laminae. The microbial mats clearly dominate the sedimentary processes prohibiting the formation of

physically derived sedimentary structures such as ripple marks (Noffke et al., 2003a). A few complete shells of bivalves and gastrodods record that the macroorganisms were well protected against wave action or bottom currents by the sandstabilizing mats, and that they became buried in situ as biocoenosis. In the lower portions of the relief casts, the spacings between relict mat layers are irregular, and the buried mat layers are sub-parallel to the surface. The mat thickness also is decreased. I interpret these lower portions of the relief casts as sediments of a former intertidal zone, the predominant colonization site of *O. limosa* mats. The change in orientation of the mat laminae from parallel to less parallel indicates a soft mat cover less affected by physical sedimentary processes that merely adapts to the preceeding surface morphology rather than altering it (Noffke et al., 2003a). Shell fragments are also found in between some of the mat layers, indicative of the more turbulent currents of a intertidal zone. The shell fragments are redeposited after transport and represent a typical taphocoenosis.

The spacings between the mat layers in the relief casts record time intervals that are not easily quantifiable. However, accurate generalizations can be made regarding the depositional environment and development of the tidal flats. The frequency of preserved mat layers indicates the frequency of deposition and microbial mat development (Noffke and Krumbein, 1999). Where there is regular spacing, there was constant deposition in regular distances. With response to this regular pattern of deposition, the mat building cyanobacteria were constantly migrating upward to establish new microbial mat generations (each represented by a laminum). This is typical for the lower supratidal zone (Noffke, 1998). It is interesting that the microbial mats pile up. It means that the tidal flat

actually must tectonically sink down (or that the sea level constantly rises). However, I cannot relate laminae to specific flooding events such as storms or the spring high tide flood.

The irregular spacing visible in the lower portions of the relief casts is indicative of a more irregular pattern of deposition that is typical for the upper intertidal zone (Noffke, 1998). The lowermost portions of the relief casts normally do not contain any buried mat layers (Fig. 24). These portions represent the lower intertidal zone, where the constant change between immense deposition and strong erosion of the sandy substrates simply prohibits the formation of a cohesive microbial mat.

2. Biofacies Zones in the Wit Mfolozi River Gorge

In the 46 m thick sandstone succession that crops out in the Wit Mfolozi River Gorge, a multitude of excellently preserved MISS have been detected (Noffke et al., 2008) (Fig. 25). The structures include multidirected ripple marks, erosional remnants and pockets, gas domes, polygonal oscillation cracks, microbial mat chips, and many more. It is most noteworthy that these structures are related to the lower and upper intertidal facies zones, as well as lower supratidal (Gerdes and Klenke, 2003). That is that the MISS preserved at this site are identical to those found in the equivalent tidal zones on Fishermans Island today. This finding has been highlighted in a review by the journal Nature.

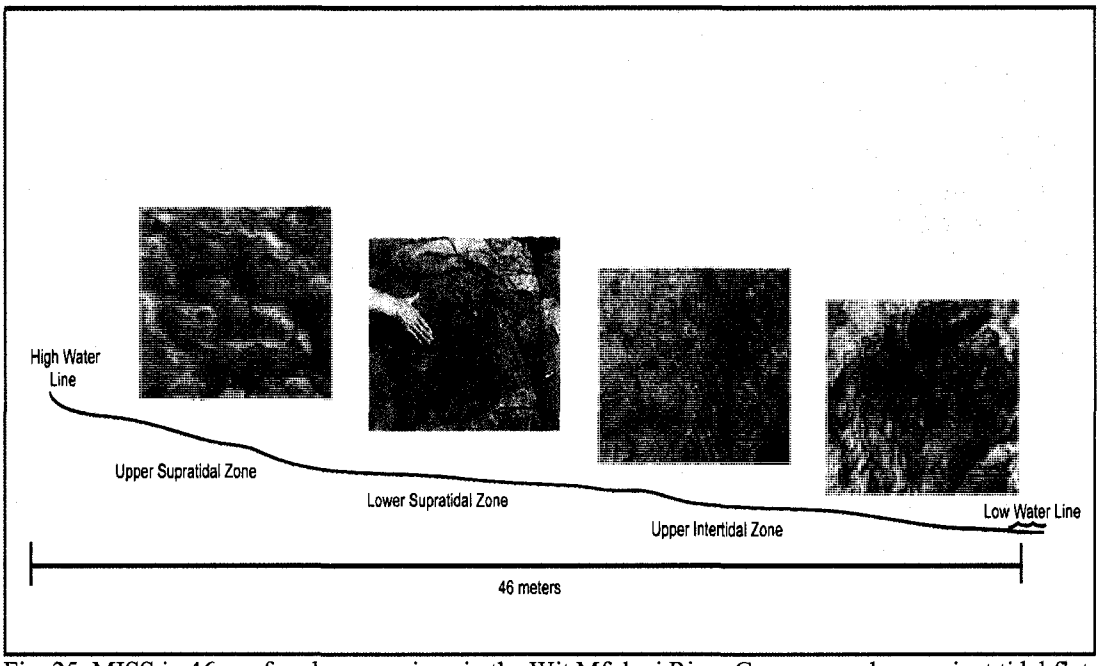

Fig. 25. MISS in 46 m of rock successions in the Wit Mfolozi River Gorge record an ancient tidal flat. (A) Polygons and gas domes in the upper portion of the succession record the upper supratidal zone. (B) Erosional remnants and pockets record the lower supratidal zone. (C), (D) Multi directed ripple marks record the upper intertidal zone.

The fossil multidirected ripple marks are beautifully preserved on 3 upper bedding planes and record microbial mats colonizing an ancient upper intertidal area that was characterized by a slow and steady movement of periodic tidal currents (Noffke and Krumbein, 1999). The erosional remnants and pockets exceptionally displayed on 17 rock bed surfaces rose from the alternation between growth of microbial mats in the lower supratidal zone and their partial erosion during episodic flooding, perhaps rare storms, or strong spring high tides. This erosion of the microbial mats ripped off fragments, mat chips, from the margins of the erosional pockets. Those fragments were spattered at random all across the tidal flat surface, recording the velocity and direction of the ancient flood currents (Noffke et al., 2008).

While not seen on Fishermans Island, impressive polygons up to about 40 cm in diameter are preserved in the Wit Mfolozi River Gorge (Fig. 25). These MISS record areas even higher up into the supratidal zone, which were characterized by longer periods without water inundation (Noffke et al., 2008). In fact, such polygonal patterns of oscillation cracks rise from the seasonal change of meteorological conditions in a semiarid climate (Gerdes and Klenke, 2003). This conclusion on the character of the ancient climate is of great interest for studies of the development of Earth's paleoclimate. Much like abiotic mudcracks, the microbial mats slowly shrink in a polygonal pattern from de-watering during periods of dessication. During the subsequent rainy season, the mats recover, fill with water, and expand laterally by this closing the polygonal cracks inbetween the patches. Unlike abiogenic mud cracks, there are holes in the center of many of these polygons. The holes are the result of gas domes that originally formed during desiccation and gas accumulation possibly during hot summers. As soon as a gas dome became too high, its tip ruptured and the gas escaped leaving the hole in the mat layer behind. The formation of these structures was described in on the southern coast of Tunisia (Noffke et al., 2001b).

As discussed in the methods section, the visibility of the MISS on the bedding planes was dependent on the angle of solar illumination. At midday, the light from the sun shone directly on to the rock surfaces. At this perpendicular angle, the light was mainly reflected from the surface, and the outlines of the MISS were not clearly distinct (Fig. 26). Later in the day, when the sun was lower in the sky, the incident light hit the rock

surface at an angle close to 45° from the horizontal surface. At this angle, the light was not completely reflected off the surface, and the outlines of the MISS were distinctly clear (Fig. 26).

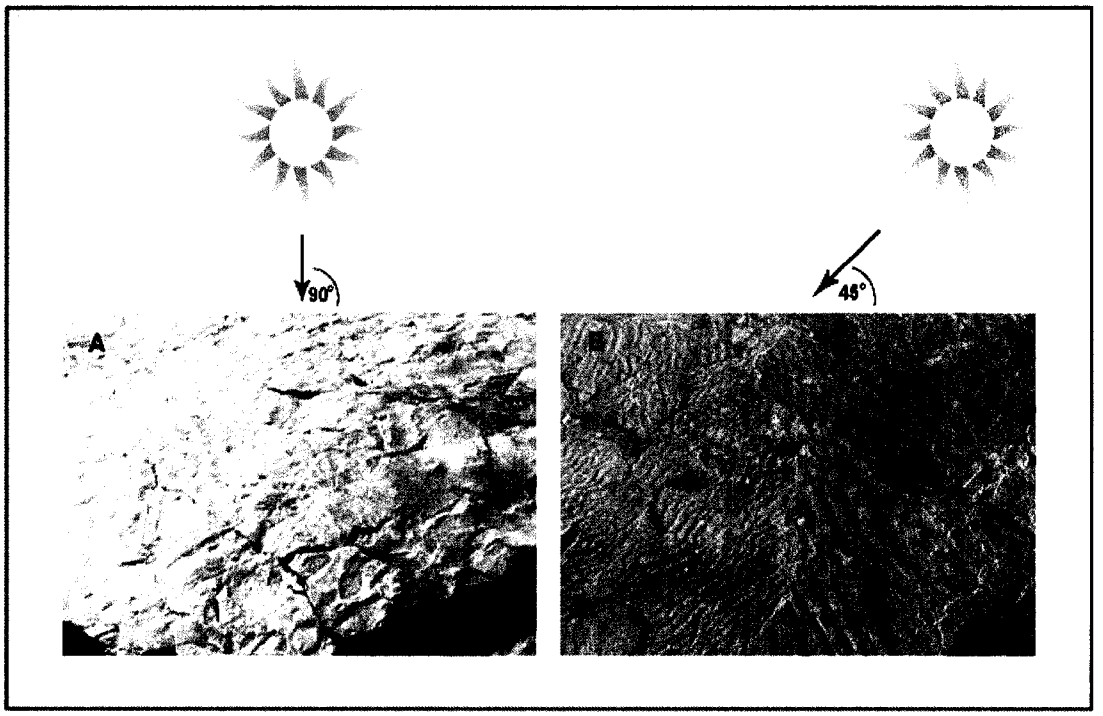

Fig. 26. Visibility of MISS on sandstone surfaces, Wit Mfolozi River Gorge. In the field, the visibility of the MISS is greatly affected by the direction of sunlight on the surface. (A) Light is reflected off the surface when the angle of light is perpendicular to the surface, obscuring the visibility of the multi directed ripple marks. (B) Surface features are visible with a decreased angle of the sun.

These simple observations will assist in the detection of surface features of mm and cm scale on the sedimentary surface of Mars. I propose that the future Mars rovers be equipped with powerful lamps that illuminate the sedimentary surface in question and thus increase the contrast of morphologies significantly. Due to atmospheric differences between Earth and Mars, it is likely that different light spectra would work better on Mars, but such investigations are beyond the scope of this study.

3. Cyanobacteria and Mat Textures (Modern and Ancient) - Optical Microscopy

The microbial mats from Fishermans Island were about 1-2mm in thickness. The overall orientation of the filaments in the microbial mats was parallel to the surface, and some filaments were sub-parallel by up to 10° from the surface (Fig. 27). The microbial mat filaments and EPS were interwoven with sand grains (Fig. 27).

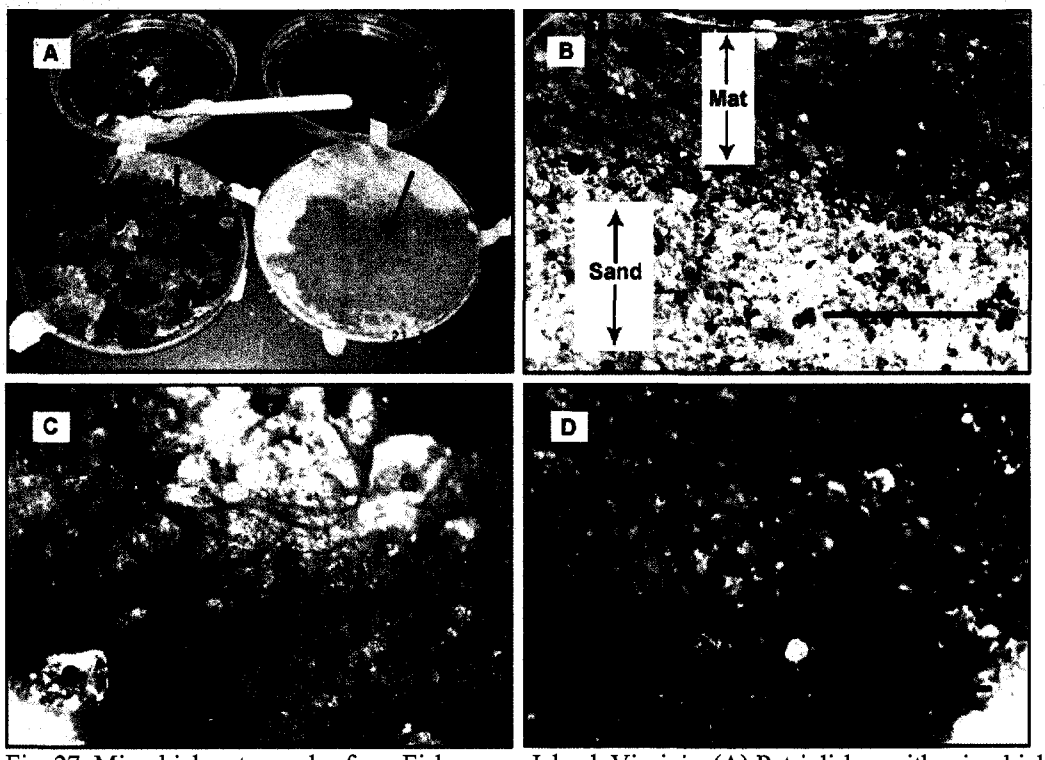

Fig. 27. Microbial mat samples from Fishermans Island, Virginia. (A) Petri dishes with microbial mat samples, arrows point to microbial mats. (B) Stereomicroscope image of cross-view through microbial mat with mat layer and sand layer, scale = 1 mm. (C) Stereomicroscopic image of mat fabrics intertwined with sand grains, Q = quartz, M = mat fabric, scale = 500μm. (D) Close-up stereomicroscopic image of microbial mat surface showing mat fabrics scale = 2mm.

According to the scale by Powers (1953), the roundness of the sand grains averaged 2.5, meaning most were sub-angular. The average sphericity of the sand grains was 4.5, meaning most were spherical. The sand grains were well-sorted and fine grained, with an average grain size of 0.205mm. The sands were made up of at least 65% quartz, 20% feldspars, 10% micas, and about 5% heavy minerals for all samples (Fig. 28).

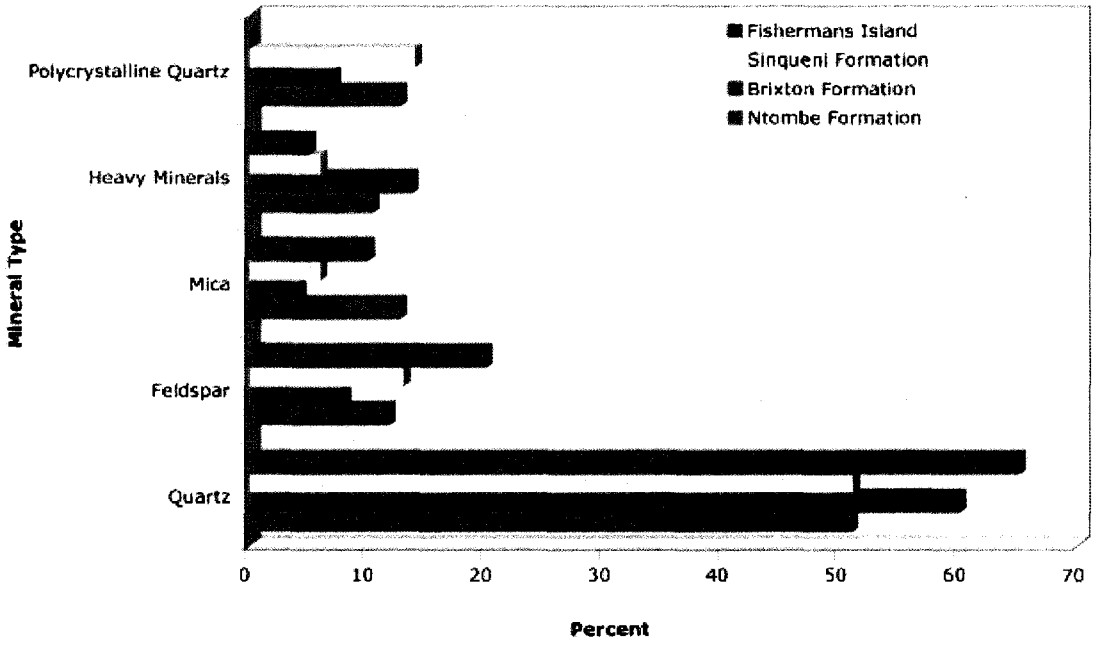

Fig. 28. Comparison of mineral grains in modern microbial mats and Mesoarchean microtextures. In all samples, quartz is the most abundant component.

Examinations of unfixed microbial mats show that the dominant mat building species are two filamentous cyanobacteria *Microcoleus chthonoplastes* and *Oscillatoria limosa*, and one coccoid species, *Merismopedia punctata*. *M. chthonoplastes* forms ensheathed bundles of trichomes (Fig. 29). Each trichome is about 15μm in thickness, and the

bundles typically are about 100μm in thickness. *O. limosa* forms individual trichomes of about 50μm thickness (Fig. 29). The coccoids are close to 20μm in diameter.

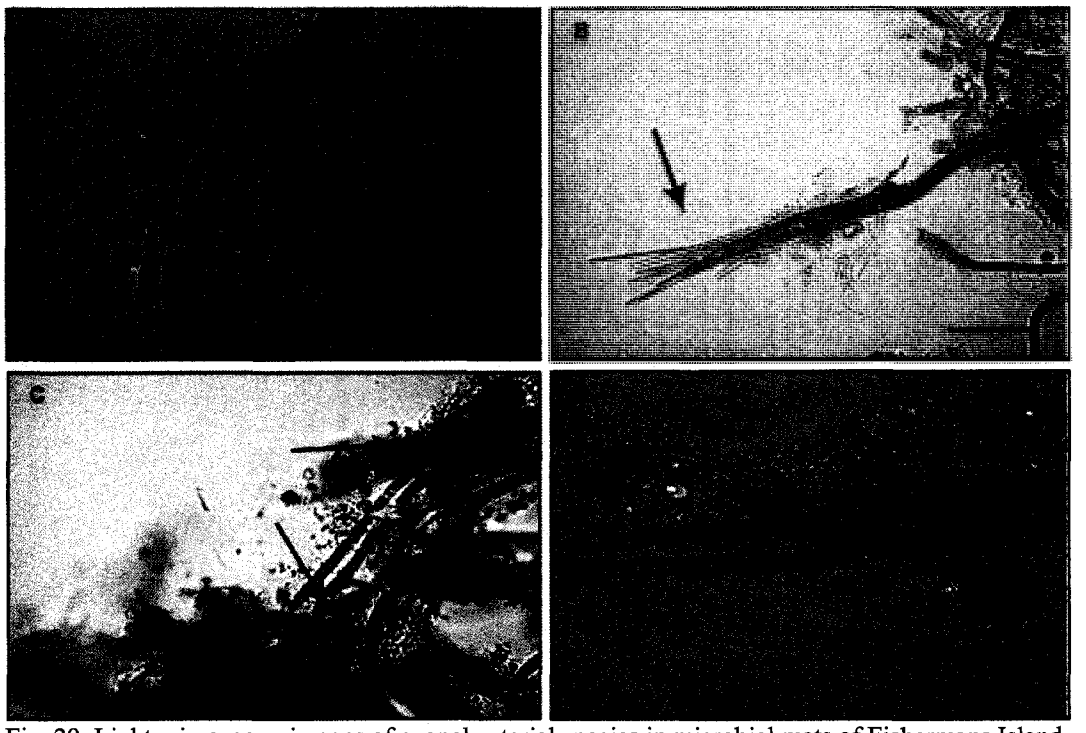

Fig. 29. Light microscopy images of cyanobacterial species in microbial mats of Fishermans Island, Virginia. (A) Thick trichomes of *O. limosa*, scale = 200μm. (B) Bundles of thinner *M. chthonoplastes*, scale = 300μm. (C) Clusters of coccoids of *M. punctata*, scale =300μm. (D) *O. limosa* (O), *M. chthonoplastes* (Mc), and *M. punctata* (Mc) together in one slide, scale = 200μm.

O. limosa was the dominant species in all but one sample, accounting for at least 40% of the total population (Fig. 30). *M. chthonoplastes* was present in all samples, accounting for at least 17% of the total population. *M. punctata* constituted close to 5% of the total population. The species composition of the microbial mats on Fishermans Island is comparable to those found in the peritidal siliciclastic environments of Mellum Island, North Sea, where *M. chthonoplastes*, *O. limosa*, *M. punctata*, and *L. aestuarii* are the

dominant mat building cyanobacterial species (Gerdes and Klenke, 2003). Other studies show that these mat building speices are cosmopolitic, that is typical members of the microflora in temperate coastal habitats (Stal, 2000; Stolz, 2000; Noffke, 2003).

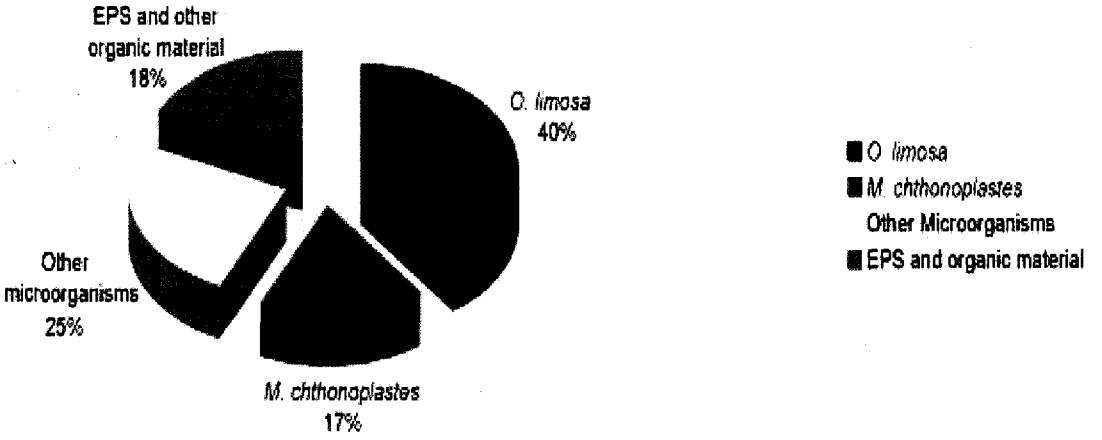

Fig. 30. Percent composition of a typical microbial mat from the tidal flats of Fishermans Island, Virginia using optical analyses. *O. limosa* is the most abundant component and makes up an average of about 40% of the total mat material. *M. chthonoplastes* makes up about 17% of the total. The coccoid species, *M. punctata*, makes up less than 5% of the total and is included with the category "other microorganisms". EPS and other organic material includes cyanobacterial sheaths and are substantial components of the microbial mats.

Pennate and centric diatoms were present in all samples, but only constituted about 5% of the total population. Seasonal changes in the species composition were not monitored. Other microorganisms including protists, bacteria, and fungi, collectively constituted almost 15% of the total population, but were not specifically identified, as this would require a special microbiological training. Extracellular polymeric substances (EPS) and other organic material such as occasional roots, plant debris, or fecal pellets made up about 18% of the microbial mat volume.

Under the microscope, examinations of thin sections from the Pongola Supergroup show dark laminae. Those laminae are composed of filamentous textures that are arranged into a carpet-like network that is comparable with modern microbial mat fabrics and the cyanobacterial filaments that constructed them. Similarly as observed in the relief cats from the modern microbial mat-overgrown sands, the orientation of the laminae in thin section is consistently parallel to the sedimentary surface (Fig. 31). Specific orientations and morphological characteristics will be discussed for each group of samples in the following section.

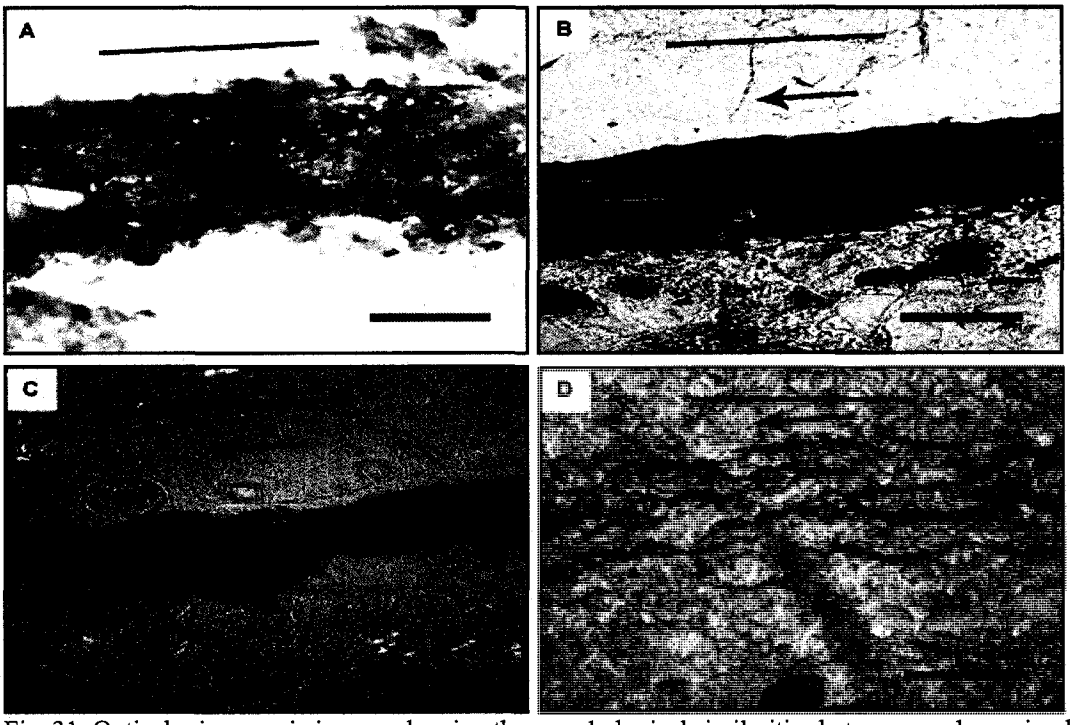

Fig. 31. Optical microscopic images showing the morphological similarities between modern microbial mat textures and ancient microtextures. (A) Photo of a modern microbial mat from Fishermans Island; cyanobacterial filaments form laminae parallel to the sediment surface among quartz sands, scale = 1 mm. (B) Photo of a thin section from the Ntombe Formation; microtextures and laminae parallel to the sediment surface, scale = 200 μm. (C) Photo of a thin section from the Brixton Formation (under reflected light); microtextures and laminae parallel to the sediment surface, scale = 300 μm. (D) Photo of a thin section from the Sinqueni Formation; microtextures separated by quartz grains with orientations about 5° from the horizontal, scale = 300 μm. Lines in each photo are parallel to the surface.

Ntombe Formation, Pongola Supergroup

In the thin sections from the Ntombe Formation, the microtextures collectively form laminae that are located only at the uppermost edge of the thin sections (Fig. 32). The uppermost edge of the thin section represents the surface of the MISS, and the laminae are therefore likely the remains of an ancient microbial mat.

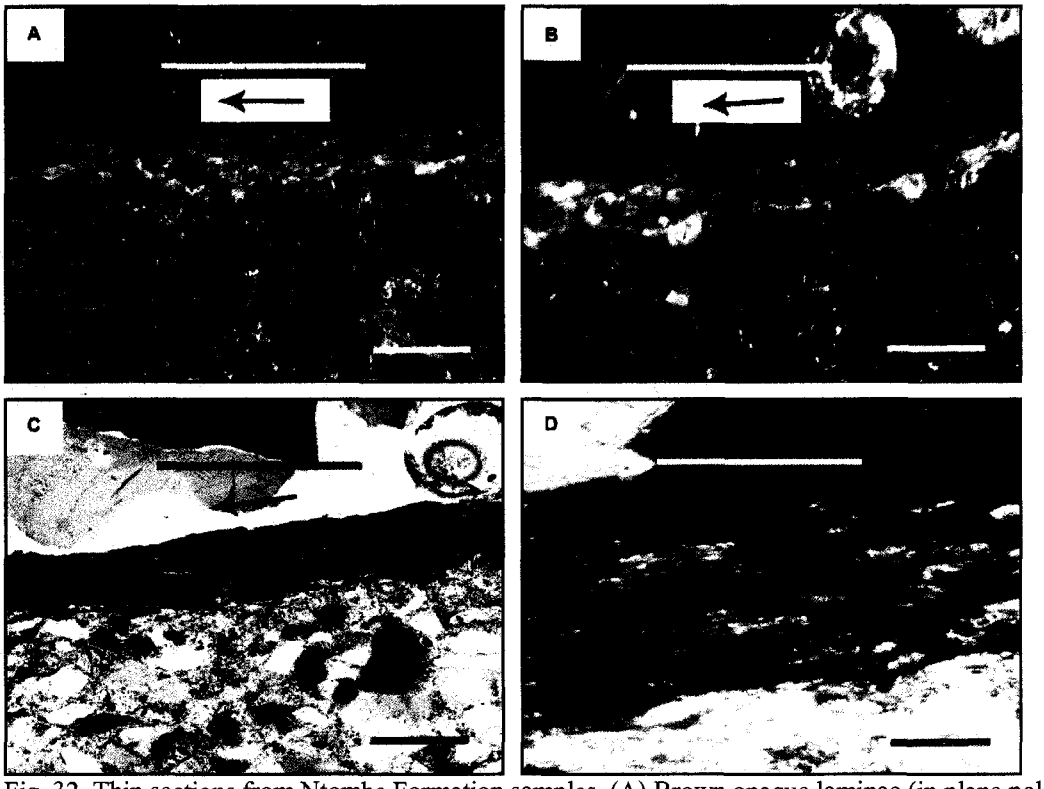

Fig. 32. Thin sections from Ntombe Formation samples. (A) Brown opaque laminae (in plane polarized light) located at the top of the thin section is an actual slice through the MISS. The arrow indicates overall orientation of laminae, which is parallel to the surface (line), 100x magnification, scale = 200μm. (B) Brown, opaque laminae (in plane polarized light) oriented about 10° from the surface, 100x magnification, scale = 200μm. (C) Brown, opaque laminae (under cross polars) is oriented about 20° from the surface, 100x magnification, scale = 200μm. (D) Close-up of laminae showing individual microtextures as indicated by arrows, 200x magnification, scale = 200μm.

In close-up, these laminae are rope-like in morphology and do not exhibit irregularities such as branching (Fig. 33). This is an important observation. Branching is usually

indicative of the migration of fluid through the rocks or from the dissolution of minerals as a result of pressure solution during deformation of the host rock (Davis and Reynolds, 1996). That means that such branching laminae would be of abiotic origin. In statistical analyses, the laminae in the MISS samples are along one line of reference and therefore not the result of hydrothermal or tectonic overprint.

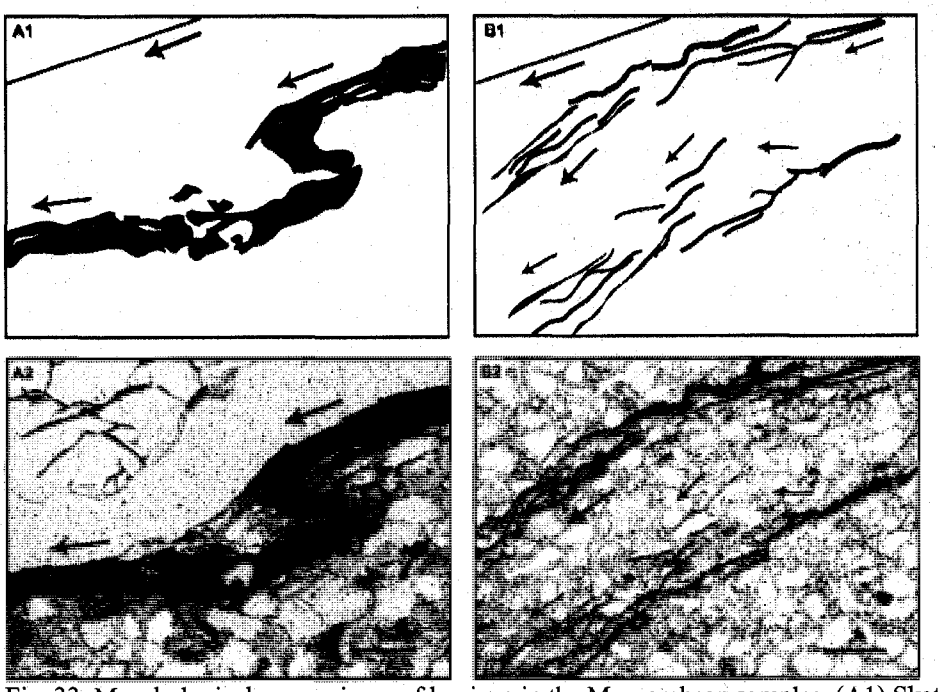

Fig. 33. Morphological comparisons of laminae in the Mesoarchean samples. (A1) Sketch and outlining the rope-like morphology of the laminae seen in the thin sections (A2) from the Ntombe Formation. The laminar structure is a thick, solid mass up to 200 μm thick, scale = 200 μm. (B1) Sketch outlining the branching morphology of the laminae seen in the thin sections (B2) from the Sinqueni Formation. The laminae are separated from each other and do not form a thick, solid mass, scale = 100 μm. The arrows indicate the overall direction of orientation. In the images from the Ntombe Formation, the laminae are close to parallel. In the images from the Sinqueni Formation, the laminae are branching with variable orientations relative to the horizontal surface.

The orientations of the laminae are between 0 – 20° from the horizontal surface (Fig. 32). The laminae are between 100μm and 200μm in thickness and are made up of brownish opaque minerals (Fig. 32). The filamentous textures that compose those laminae have

average widths between 10μm and 50μm (Fig. 32). The thicknesses of these microtextures are consistent with that of trichomes of modern cyanobacteria belonging to the group Oscillatoriales. The microtextures are all oriented parallel to subparallel to the surface (Fig. 32).

The results of petrographic analyses indicate the samples are composed of about 50.9% undulose quartz, 11.8% feldspars, 12.7% micas, 12.7% chert, and close to 10.4% heavy minerals (Fig. 28). This mineral composition is comparable to the composition of sand grains in modern microbial mats, of course with the exception of chert. The chert is a result of diagenetic processes representing perhaps fossil EPS, and is not component in modern samples.

Sinqueni Formation, Pongola Supergroup

The laminae in the Sinqueni thin sections are not concentrated close to the upper edge (the ancient sedimentary surface). (Fig. 34). Also, the laminae are not completely planar, but appear in a branching, zigzag pattern (Fig. 33). My initial interpretation is that these laminae are stylolitic, meaning that they derive from pressure solution of a perhaps organic rich clay-containing sand. However, I cannot rule out the biogenicity of the structures though their formation may have differed (see discussion below). The widths of the laminae in these samples average around 35μm in thickness. The spaces between

the laminae vary from 2μm to 100μm. These laminae are oriented between 0 – 45° from the horizontal surface.

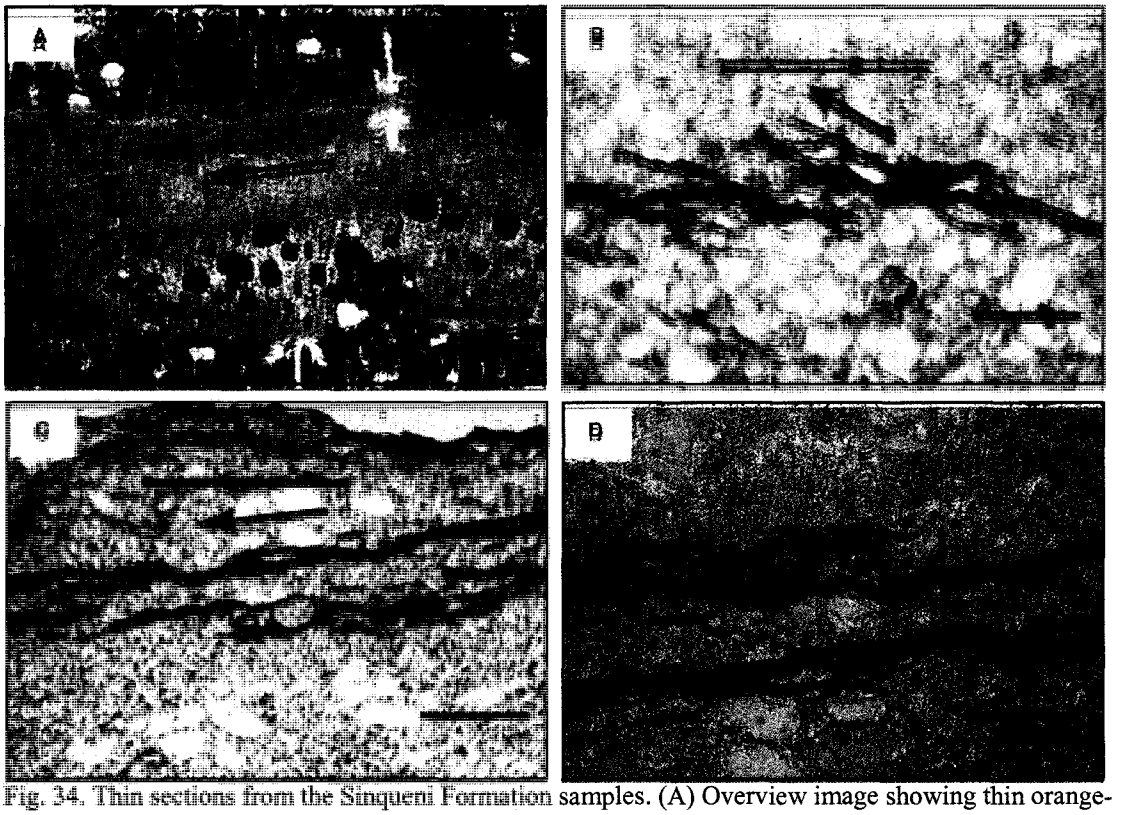

Fig. 34. Thin sections from the Sinqueni Formation samples. (A) Overview image showing thin orange-brown opaque laminae. Line is parallel to surface; arrow indicates the overall orientation of the laminae is close to parallel. The photo also shows the location of microprobe analysis (2 white arrows); 50x magnification, scale = 3 mm. (B) Brown, opaque, branching laminae (in plane polarized light), arrow indicates a deviation from the horizontal surface of close to 45° for the branches of laminae, scale = 200μm. (C) Brown, opaque laminae in 3 portions of the thin section with an average orientation of about 10° from the horizontal. Sample contains heavy minerals oriented parallel to the laminae, scale = 500μm. (D) Close-up of photo (C) showing heavy mineral in the laminae, scale = 250μm.

In contrast to the Ntombe samples, the laminae in the Sinqueni samples are located in a variety of regions in the thin sections rather than just at the uppermost edge. The uppermost laminae are part of the MISS preserved in the rocks. However, the laminae in the lower portions of the thin sections may be the remains of buried microbial mats. This is comparable to the microbial mat layers preserved in relief casts from Fishermans

Island (Fig. 24). The uppermost layer of the relief cast consists of the most recent microbial mat on the sediment surface, while the intrasedimentary layers consist of buried microbial mats. The spacings between the layers in the relief casts tend to increase with depth, though the thickness of the buried mat layers doesn't significantly change (Fig. 35). Although on a smaller scale, this is similar to what is seen in the Sinqueni samples with spacings between laminae of mostly uniform thickess.

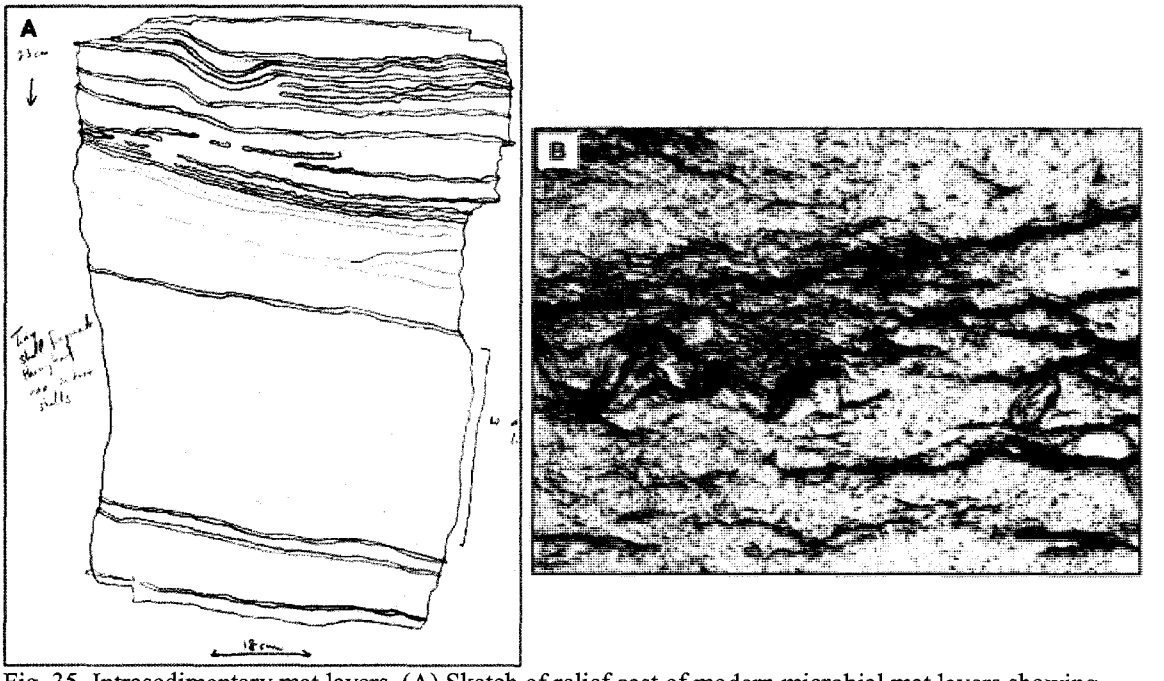

Fig. 35. Intrasedimentary mat layers. (A) Sketch of relief cast of modern microbial mat layers showing spacing between layers and slight deviation from the horizontal. (B) Optical microscopic image of similar mat-like textures from the Sinqueni Formation, scale = 200μm.

Within the laminae of the Sinqueni samples, the grain sizes ranged from around 75μ to 225μ, defining very fine to fine grained sands. Directly below the laminae, the grain sizes ranged from around 50μ to 200μ, indicating fine grained sands. Three mm below the

laminations, the grain sizes ranged between 400μ to 1mm, defining medium to coarse sands.

Since the laminae in the Sinqueni samples are not restricted to the surface, petrographic analyses were done in three portions of the thin section (Fig. 34). Monocrystalline undulose quartz made up almost 27%, feldspars made up over 10%, chert made up close to 13%, micas made up close to 10%, and heavy minerals made up almost 30% of the minerals within the laminae (Fig. 28). The clay/chlorite matrix made up close to 15%. The laminae are composed of brown and black opaque minerals. Directly beneath the laminae, the matrix made up about 38% of the counts, with monocrystalline undulose quartz comprising 14%, feldspars comprising 18%, micas comprising 7%, chert comprising 8%, and heavy minerals comprising 22% of the grains >50μ. The area 3mm below the laminae had the least amount of matrix, at just over 10%. Monocrystalline undulose quartz grains made up 51% of the grains in this portion of the thin section, followed by 14% chert, 13% feldspars, 6% micas, and 6% heavy minerals. The majority of these heavy minerals are adjacent to the layers of microtextures and are also oriented long-axis parallel to the microtextures. The main species include subangular rutile and abraded tourmaline.

The grains >50μ were fairly sorted and mostly subangular within the laminae, with the long axis of the grains mainly oriented parallel to the laminae. Directly below the laminae, the >50μ size fraction was fairly sorted, angular to subangular, with long axis orientations parallel to laminae. The sorting and angularity of the grains within and

directly below the laminae supports the idea of sand grains being entrained within an ancient mat fabric. In contrast, the portion 3mm below the laminae was poorly sorted, with angular to subrounded grains mainly oriented parallel to the laminae. These grains were not part of the original mat fabrics.

Brixton Formation, Witwatersrand Supergroup

The laminar textures in the Brixton samples are similar to those from the Ntombe Formation. The laminae are located only at the uppermost edge of the thin section where the MISS are preserved. These laminae are also rope-like in morphology and do not exhibit branching (Fig. 31). The laminae are between 100μm and 200μm in thickness and are made up of brownish opaque minerals. These laminae are oriented between 0-20° from the horizontal.

There is also some differentiation of individual filaments within the laminae with average filament thicknesses between 10μm and 50μm. One feature that is seen exclusively in the Brixton samples is the preservation of "segmented" filamentous textures within the laminae (Fig. 36). These "segments" are found in 25μm thick filaments and measure about 20μm in width, which is comparable to the segments in modern mat building cyanobacteria, *Beggiatoa sp.* and *M. chthonoplastes*. However, I am careful with my interpretation, because these segments also resemble the dissolution domain boundaries of pure synthetic goethite crystals (Cornell and Schwertmann, 1996).

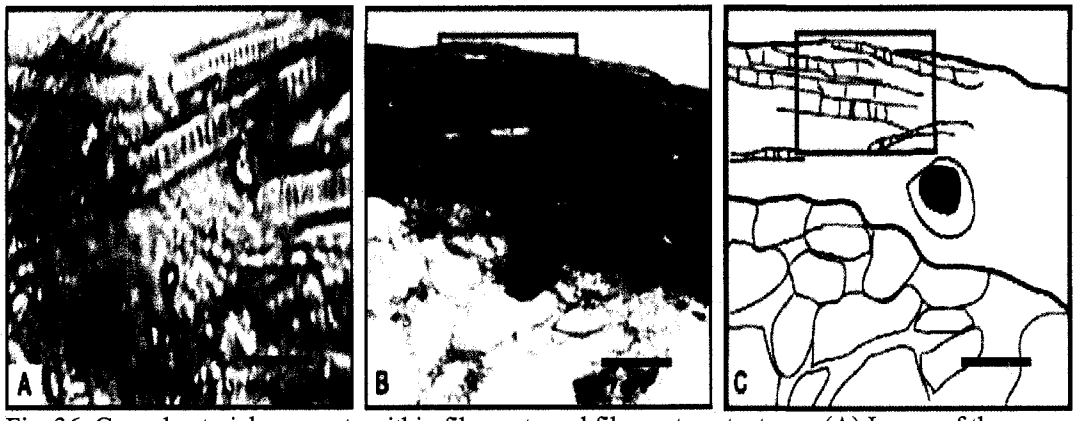

Fig. 36. Cyanobacterial segments within filaments and filamentous textures. (A) Image of the segmented trichomes of a modern cyanobacteria, *O. limosa*, scale = 120 μm. (B) Image of a thin section containing segmented filamentous textures (within the red box) from the Brixton Formation, scale = 100 μm. (C) Sketch outlining the segmented filamentous textures in the Brixton Formation thin section. The textures resemble the segmented trichomes of modern microbial mat building cyanobacteria.

The results of the petrographic analyses show that the samples from the Brixton Formation are composed of almost 60% undulose quartz, 8% feldspars, 4.2% micas, 7.1% chert, and 13.7% heavy minerals (Fig. 28).

Summary of Microscopy Results

The laminae, microtextures, and mineral grains in the Ntombe, Sinqueni, and Brixton Formation samples are likely the remains of mat fabrics and the entrained fine sands of ancient microbial mats. The laminae in the Mesoarchean samples are all predominantly oriented parallel to the rock surface; modern microbial mats are formed and buried on horizontal surfaces. The individual microtextures from the Mesoarchean samples have an average thickness that is comparable to the individual and bundled trichomes of modern mat building cyanobacteria. The mineral assemblages associated with the laminae and

microtextures in the Mesoarchean samples are analogous to the siliciclastic sands that are associated with the modern microbial mats on Fishermans Island.

Stratigraphic studies of the Pongola and Witwatersrand Supergroups show that the Ntombe, Brixton, and Sinqueni Formations were each deposited in shallow marine environments (Beukes and Cairncross, 1991; Nhleko, 2004). The Ntombe and Brixton Formations were deposited specifically in storm dominated shelf environments and the Sinqueni Formation was deposited in a tidal flat environment (Beukes and Cairncross, 1991). This is reflected in the types of structures preserved in each formation. The samples from the Ntombe and Brixton Formations have thick, rope-like laminae with individual microtextures within the laminae. (Beukes and Cairncross, 1991). These were formed in an environment similar to the storm-influenced shelf successions of the Neoproterozoic Nudaus Formation, Nama Group, Namibia, where the same rope-like textures and mineral assemblages occur (Noffke et al., 2002).

In contrast, the samples from the Sinqueni Formation do not have thick rope-like laminae, but instead have individualized layers of laminae separated by spaces. While these laminae resemble abiogenic stylolites, there are some biogenic explanations. As discussed above, these separated layers are reminiscent of the intrasedimentary mat layers preserved in relief casts from the tidal flats of Fishermans Island. Also, similar textures have been interpreted to be preserved mat layers in the Paleozoic sandstones of the Montagne Noire, France and the 3.2 Ga Moodies Group, South Africa (Noffke, 2000; Noffke et al., 2006b). For example, in the sandstones of the Montagne Noire recording an

intertidal facies zone, there are stacked laminae in layers up to 3 cm thick (Noffke, 2000). This is much like the layers of individual laminae in the Sinqueni samples.

4. Textures of Microbial Mats (Modern and Ancient) in CSLM

In samples from modern microbial mats, CSLM reveals filaments and mat fabrics in three dimensions and distinguishes textures related to extracellular polymeric substances (EPS). Whereas the optical analyses with the light microscope gave the impression of a predominance of *O. limosa* over all other components that form the mat fabrics, the much more detailed view using CSLM shows that it is the EPS taking up the most space of at least ¾ of the total microbial mat volume (Fig. 37). The tubular filaments of O. limosa are between 12 and 30μm in diameter and make up about 1/8 of the total volume (Fig. 37). The void spaces also make up about 1/8 of the total microbial mat volume (Fig. 37). The amount of EPS in a microbial mat can be regulated by many external parameters, and is not merely result of the species composition of a microbial mat (which, of course, has some influence). The EPS increases in many microbial mats with an increase in salinity, or – for tidal flat ecosystems – with the duration of subaerial exposure of the organic layers. Other studies using CSLM to investigate the microstructure of microbial mats have also proved that EPS can make up to 87% of the total biomass (Lawrence et al., 1998, 2003; De Los Rios et al., 2004). Void spaces are an interesting phenomenon visible

in modern mat fabrics. These voids are often filled with water, but also can in fact contain highly complicated biomolecules of polysaccharine bridged by a great variety of ions (Decho, 2000b).

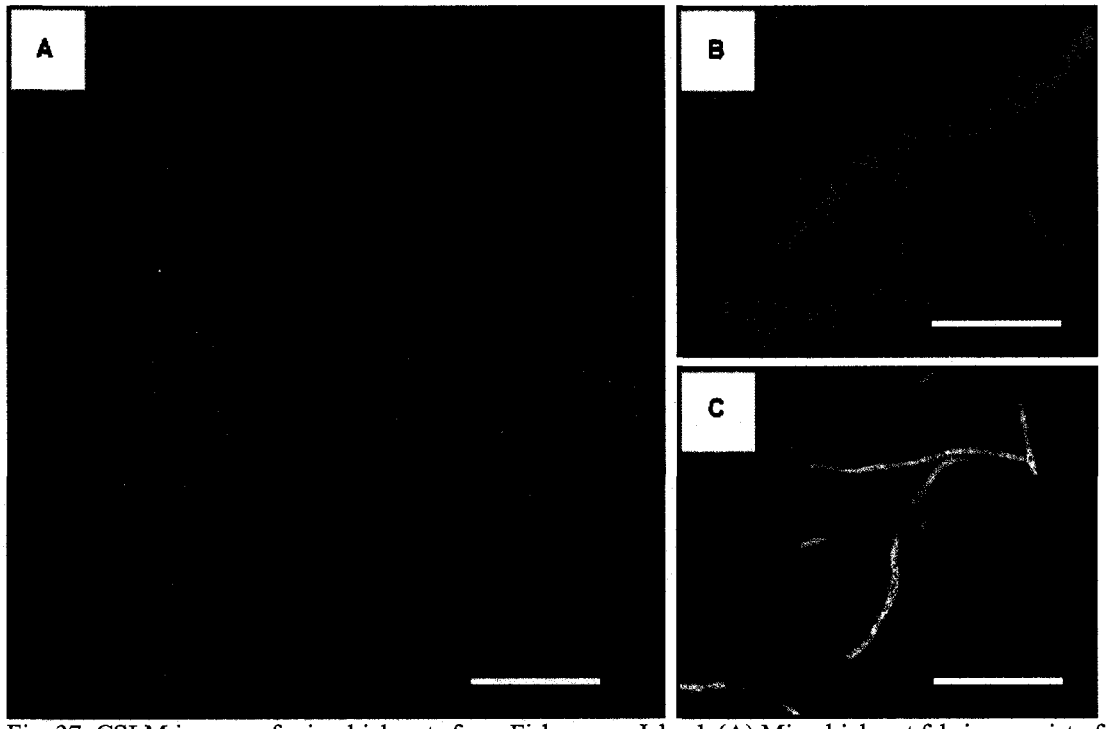

Fig. 37. CSLM images of microbial mats from Fishermans Island. (A) Microbial mat fabrics consist of cyanobacterial filaments (C), extracellular polymeric substances (EPS), and void spaces (V). This image was taken using a FITC filter at 200x magnification, scale = 500 μm. (B) Image of microbial mat fabrics taken using a TRITC filter at 600x magnification in which there are quartz grains (Q) and cyanobacterial filaments (C), scale = 100 μm. (C) Composite image taken at 400x magnification without a filter in which cyanobacterial filaments (C) are seen, scale = 350 μm.

Similar fabrics were observed in the Mesoarchean microbial mats (Figs. 38, 39). However, the outlines of the textures are more diffuse than those seen in the modern samples. This is not a surprise, because post-mortem decay of organic matter includes the diffusion of chemical compounds away from their original site, as well as the ionic

exchange between dead organic matrix and sea water solutes. Also the diagenetic recrystallization that forms sand into sandstones, dehydration, as well as hydrothermal overprint all add to the dissolution of former discrete material.

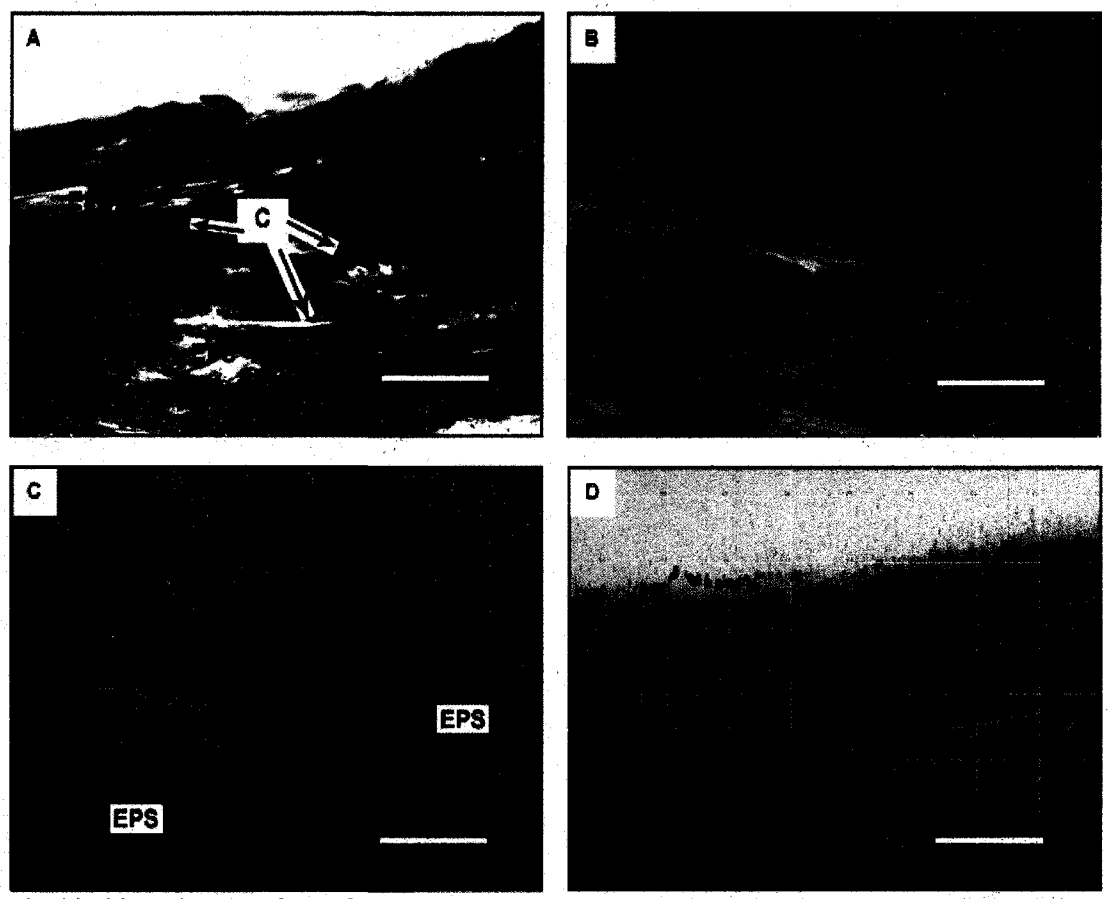

Fig. 38. CSLM images of samples from the Ntombe Formation. (A) Image taken without using a filter at 200x shows opaque filamentous textures (C) surrounded by transparent material (EPS), scale = 75 μm. (B) Image taken without using a filter and 600x magnification shows opaque filamentous textures (C) and transparent surrounding material (EPS), scale = 20 μm. (C) Image taken using TRITC filter at 1000x magnification shows filamentous textures (C) surrounded by darker, denser material (EPS), scale = 5 μm. (D) Image taken using TRITC filter at 200x magnification shows filamentous textures (C) with shadowy outlines surrounded by diffuse material (EPS), scale = 45μm. Image was saved with a grid to quantify the microtextures.

The microtextures in the Mesoarchean samples are seen as filamentous channels within the laminae (Fig. 39). These microtextures are about 15μm in diameter and are opaque. The minerals surrounding the microtextures are cloudy and transparent (Figs. 38,39).

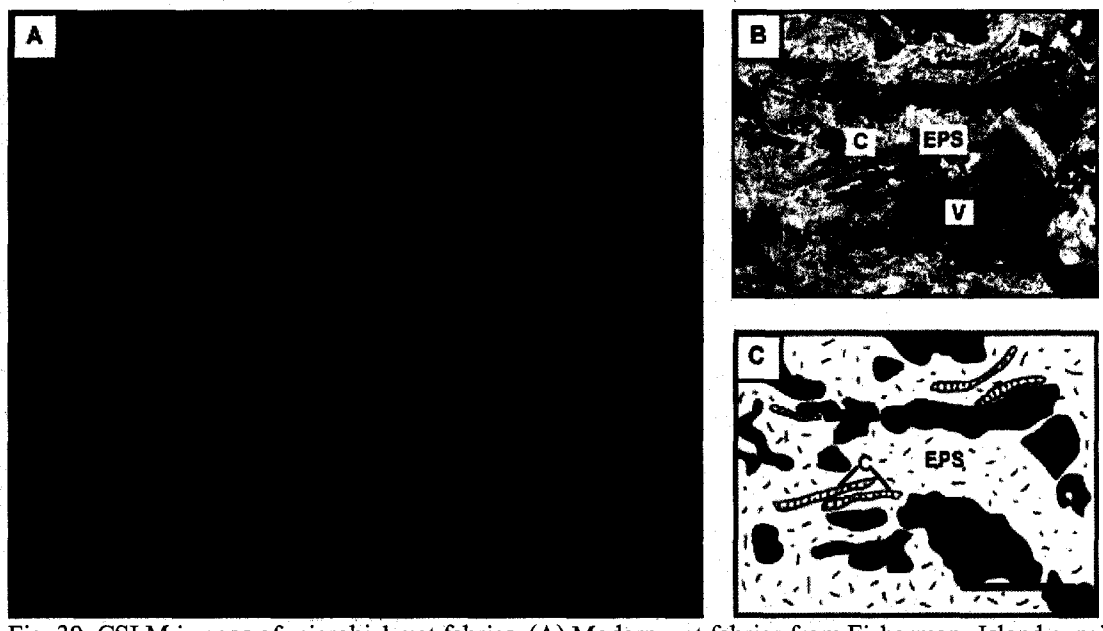

Fig. 39. CSLM images of microbial mat fabrics. (A) Modern mat fabrics from Fishermans Island consist of cyanobacterial filaments (C), extracellular polymeric substances (EPS), and void spaces (V). This image taken using a FITC filter at 200x magnification, scale = 400 μm. (B) In comparison, there are similar features from the Mesoarchean Ntombe Formation, with filamentous textures (C), denser areas (EPS), and void spaces (V). 3-dimensional composite image taken without filters at 400x magnification, scale = 150 μm. (C) Sketch of thin section B outlines the features of the microfabrics.

I consider the opaque microtextures to be the remains of microbial filaments and the surrounding transparent material to be mineralized EPS (Fig. 39). The matrix-like structure of EPS creates a large surface area where chemical reactions take place. EPS can be negatively charged, so it incorporates positively charged ions, such as Ca^{+2} or Mg^{+2} and metals, such as Fe^{+2} or Ti^{+2} into its structure, resulting in the precipitation of clays or poorly ordered iron-rich minerals (Cornell and Schwertmann, 1996; Fortin et al, 1997; Konhauser, 1998). In this case of the fossil microbial mats, the possible "filaments" make up about 1/5 of the total volume. The possible "void spaces" make up about ¼ of the total volume. The possible "EPS" makes up almost ½ of the total volume. As shown above, this is similar to the modern examples where EPS is the most dominant constituent of a microbial mat.

5. Carbon Isotopes of Fossil Filament-like Textures

Any study on ancient fossils, especially of microscopic scale, must include geochemical investigations as well. Most important are isotopes that strongly support that possibly preserved carbon could be indeed remains of the original organic matter, and not products of abiotic graphite formation – a common process especially in Archean sediments. My carbon isotope analyses on fossil microbial mat layers separated from the host rock by careful cutting show $\delta^{13}C$ values around -24.2 +/- 0.5 ‰ (Ntombe Formation), and around -22.8 +/- 0.1‰ (Sinqueni Formation). Previous analyses on samples from the Brixton Formation are consistent to my values, and showed $\delta^{13}C$ of around -22 +/-0.1 ‰. The isotopic values in all three sets of samples indicate a possible biogenic source which could have been from ancient cyanobacteria. The known $\delta^{13}C$ values for modern cyanobacteria are between -31‰ and -3.0 ‰ (Schidlowski, 1988). The carbon enriched in modern abiogenic marine carbonates has an isotopic composition between -4.0 ‰ and +2.0 ‰ – clearly different from my values derived from the fossil material (Schidlowski, 1988; Ueno et al., 2002).

As mentioned above, more recent studies of microfossils in Archean rocks have shown that $\delta^{13}C$ values close to -28‰ could be the result of the abiogenic production of graphite as well, for example as result of metamorphosis from ferrous carbonates under high temperatures and pressures (Van Zuilen et al., 2002). However, the abiogenic production of carbon isotopic signatures in the microtextures from the Ntombe, Sinqueni,

and Brixton Formations is not likely, because these rocks are sandstones,and in addition, have only experienced low grade metamorphosis of lower greenschist facies.

6. Micro Raman Spectroscopy of Fossil Filament-like Textures

In order of predominance, the microtextures in the microbial mats from the Ntombe Formation are mainly composed of iron hydroxides (goethite), titanium oxides (rutile and anatase), mica (muscovite), and iron oxides (hematite) (Table 2) (Figs 40-42). In the samples from the Sinqueni Formation, the microtextures are also mainly composed of iron hydroxides, titanium oxides, muscovite, and graphitic carbon (Figs 4-10). The grains directly associated with (and also within) the microtextures in samples from both rock successions are composed of quartz, potassic feldspars, and muscovite. Close examination of the filamentous textures in some of the samples reveal banding of either graphitic carbon (1355 and 1593cm^{-1}), rutile (445 and 615 cm^{-1}), anatase (145, 397, 514, and 643^{-1}) or goethite (245, 300, 479, 682 cm^{-1}). This suggests that the mineral nucleation was controlled by a preexisting structure identical to cyanobacterial filaments. I conclude therefore that the minerals formed along the filamentous cell walls of ancient microbial mat building cyanobacteria, and will discuss this issue in detail below. (Figs 2, 5,6).

Sample	Type of Scan	Location of Laminae	Minerals/Elements Present
Modern Mat	Spot Scans	Throughout sample	Quartz, sulfides, carbon
P2	Spot Scans	Upper,outer edge of thin section/parallel to surface	Rutile, Feldspar, Mica, Graphite
P4	4hr 35min 60x30μm 6sec dwell time	Upper,outer edge of thin section/parallel to surface	Goethite, Rutile, Anatase, clays, graphitic carbon
P5	3hr 3min 60x30μm 4sec dwell time	Upper,outer edge of thin section/parallel to surface	Goethite, Rutile, Anatase
RCH2	80 x 20μm 9h10m 4s dwell time	upper portion of thin section/within matrix	Goethite, rutile, muscovite
RCH2	40x20μm 4s dwell time 1hr 24min	Heavy mineral in laminae	Tourmaline w/Graphitic carbon band
RCH11	1 hr 43 min 40x20μm 5sec dwell time	Upper portion of thin section,within matrix/parallel to surface	Muscovite, Quartz, graphite, rutile
RCH12 -1	60x60μm 6s int time 9hr 10min	lower portion of thin section/within matrix	Quartz, anatase, muscovite,graphite
RCH13 -1	20x20μm 6s int time 1hr 3min	lower/outer edge of thin section	Carbon from polymer
RCH18	40x20μm 5s int time 1hr 45min	Upper portion of thin section;marked by arrows	Muscovite,rutile, feldspar
RCH21	12hr 15 min 60x80μm 6sec dwell time	Lower portion of thin section,within matrix/parallel to surface	Rutile, Quartz, Muscovite, Feldspar

Table 2. Thin sections used for micro Raman analyses. P = Ntombe Formation, RCH = Sinqueni Formation Column 2: scan areas, scan lengths. Column 3: area of thin section analyzed. Column 4: Dominant mineral components.

Formation of Mineral Phases Within Microtextures
Case 1: Goethite (α-FeO(OH))

The majority of the microtextures from the samples from the Ntombe Formation are composed of goethite. Goethite is typically a weathering product of biotite, amphibole, pyroxene, magnetite, hematite, or other iron-bearing minerals (Nesse, 2000). In natural abiotic systems, goethite can also form as an initial hydrated iron precipitate (Cornell and Schwertmann, 1996).

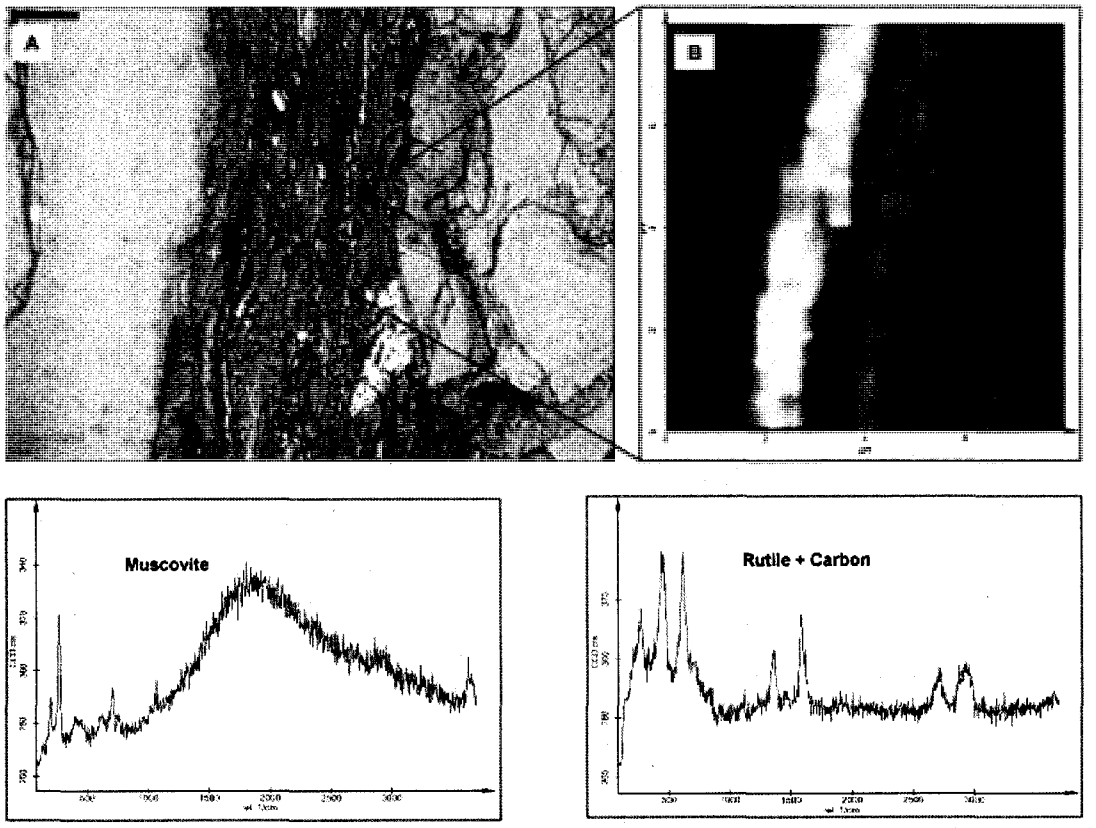

Fig. 40. Raman analysis of laminae, Ntombe Formation (P2). (A) Photo through confocal microscope using reflected light of scan area, scale = 10μm. Scan area was 30μm x 30μm. (B) Red reflectivity composite map of the scan area showing muscovite (yellow), rutile and carbon (black), and mixtures of mica, feldspars, and goethite (red). Individual spectra for muscovite, and rutile with carbon are also shown.

In laboratory controlled biomineralization studies, microbial biofilms and EPS provided substrates for the precipitation of iron oxides such as hematite and magnetite, whereas iron hydroxides only precipitated in the absence of organic material (Brown et al., 1998). The Raman measurements showed trace amounts of hematite still preserved within the microtextures of the Ntombe and Sinqueni samples. I conclude that this hematite could have been the first mineral to precipitate on the original organix matrix of a decaying microbial mat. Much later, this hematite was transformed into goethite in the course of weathering.

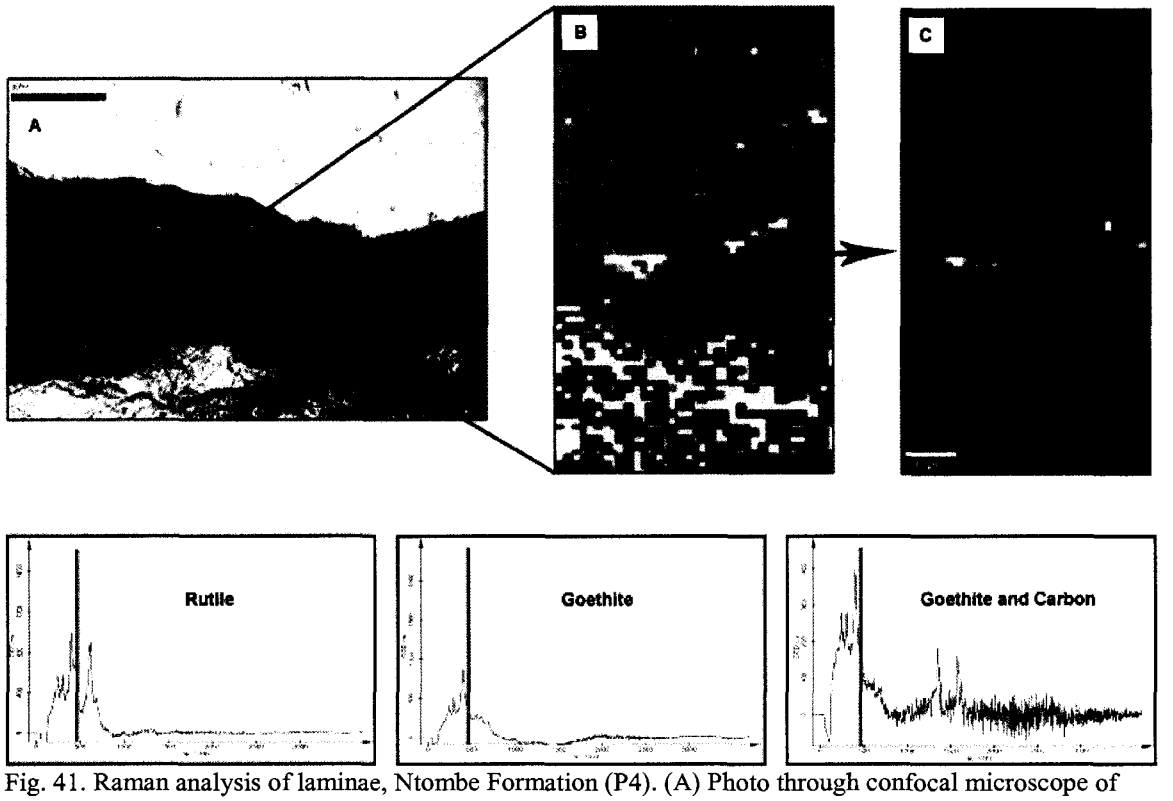

Fig. 41. Raman analysis of laminae, Ntombe Formation (P4). (A) Photo through confocal microscope of scan area, scale = 80μm. Scan area was 60μm x 30μm. (B) Color composite map of the scan area showing rutile (gray), goethite (blue), and carbon (red). (C) Red sum color map highlighting carbon band (red). Individual spectra for rutile, goethite, and goethite with carbon are also shown.

Case 2: Rutile and Anatase (TiO_2)

Rutile (titanium oxide) and anatase (titanium oxide) are also major components of the microtextures in the Ntombe and Sinqueni samples. Rutile is a common accessory mineral in igneous and metamorphic rocks, and – after weathering of those rocks, and transport - is found as allochthonous components in clastic sediments (Nesse, 2000). Anatase tends to form in low-temperature hydrothermal settings, and is a common mineral that replaces feldspars in late diagenesis of sandstones (Lindsley, 1991; Milliken, 2005). Under the petrographic microscope, rutile grains outside of the microtextures appear to be unaltered and have distinct grain boundaries and crystal habits. It is noteworthy that the rutile component within the microtextures is not visible with a petrographic light microscope. Therefore it is an important step to take a second look at samples with another technique, and indeed the Raman analyses do reveal the presence of rutile within the microtextures. This suggests the rutile within the microtextures was originally part of the heavy mineral fraction of sand grains entrained within the ancient microbial mat fabrics. As a result, this rutile (and anatase) has been affected by diagenesis along with the original organic material. The unaltered rutile grains outside of the microtextures are detrital minerals that are typical of sandstones.

There is a distinctive layering of alternating iron hydroxides and titanium oxides within the fossil textures that can be seen in the spectral maps (Fig 9). The spectra in the layers typically consist of bands around 245, 300, 479, 682 cm^{-1} for goethite, and bands around 445 and 615 cm^{-1} for rutile.

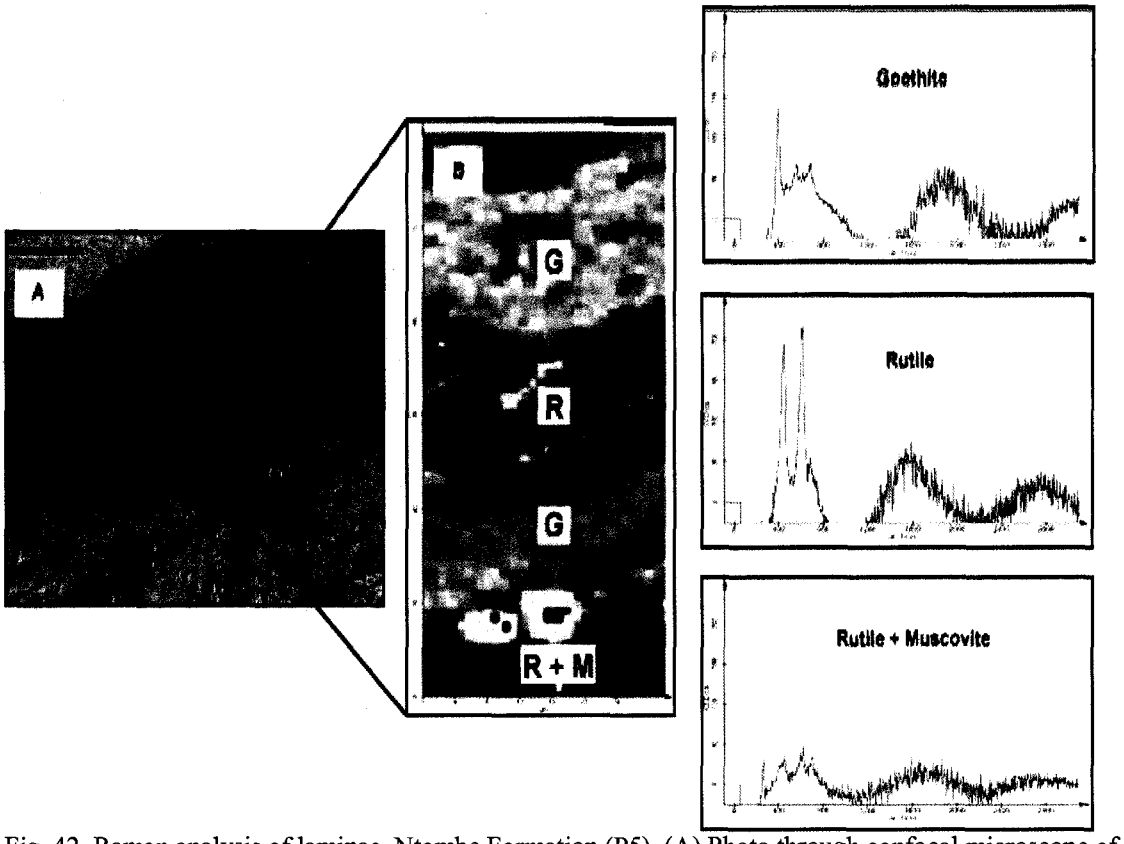

Fig. 42. Raman analysis of laminae, Ntombe Formation (P5). (A) Photo through confocal microscope of scan area, scale = 80μm. Scan area was 60μm x 30μm. (B) Color composite image of scan area in central portion of thin section. Composite image maps show changes in mineral composition and correlate with corresponding spectra; the lighter bands correspond with goethite, middle dark with rutile, and bottom dark with rutile mixed with muscovite. The spectra for each section is also shown.

The alternating compositions in the laminae could indicate differences between the chemical composition of the original cyanobacterial filaments and the EPS. The original cyanobacterial filaments and EPS could have formed alternating layers of organic material as they were buried together. Indeed, thin-sections through modern, now buried microbial mat layers show a similar banded pattern.

As discussed in the introduction chapter, the chemical composition of the filaments would have been different from the composition of the EPS, so it is not surprising these chemically different layers could have served as templates for the nucleation of different types of minerals. An alternative explanation is that the textures in the Ntombe Formation represent compacted microbial mats. These mats originally had sand grains between the layers. The compaction of the two layers together could have resulted in the banding seen in the samples now. However, it is very unlikely that the sand grains would have recrystallized under those low metamorphic grades recorded in the Ntombe Formation.

Case 3: Muscovite ($KAl_2(AlSi_3O_{10})(OH)_2$

The muscovite forming a common constituent of the Mesoarchean rocks is a mineral that is commonly found in sandstones and quartzites (Nesse, 2000). It can be detrital or can occur as the result of clay mineral reactions during diagenesis (Pettjohn et al., 1987). Studies it have also shown that clay minerals precipitate on microbial cell walls and EPS (Ransom et al., 1999; Konhauser, 1998). Many of the filamentous textures in the Mesoarchean samples are composed of muscovite lathes with anatase, rutile, and carbon in the striae (Figs 43, 44, 47). In other cases, the muscovite in the Ntombe and Sinqueni samples is aligned with the microtextures and laminae.

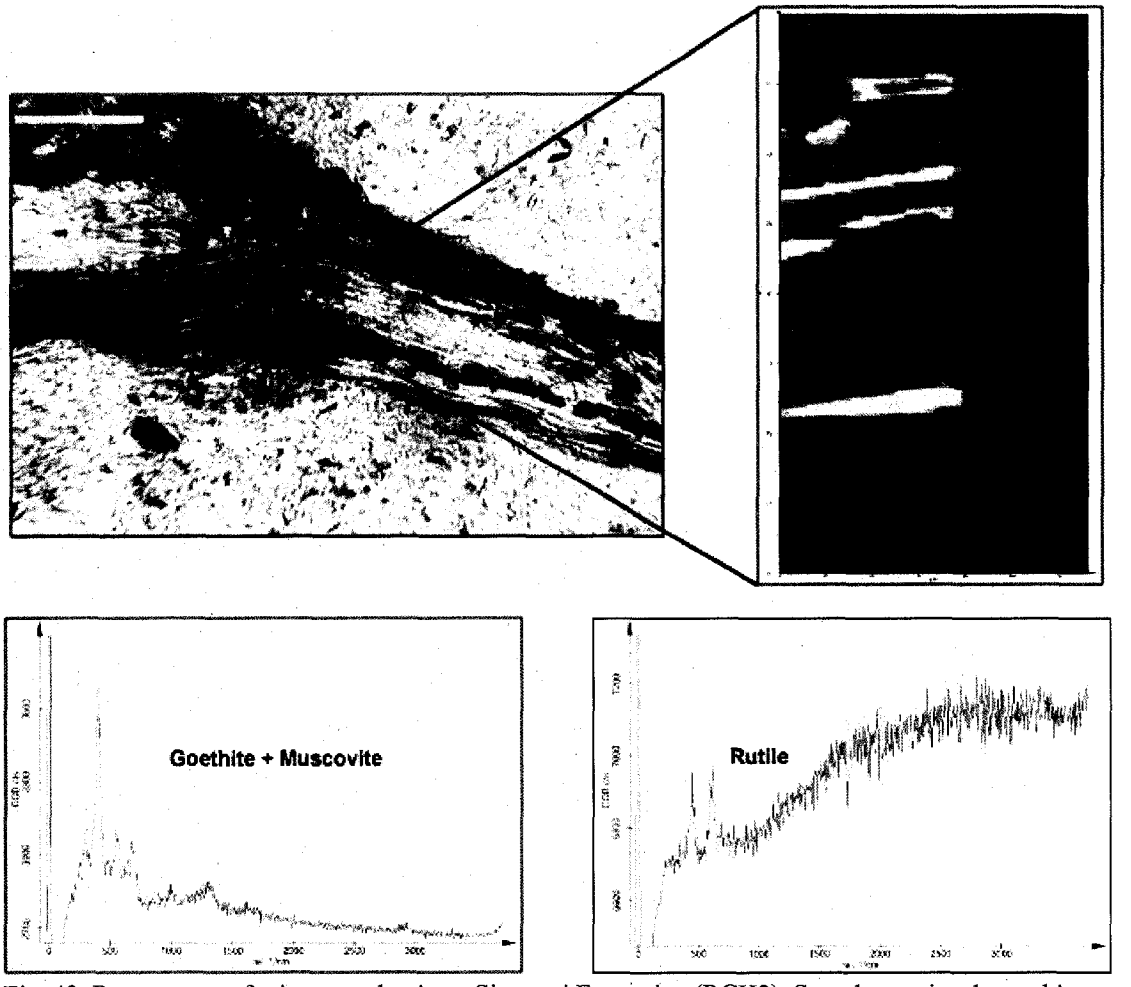

Fig. 43. Raman scan of micaceous laminae, Sinqueni Formation (RCH2). Sample previously used in microprobe analysis (A) Photo through confocal microscope of scan area showing darkened microprobe scan area and untouched portion, scale = 80μm. Scan area was 40μm x 20μm. (B) Color composite map of the scan area showing rutile (gray), goethite (green), muscovite (black), fluorescence from Al coating (yellow).

The orientation and association with the laminae and microtextures suggests i) that the muscovite grains were entrained within the mat fabrics and buried along with the microbial mat, or ii) clay minerals precipitated preferentially along the filamentous textures. Again, the incorporation of muscovite grains was commonly observed in modern microbial mats. Also, other studies regarding clay mineral –microbe interaction

showed a preferred orientation of the clays along the cellular components (Ransom et al., 1999).

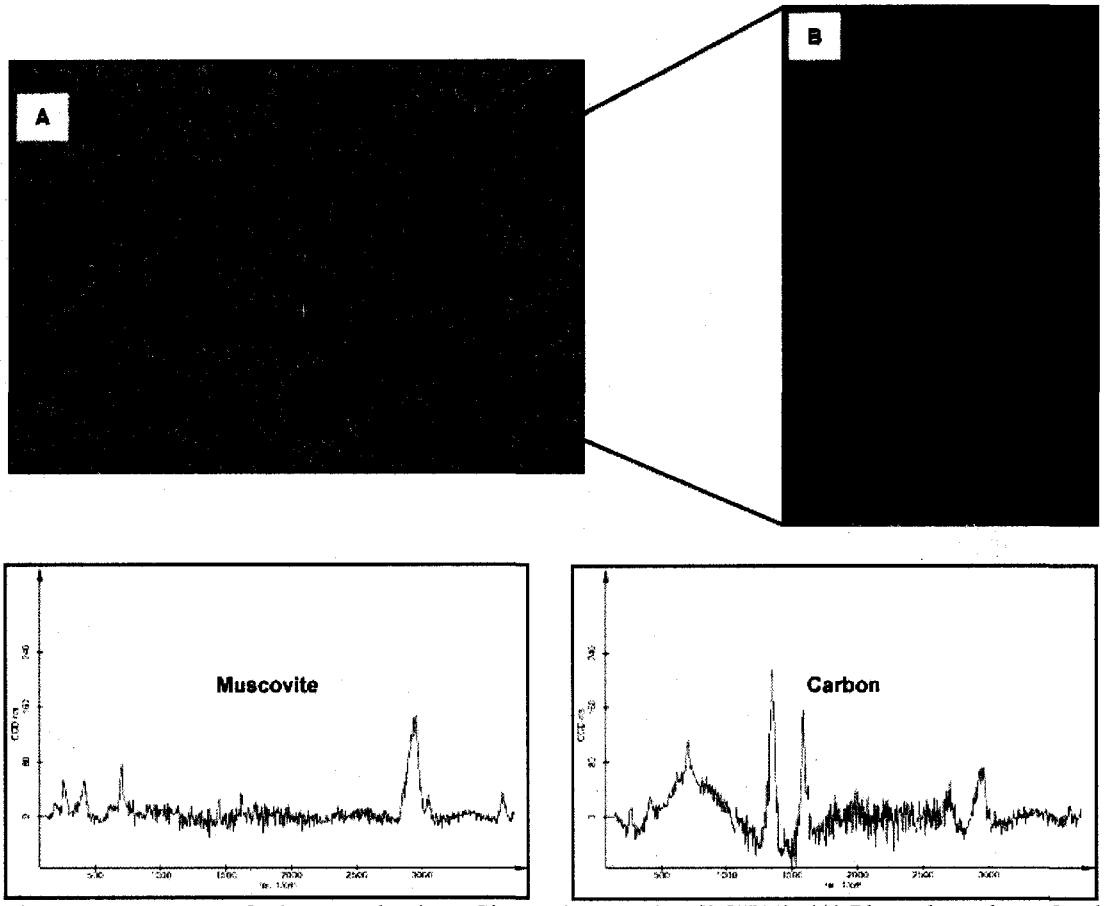

Fig. 44. Raman scan of micaceous laminae, Sinqueni Formation (RCH11). (A) Photo through confocal microscope of scan area, scale = 80μm. Scan area was 40μm x 20μm. (B) Color composite map of the scan area showing muscovite (red) with quartz (blue) and carbon (black) interlayers.

Case 4: Carbon (C)

Spectral signatures for graphitic carbon also occur within the microtextures of the Ntombe and Sinqueni samples, with typical graphitic bands for less crystalline, disordered carbon around 1350 cm^{-1} and well-crystallized, ordered graphite around 1581

cm^{-1}. The carbon occurs as a thin layer within and parallel to the microtextures (Figs 40,41, 44, 45). This suggests an original layer of organic material that was most likely part of the cell wall of an ancient filamentous cyanobacterial type of microorganism (Marshall et al., 2005). No carbon was detected outside of the laminae or microtextures in the Ntombe and Sinqueni samples. Clearly, this exclusive distribution supports that the carbon is biogenic.

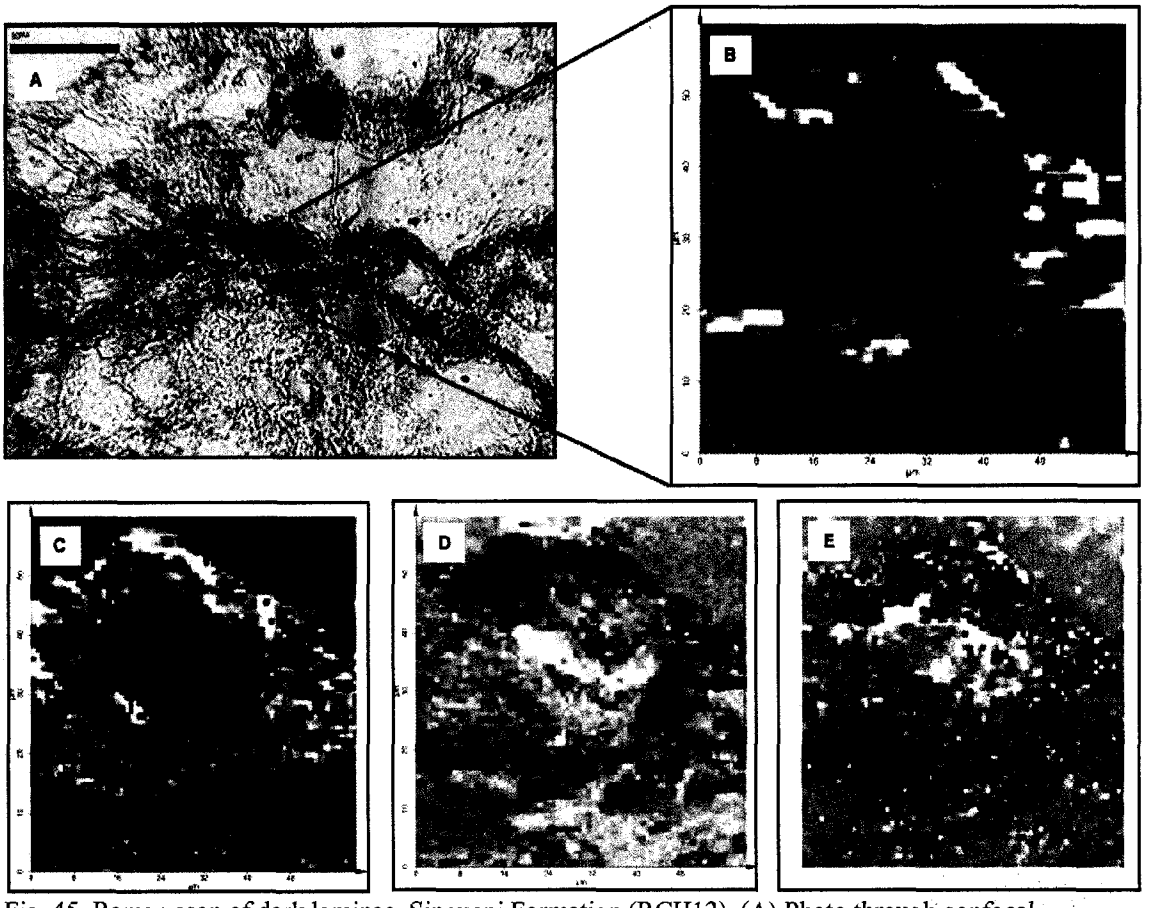

Fig. 45. Raman scan of dark laminae, Sinqueni Formation (RCH12). (A) Photo through confocal microscope of scan area, scale = 80μm. Scan area was 60μm x 60μm. (B) Color composite map of the scan area showing quartz (black), anatase (green), muscovite (light blue-gray), and graphitic carbon (dark blue). (C) Red sum color map highlighting muscovite (black). (D) Red sum color map highlighting anatase (black). Red sum color map highlighting graphitic carbon (black).

Also in support of a biogenic origin: A dravite grain located within the spacing between mat laminae in a sample from the Sinqueni Formation contains carbon too (Fig. 46). In this case, the carbon appears to be along an edge of the inner detrital core of the zoned dravite grain. This suggests that the carbon is syngenetic and was in place at the time the original mineral grain was deposited (Pettjohn et al., 1987). In this case, the mineral grain was deposited and entrained within the fabrics of the microbial mat during its growth on the former tidal flat.

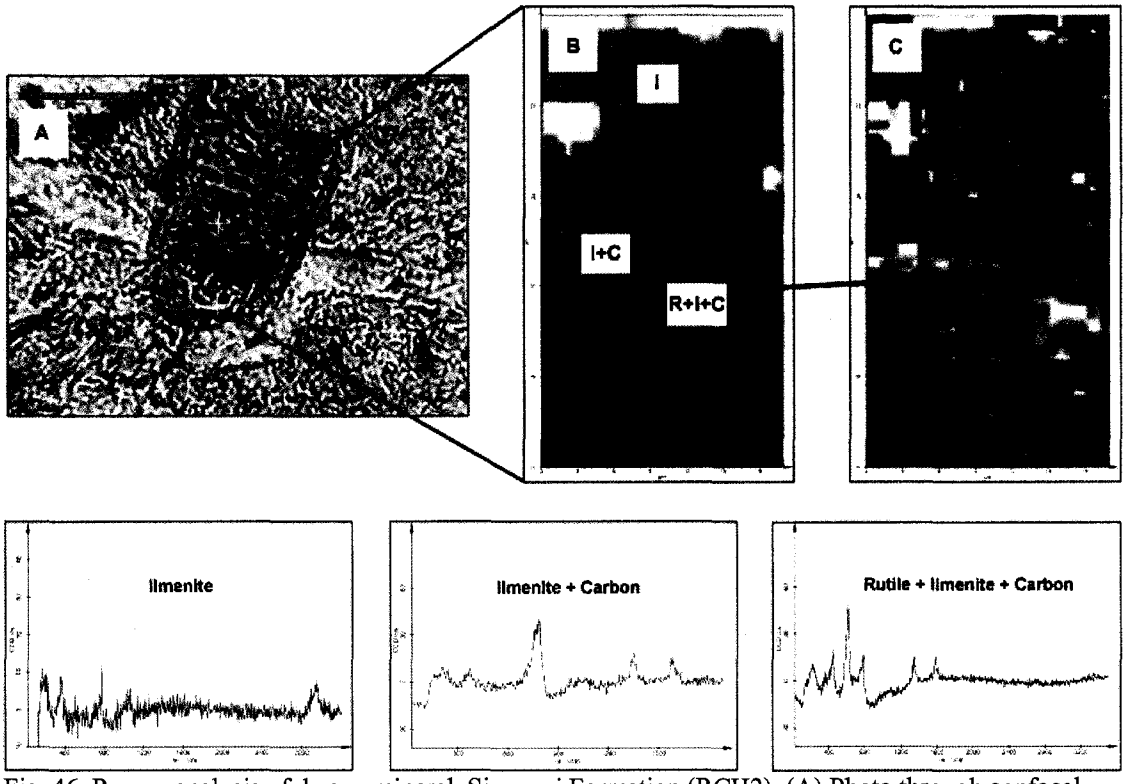

Fig. 46. Raman analysis of heavy mineral, Sinqueni Formation (RCH2). (A) Photo through confocal microscope of scan area, scale = 40μm. Scan area was 40μm x 20μm. (B) Color composite map of the scan area showing ilmenite (I) , ilmenite + carbon (I+C), and rutile + ilmenite + carbon (R+I+C). Bottom panels show the spectra for each area. (C) Sum color map with a carbon filter, arrow points to the location of carbon as highlighted by the red and orange colors.

It is important to consider that this described co-occurrence of titanium oxides and carbon can be indicative of a process called oxyexsolution, a purely abiotic process, where CO_2 introduced through hydrothermal fluids (Satish-Kumar, 2005). The CO_2 is reduced by the crystallization of Fe^{+3} bearing oxides during cooling, which results in the precipitation of graphite. However, on the other hand it is important to notice that the rocks in the Sinqueni and Ntombe Formations experienced only greenschist facies metamorphism. Because oxyexsolution typically occurs at temperatures and pressures higher than those associated with greenschist facies metamorphism, this abiotic mechanism of carbon derivation may well be excluded (Satish-Kumar, 2005).

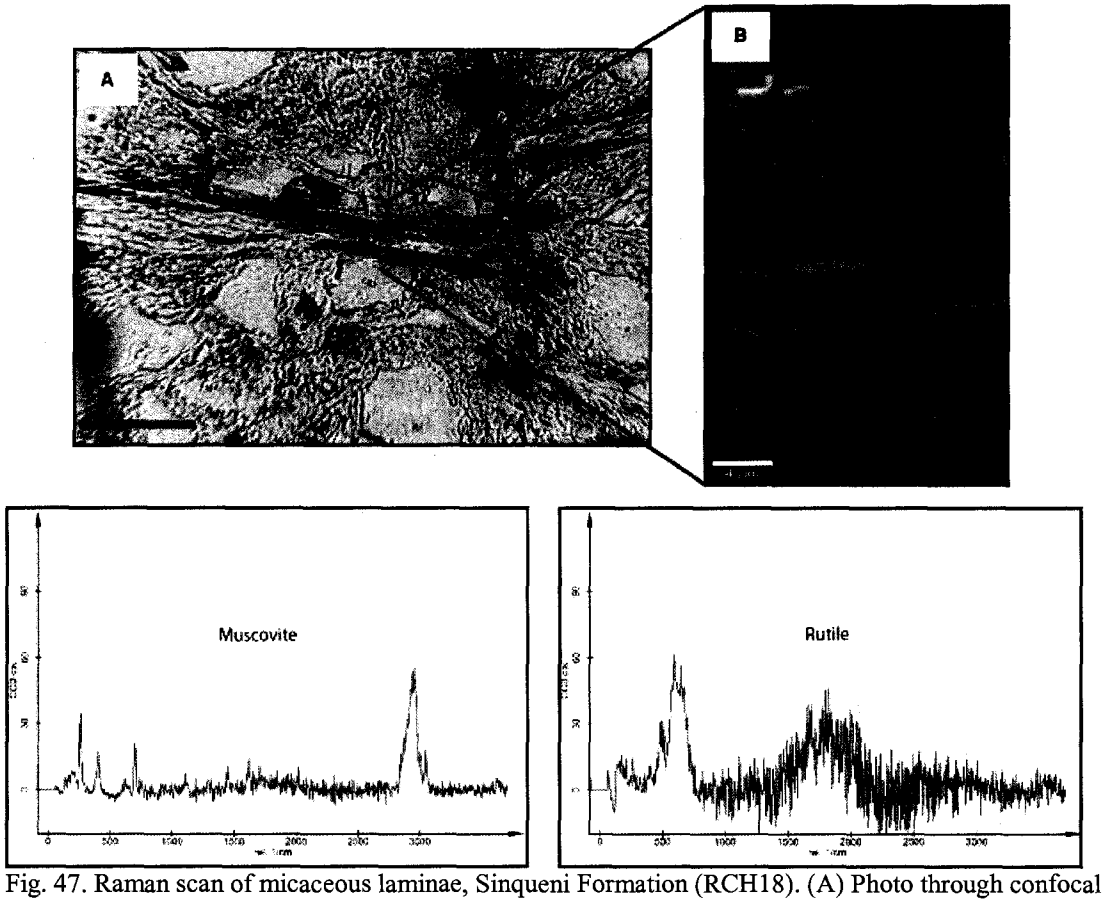

Fig. 47. Raman scan of micaceous laminae, Sinqueni Formation (RCH18). (A) Photo through confocal microscope of scan area, scale = 80μm. Scan area was 40μm x 20μm. (B) Color composite map of the scan area showing mica (green) with rutile (red) interlayers.

The graphitic carbon spectra in the microtextures of my rocks do correlate with the metamorphic grade of the rocks. It has been shown that consistently well-developed disordered and ordered carbon peaks is indicative of carbon that has already been in place at the time of metamorphism (Tice et al., 2004). Therefore, it is not likely that the carbon in the samples from the Ntombe and Sinqueni Formations is from contamination.

Modern Samples

For the modern microbial mats from Fishermans Island, the spot scans with the micro Raman instrumentation showed that the mat fabrics contained silica, sulfides, and disordered carbon grains. However, the high amount of organic material caused too much fluorescence to allow any reliable measurement, and just a few spot scans of the samples were possible. This problem can be alleviated with the use of a longer wavelength laser that is better suited for organic compounds (Wynn-Williams et al., 2002).

The Problem of Biogenicity – Another Issue to Consider with Raman Microscopy

Slight signal interference from fluorescence also occurred in the Mesoarchean samples, and there is a specific reason for this, related to the thin section preparation. The Raman microscope at the Geophysical Laboratory is equipped with a green laser, as opposed to a red laser. The green laser has a greater sensitivity than the red laser and is commonly

used for rock samples where fluorescence is not a problem (Pelletier, 1999). However, synthetic polymers typically used for thin sections are known to fluoresce when excited at the green laser wavelength of 532 nm (Pelletier, 1999).

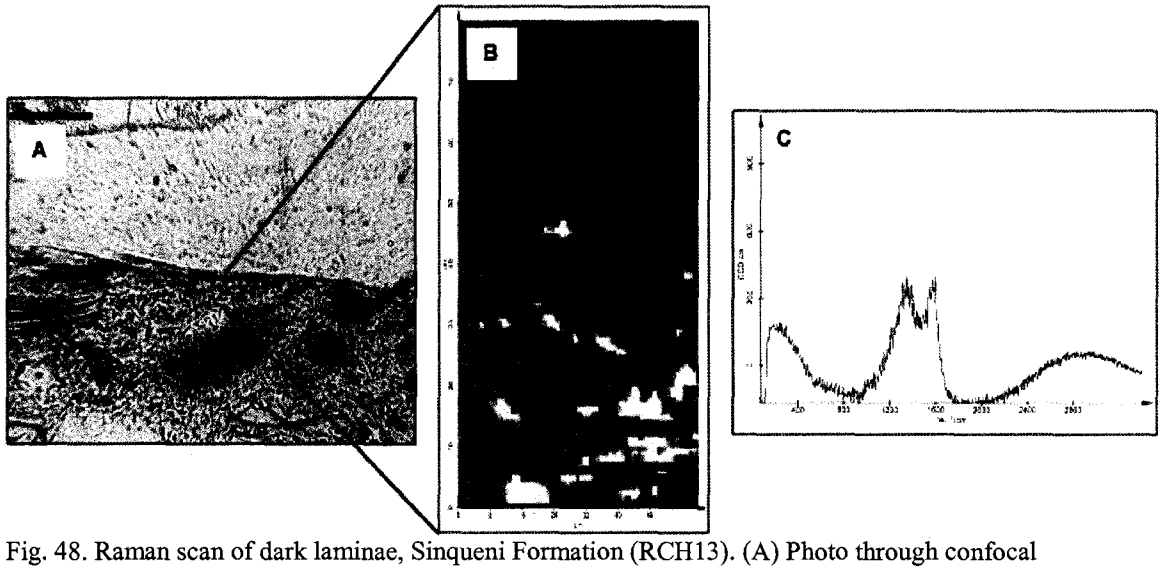

Fig. 48. Raman scan of dark laminae, Sinqueni Formation (RCH13). (A) Photo through confocal microscope of scan area, scale = 80μm. Scan area was 20μm x 20μm. (B) Color composite map of the scan area showing carbon from polymer (black and gray. (C) Spectra of carbon from polymer.

The thin sections from the Ntombe and Sinqueni, Formations were fixed using a synthetic polymer, which resulted in interference that obscured some of the Raman spectra for the constituents of the samples. The synthetic polymer also yielded Raman spectra for carbon (Fig. 48). However, this phenomenon still allowed me to interpret carbon as original and as of biological origin, because the spectra of the polymer displayed wide and poorly developed peaks that differed greatly from the narrow and well-developed carbon peaks associated with the microtextures.

7. Electron Microprobe Analysis of Fossil Filament-like Textures

The filaments in the modern microbial mat contained mainly carbon, but no heavier elements. The sandy interlayers between the filaments contained (in order of abundance) Si, Al, K, Ca, Mg, and some Fe.

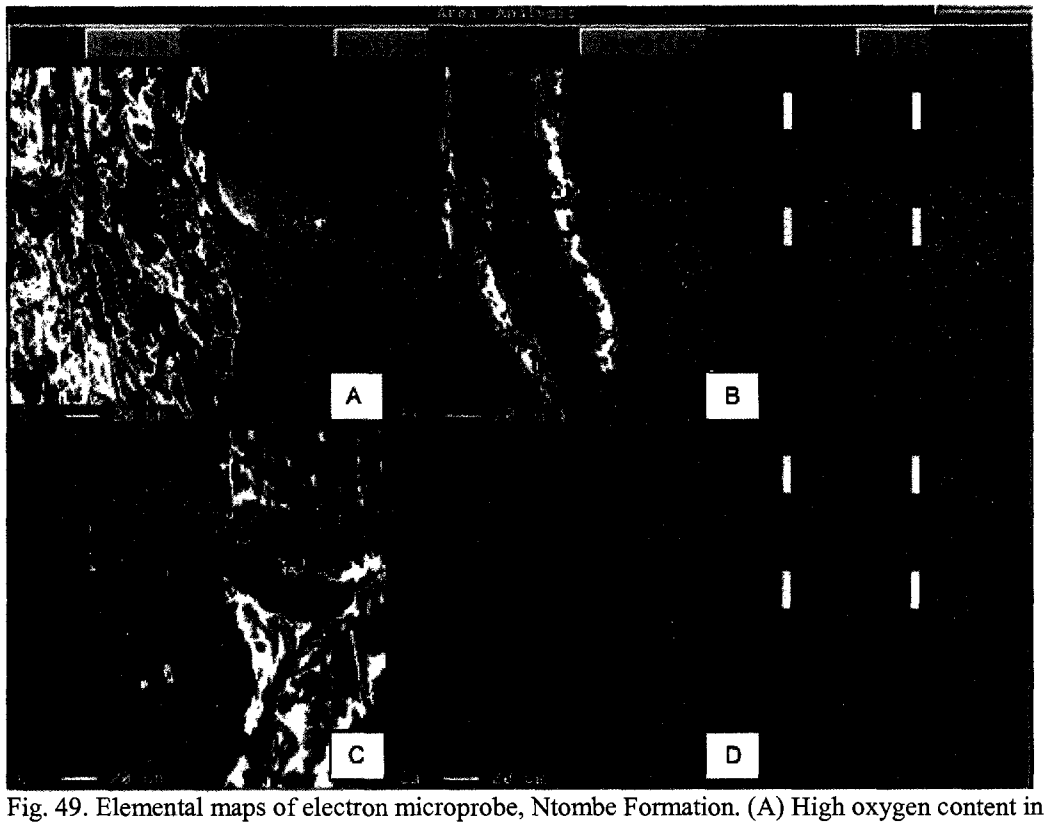

Fig. 49. Elemental maps of electron microprobe, Ntombe Formation. (A) High oxygen content in the laminae is indicated by the pinkish-red color. (B) High iron content in the laminae is indicated by the white and pink colors. The iron coupled with the oxygen constitutes the fe-oxides and fe-hydroxides in the laminae. (C) Red regions outside of the laminae indicate high content of carbon from the thin section polymer. (D) Calcium is not a significant component of this sample.

Based on the elements scanned for by the microprobe, the laminae in the Ntombe samples contained high amounts of Fe and O, followed by (in order of abundance) Si, C, and Mg (Figs 49,50). The high amounts of Fe and O are consistent with the Raman

results that reveal Fe/Ti-oxides and Fe-hydroxides as the main components of the laminae (Figs 49, 50). Also the carbon component reflects the Raman results showing graphite layers within the laminae (Figs 49, 50). Outside of the laminae, the fossil samples were composed of Si, O, Mg (Fig. 50). This also agrees with the results from the Raman and petrographic analyses that show a high component of quartz and clays outside of the laminae. In a previous study, similar results were obtained for the Brixton samples (Noffke et al., 2006a).

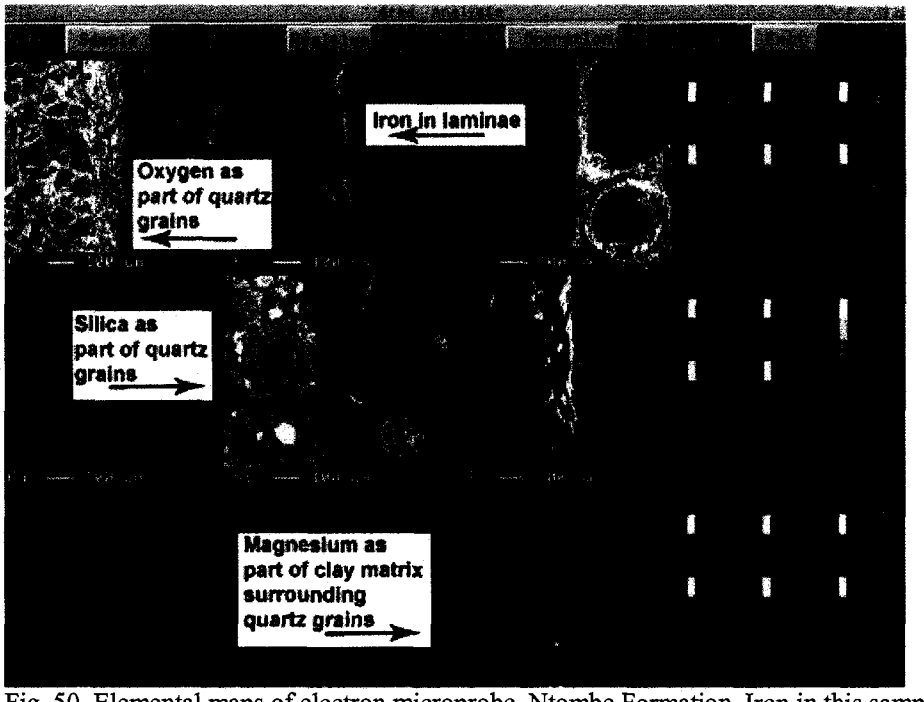

Fig. 50. Elemental maps of electron microprobe, Ntombe Formation. Iron in this sample is only associated with the laminae. Oxygen in red and silica in pink are the main constituents of the mineral grains. Magnesium, shown in blue, is a component of the clay matrix surrounding the quartz grains.

The laminae in the samples from the Sinqueni Formation include Fe and C (Fig. 51). The elemental maps confirm the petrographic analyses with the light microscope, because

they also show the spatial distribution of clay matrix and quartz grains (Figs. 51,52). In both analyses, quartz grains were surrounded by a matrix composed of clays that contain K, Mg, and Si.

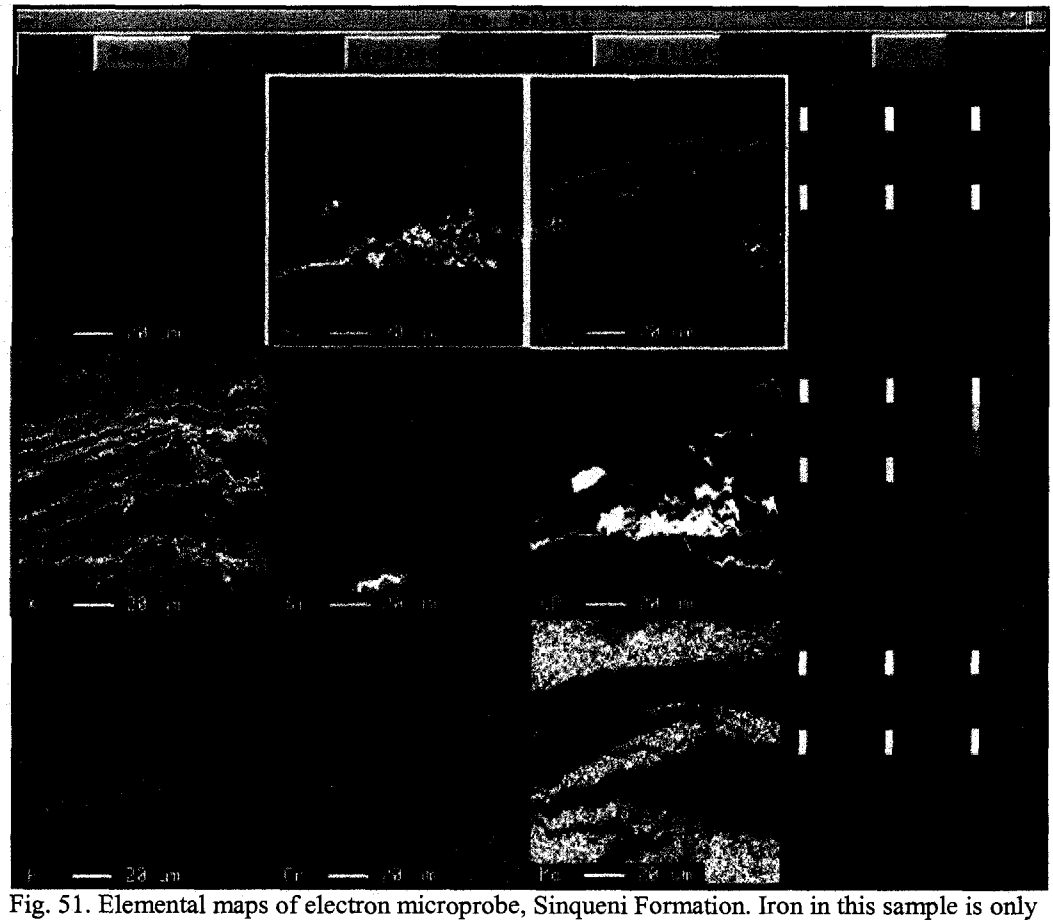

Fig. 51. Elemental maps of electron microprobe, Sinqueni Formation. Iron in this sample is only associated with the laminae. Silica in white and red is one the main constituents of the mineral grains. Potassium in this sample is a large component of the clay matrix surrounding the quartz grains.

These results are consistent with the Raman results that show a mineralic composition of potassic feldspars, clays, and quartz. Also, as in the Ntombe samples, Fe was restricted to the laminae and not a major component of the matrix. Electron microprobe analyses had been conducted earlier on similar sandstone samples from the 3.2 Ga Moodies Group,

South Africa, that contain fossil microbial mats. Also here, Fe and C dominate within the microbial microtextures and laminae (Noffke et al., 2006b).

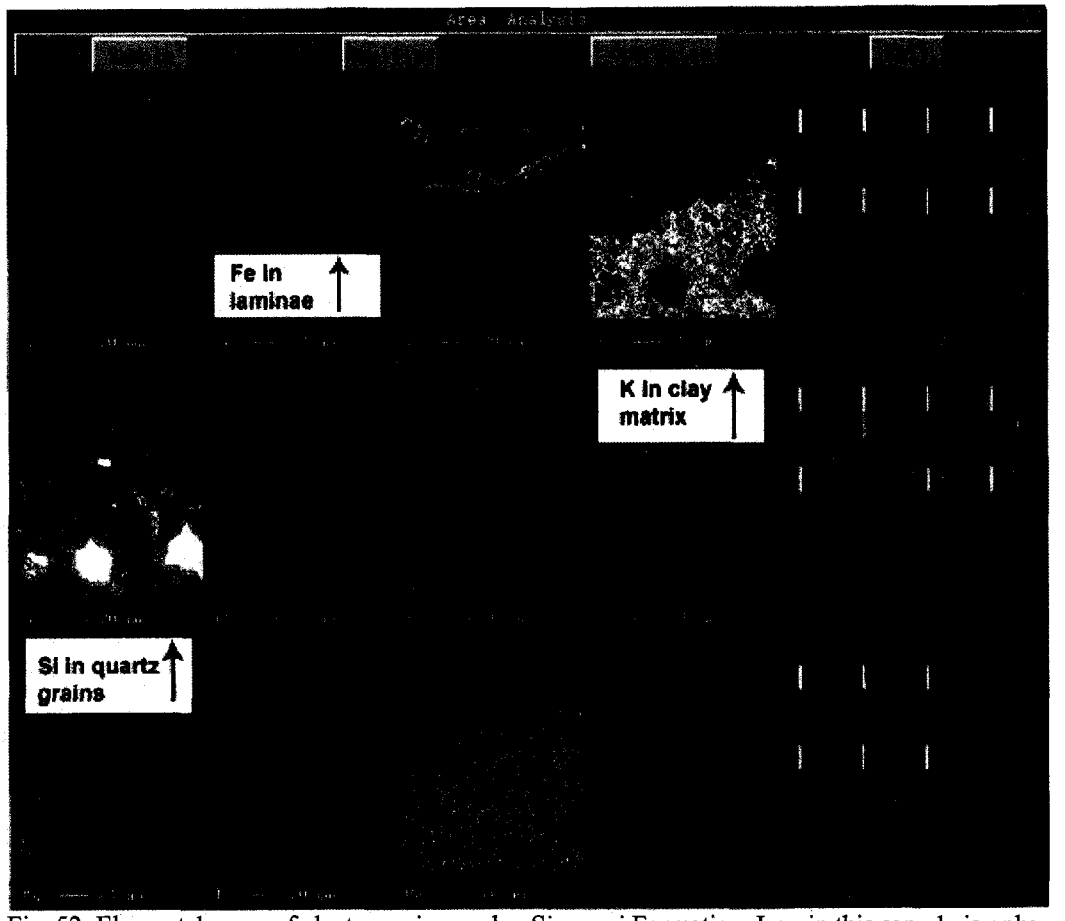

Fig. 52. Elemental maps of electron microprobe, Sinqueni Formation. Iron in this sample is only associated with the laminae. Silica in white and red is one the main constituents of the mineral grains. Potassium in this sample is a large component of the clay matrix surrounding the quartz grains. The carbon in this case is part of the synthetic polymer.

CHAPTER V

DISCUSSION

The aim of my research was to compose a catalogue of recommendations for the NASA Mars Exploration Program using analytical techniques that can be employed to find, identify, and clearly define life as life. Because sand and sandstones are abundant on Mars, and because aquatic sediments have been found on Mars, these investigations are of prime significance. I hope with this thesis to have made an important contribution to this exciting search for extraterrestrial life.

The first step of my investigations was to assist in the investigation of early life on Earth. Because both Earth and Mars had a similar early history of development, it might be possible to find similar fossils in Mars rocks like those we find in Archean sandstones on Earth. In order to accomplish this aim, I specifically studied microtextures in different Mesoarchean siliciclastic sedimentary rocks. Importantly I respectfully assert the biogenicity of these structures and textures using several lines of evidence, because many debates have legitimately addressed this issue (Schopf, 2004, 2006; Brasier et al., 2006, 2005).

The biogenicity of the MISS and microtextures is suggested by three important factors. The first factor is geologic context, which has been thoroughly studied by earlier work. The Ntombe, Sinqueni, and Brixton Formations represent ancient shallow marine tidal

and shelf environments in the Archean (Beukes and Cairncross, 1991; Noffke et al., 2003b, 2006a,b; Nhleko, 2004). These environments would have been similar to the modern siliciclastic intertidal environments of Fishermans Island, Virginia and Mellum Island, North Sea. Cyanobacterial mats thrive in such environments today, and it is possible their ancestral counterparts could have colonized the tidal flats or shallow shelves of the Mesoarchean (Noffke et al., 2008).

In establishing biogenicity, the morphological character of microtextures is important, as microfossils could be microbial fossils but also abiotic textures of various hydrothermal, diagenetic, metamorphic or tectonic origins. The sandstones of the Ntombe, Sinqueni, and Brixton Formations each contain MISS that are similar to those seen in modern environments. Fishermans Island contains MISS that result from the preservation of microbial mats constructed mainly by filamentous cyanobacteria. Without the interaction of the cyanobacteria with the sedimentary dynamics of erosion and deposition, the MISS would not be formed (Noffke, 1998; Noffke and Krumbein, 1999; Noffke et al., 2001a, 2003a; Gerdes and Klenke, 2003). Similar examples of MISS are also seen in sandstones of younger ages (Schieber, 1998, 2004; Noffke et al., 2001b, 2002; Draganits and Noffke, 2004; Banerjee and Jeevankumar, 2005; Parizot et al., 2005).

Closer inspection of Pongola and Witwatersrand samples showed laminae and filamentous microtextures. These laminae and microtextures are comparable to modern mat building cyanobacterial filaments and mat fabrics in dimension and orientation, suggesting that the microtextures are remnants of ancient filamentous cyanobacteria.

These laminae and microtextures are also similar to textures seen in MISS bearing sandstones of younger ages (Noffke et al., 2001b, 2002; Banerjee and Jeevankumar, 2005).

A necessary and beneficial aid in evaluating the biogenicity of a microfossil in question is a biologic geochemical signature. The electron microprobe, Raman, and carbon isotope analyses all show that carbon is associated with the microtextures in the Ntombe and Sinqueni samples. These results agree with previous carbon isotope and microprobe analyses on both the Ntombe and Brixton samples (Noffke et al., 2003b, 2007). The carbon signature in the Mesoarchean samples occurs exclusively within the mat laminae and microtextures, and not in the surrounding material. The host rocks only experienced greenschist facies metamorphism and little tectonism, and not conditions conducive to abiogenic metamorphic graphitization (Ueno et al., 2002; Tice et al., 2004; Satish-Kumar, 2005). The concentration of the carbon along morphologically convincing features, along with the low grade metamorphic history, supports a biologic origin.

The graphite in the samples from the Ntombe and Sinqueni Formations is texturally aligned with Fe hydroxides, Ti-oxides, and clay minerals in the microtextures. The cell walls and EPS buried in the sediments acted as sites of mineral nucleation and mineral replacement of organic material (Ferris et al., 1986, 1988; Konhauser and Urrutia, 1999). As shown with the CSLM analyses, EPS is a major component of microbial fabrics. Together the ancient cyanobacterial filaments and EPS both provided ample organic material and mineral nucleation sites that over 2.9 Ga years resulted in the Fe – Ti-rich

components and small remnants of carbon in the textures preserved in the Ntombe, Sinqueni, and Brixton Formations.

The results of this work can be applied to the exploration of life on other Earth-like planets, such as Mars. The methods I used to examine the MISS and the microtextures associated with MISS can be used by a rover to detect biosignatures on the surface of Mars (Edwards et al., 2003, 2007; Bishop et al., 2004; Erickson et al., 2007). A Mars rover is limited by time and onboard space, and instruments, such as cameras and miniaturized Raman spectrometers, provide quick and informative results. The rover can detect and photograph the MISS while doing a surface scan. A point on the MISS can be targeted and scanned using Raman, and geochemical information can be obtained. I hope that this thesis contribution will support NASA in the challenging search for life on other planets.

REFERENCES

Al-Hanbali, H.S., Sowerby, S.J., Holm, N.G., 2001. Biogenecity of silicified microbes from a hydrothermal system: relevance to the search for evidence of life on earth and other planets. Earth and Planetary Science Letters 191, 213-218.

Altermann, W., Kazmierczak, J., 2003. Archean microfossils: reappraisal of early life on Earth. Research in Microbiology 154, 611-617.

Aplin, A.C., Macleod, G., Lartere, S.R., Pederson, K.S., Sorensen, H., Booth, T., 1999. Combined use of Confocal Laser Scanning Microscopy and PVT simulation for estimating the composition and physical properties of petroleum in fluid inclusions. Marine and Petroleum Geology 16, 97-110.

Banerjee, S., Jeevankumar, S., 2005. Microbially originated wrinkle structures on sandstone and their stratigraphic context: Palaeoproterozoic Koldaha Shale, central India. Sedimentary Geology 176, 211-224.

Banfield, J.F., Hamers, R.J., 1997. Processes at minerals and surfaces with relevance to microorganisms and prebiotic synthesis. In: Banfield, J.F., Nealson, K.H. (Eds), Geomicrobiology: interactions between minerals and microbes. Mineralogical Society of America, Washington, D.C.

Bell, J.F. III, Squyres, S.W., Arvidson, R.E., Arneson, H.M., Bass, D., Calvin, W., Farrand, W.H., Goetz, W., Golombek, M., Greeley, R., Grotzinger, J., Guinness, E., Hayes, A.G., Hubbard, M.Y.H., Herkenhoff, K.E., Johnson, M.J., Johnson, J.R., Joseph, J., Kinch, K.M., Lemmon, M.T., Li, R., Madsen, M.B., Maki, J.N., Malin, M., McCartney, E., McLennan, S., McSween, H.Y. Jr., Ming, D.W., Morris, R.V., Noe Dobrea, E.Z., Parker, T.J., Proton, J., Rice, J.W. Jr., Seelos, F., Soderblom, L.A., Sohl-Dickstein, J.N., Sullivan, R.J., Weitz, C.M., Wolff, M.J., 2004. Pancam multispectral imaging results from the Opportunity rover at Meridiani Planum. Science 306, 1703-1709.

Beukes, N.J., Cairncross, B., 1991. A lithostratigraphic-sedimentological reference profile for the Late Archaean Mozaan Group, Pongola sequence: application to sequence stratigraphy and correlation with the Witwatersrand Supergroup. South African Journal of Geology 94, 44-69.

Bishop, J.L., Anglen, B.L., Pratt, L.M., Edwards, H.G.M., Des Marais, D.J., Doran, P.T., 2003. A spectroscopy and isotope study of sediments from the Antarctic Dry Valleys as analogues for potential paleolakes on Mars. International Journal of Astrobiology 2, 273-287.

Bishop, J.L., Munrad, E., Lane, M.D., Mancinelli, R.L., 2004. Multiple techniques for mineral identification on Mars: a study of hydrothermal rocks as potential analogs for astrobiology sites on Mars. Icarus 169, 311-323.

Bleeker, W., 2002. Archaean tectonics: a review, with illustrations from the Slave craton. In: Fowler, C.M.R., Ebinger, C.J., Hawkesworth, C.J. (Eds), The early Earth: physical, chemical and biological development. The Geological Society Publishing House, London.

Bouougri, E., Porada, H., 2002. Mat related sedimentary structures in Neoproterozoic peritidal passive margin deposits of the West African Craton (Anti-Atlas, Morocco). Sedimentary Geology 153, 85-106.

Bower, D.M., Noffke, N., 2004. Investigations by confocal scanning laser microscopy on modern microbial mats and comparisons with 2.9 Ga bacterial textures from the Pongola Supergroup, South Africa. Geological Society of America Annual Meeting, paper#80310.

Boyce, C.K., Hazen, R.M., Knoll, A.H., 2001. Nondestructive, *in situ*, cellular-scale mapping of elemental abundances including organic carbon in permineralized fossils. PNAS 98, 5970-5974.

Boyce, J.M., Mouginis-Mark, P., Garbeil, H., 2005. Ancient oceans in the northern lowlands of Mars: evidence from impact crater depth/diameter relationships. Journal of Geophysical Research 110, 1-15.

Brack, A., 1996. Why exobiology on Mars? Planetary Space Science 44, 1435-1440.

Brasier, M.D., Green, O.R., Jephcoat, A.P., Kleppe, A.K., Van Kranendonk, M.J., Lindsay, J.F., Steele, A., Grassineau, N.V., 2002. Questioning the evidence for Earth's oldest fossils. Nature 416, 76-81.

Brasier, M.D., Green, O.R., Lindsay, J.F., McLoughlin, N., Steele, A., Stoakes, C., 2005. Critical testing of Earth's oldest putative fossil assemblage from the ~ 3.5 Ga Apex xhert, Chinaman Creek, Western Australia. Precambrian Research 140, 55-102.

Brasier, M.D., McLoughlin, N., Green, O., Wacey, D., 2006. A fresh look at the fossil evidence for early Archean cellular life. Philosophical Transactions of the Royal Society, B 361, 887-902.

Brown, D.A., Sawicki, J.A., Sherriff, B.L.,1998. Alteration of microbially precipitated iron oxides and hydroxides. American Mineralogist 83, 1419-1425.

Bryant, D.A., Frigaard, N., 2006. Prokaryotic photosynthesis and phototrophy illuminated. Trends in Microbiology 14, 488-496.

Cabrol, N.A., Wynn-Williams, D.D., Crawford, D.A., Grin, E.A., 2001. Recent aqueous environments in Martian impact craters: and asrobiological perspective. Icarus 154, 98-112.

Canfield, D.E., 1999. A breath of fresh air. Nature 400, 503-505.

Canfield, D.E., 2005. The early history of atmospheric oxygen: homage to Robert M. Garrels. Annual Review of Earth and Planetary Science 33, 1-36.

Canfield, D.E., Habicht, K.S., Thamdrup, B., 2000. The Archean sulfur cycle and the early history of atmospheric oxygen. Science 288, 658-661.

Catling, D.C., Zahnle, K.J., McKay, C.P., 2001. Biogenic methane, hydrogen escape, and the irreversible oxidation of early Earth. Science 293, 839-843.

Catuneanu, O., 2001. Flexural partitioning of the Late Archean Witwatersrand foreland system, South Africa. Sedimentary Geology 141-142, 95-112.

Cockell, C.S., 2000. The ultraviolet history of the terrestrial planets – implications for biological evolution. Planetary and Space Science 48, 203-214.

Cockell, C.S., Raven, J.A., 2004. Zones of photosynthetic potential on Mars and the early Earth. Icarus 169, 300-310.

Cook, R.A., 2005. The Mars exploration rover project. Acta Astronautica 57, 116-120.

Cordoba-Jabonero, C., Lara, L.M., Mancho, A.M., Marquez, A., Rodrigo, R., 2003. Solar ultraviolet transfer in the Martian atmosphere: biological and geological implications. Icarus 51, 399-410

Cornell, R.M., Schwertmann, U., 1996. The iron oxides – structure, properties, reactions, occurrence, and uses. VCH Verlagsgesellschaft, Weinheim.

Davis, G.H., Reynolds, S.J., 1996. Structural geology of rocks and regions. John Wiley and Sons, Inc., New York.

De Beer, J.H., Eglington, B.M., 1991. Archean sedimentation on the Kaapvaal caton in relation to tectonism in the granite-greenstone terrains. Journal of African Earth Sciences 13, 27-44.

Decho, A.W., 1990. Microbial exopolymer secretions in ocean environments: their roles in food webs and marine processes. Oceanography and Marine Biology Annual Review 28, 73-153.

Decho, A.W., 2000a. Microbial biofilms in intertidal systems: an overview. Continental Shelf Research 20, 1257-1273.

Decho, A.W., 2000b. Exopolymer microdomains as a structuring agent for heterogeneity within microbial biofilms. In: Riding, R.E., Awramik, S.M. (Eds), Microbial Sediments Springer-Verlag, Berlin.

De Gregorio, B.T., Sharp, T.G., 2003. Determining the biogenecity of microfossils in the Apex chert, Western Australia, using transmission electron microscopy. Lunar and Planetary Science XXXIV, 1267.

De Los Rios, A., Ascaso, C., Wierzchos, J., Fernandez-Valiente, E., Quesada, A., 2004. Microstructural characterization of cyanobacterial mats from the McMurdo ice shelf, Antarctica. Applied and Environmental Microbiology 70, 569-580.

De Wit, M. J., Roering, C., Hart, R.J., Armstrong, R.A., de Ronde, C.E.J., Green, R.W.E., Tredoux, M., 1992. Formation of an Archean continent. Nature 357, 553-562.

Dimroth, E., Lichtblau, A.P., 1978. Oxygen in the Archean ocean. Neues Jahrbuch fur mineralogy 133, 1-22.

Doran, P.T., Clifford, S.M., Forman, S.L., Nyquist, L., Papanastassiou, D.A., Stewart, B.W., Sturchio, N.C., Swindle, T.D., Cerling, T., Kargel, J., McDonald, G., Nishiizumi, K., Poreda, R., Rice, J.W., Tanaka, K., 2004. Mars chronology: assessing techniques for quantifying surficial processes. Earth-Science Reviews 67, 313-337.

Draganits, E., Noffke, N., 2004. Siliciclastic stromatolites and other microbially induced sedimentary structures in an early Devonian barrier-island environment (Muth Formation, NW Himalayas). Journal of Sedimentary Research 74, 191-202.

Dupraz, C., Visscher, P., 2005. Microbial lithification in marine stromatolites and hypersaline mats. Trends in Microbiology 13, 429-438.

Dvornyk, V., Nevo, E., 2003. Genetic polymorphism of cyanobacteria under permanent natural stress: A lesson from the "Evolution Canyons". Research in Microbiology 154, 79-84.

Edwards, H.G.M., Newton, E.M., Dickensheets, D.L., Wynn-Williams, D.D., 2003. Raman spectroscopic detection of biomolecular markers from Antarctic materials: evaluation for putative Martian habitats. Spectrochimica Acta Part A 59, 2277-2290.

Edwards, H.G.M., Moody, C.D., Newton, E.M., Jorge Villar, S.E., Russell, M.J., 2005. Raman spectroscopic analysis of cyanobacterial colonization of hydromagnesite, a putative martian extremophile. Icarus 175, 372- 381.

Ehrlich, H.L., 1990. Geomicrobiology. Marcel Dekker, Inc. New York.

Erickson, J.K., Callas, J.L., Haldemann, A.F.C., 2007. The Mars Exploration Rover project: 2005 surface operations results. Acta Astronautica 61, 699-706.

Ericksson, P.G., Condie, K.C., Tirsgaard, H., Mueller, W.U., Altermann, W., Miall, A.D., Aspler, L.B., Catuneanu, O., Chiarenzelli, J.R., 1998. Precambrian clastic sedimentation systems. Sedimentary Geology 120, 5-53.

Ericksson, P.G., Catuneanu, O., Nelson, D.R., Mueller, W.U., Altermann, W., 2004. Towards a synthesis. In: Ericksson, P.G., Altermann, W., Nelson, D.R., Mueller, W.U., Catuneanu, O. (Eds), The Precambrian Earth: tempos and events (Elsevier, Netherlands.

Ericksson, P.G., Catuneanu, O., Sarkar, S., Tirsgaard, H., 2005a. Patterns of sedimentation in the Precambrian. Sedimentary Geology 176, 17-42.

Ericksson, P.G., Catuneanu, O., Els, B.G., Bumby, A.J., Van Rooy, J.L., Popa, M., 2005b. Kaapvaal craton: changing first- and second-order controls on sea level from c. 3.0 Ga to 2.0 Ga. Sedimentary Geology 176, 121-148.

Eriksson, K.A., Fedo, C.M., 1994. Archean synrift and stable-shelf sedimentary successions. Developments in Precambrian Geology 11, 171-204.

Ferris, F.G., Beveridge, T.J., Fyfe, W.S., 1986. Iron-silica crystallite nucleation by bacteria in a geothermal sediment. Nature 320, 609-615.

Ferris, F.G., Fyfe, W.S., Beveridge, T.J., 1988. Metallic ion binding by *Bacillus subtilis*: implications for the fossilization of microorganisms. Geology 16, 149-152.

Fortin, D., Ferris, F.G., Beveridge, T.J., 1997. Surface-mediated mineral development by bacteria. In: Banfield, J.F., Nealson, K.H. (Eds), Geomicrobiology: interactions between microbes and minerals. Mineralogical Society of America, Washington, D.C.

Franck, S., Block, A., Von Bloh, W., Bounama, C., Schellnhuber, H.J., Svirezhev, Y., 2000. Habitable zone for Earth-like planets in the solar system. Planetary and Space Science 48, 1099-1105.

Fries, M., Steele, A., 2005. Inclusions within chondrule mineral grains as characterized using confocal Raman imaging. Lunar and Planetary Science XXXVI.

Garcia-Ruiz, J.M., Hyde, S.T., Carnerup, A.M., Christy, A.G., Van Kranendonk, M.J., Welham, N.J., 2003. Self-assembled silica-carbonate structures and detection of ancient microfossils. Science 302, 1194-1197.

Gee, H., 2002. That's life? Nature 416, 28.

Gerdes, G., Klenke, T., 2003. Geological importance of ecological time spans in biogenic bedding (microbial mats, potential stromatolites). Mitt. Ges. Geol. Bergbaustud. Osterr. 46, 35-49.

Gold, D.J.C., Von Veh, M.W., 1995. Tectonic evolution of the Late Archean Pongola-Mozaan basin, South Africa. Journal of African Earth Sciences 21, 203-212.

Golubic, S., Seong-Joo, L., 1999. Early cyanobacterial fossil record: preservation, paleoenvironments and identification. European Journal of Phycology 34, 339-348.

Golubic, S., Seong-Joo, L., Browne, K.M., 2000. Cyanobacteria : Architects of sedimentary structures. In: Riding, R.E., Awramik, S.M. (Eds), Microbial Sediments Springer-Verlag, Berlin.

Griffiths, A.D., Coates, A.J., Josset, J.L., Paar, G., Hofmann, B., Pullan, D., Ruffer, P., Sims, M.R., Pillinger, C.T., 2005. The Beagle 2 stereo camera system. Planetary and Space Science 53, 1466-1482.

Gutzmer, J., Nhleko, N., Beukes, N.J., Pickard, A., Barley, M.E., 1999. Geochemistry and ion microprobe (SHRIMP) age of quartz porphyry sill in the Mozaan Group of the Pongola Supergroup. South African Journal of Geology 102, 139-146.

Habicht, K.S., Gade, M., Thamdrup, B., Berg, P., Canfield, D.E., 2002. Calibration of sulfate levels in the Archean ocean. Science 298, 2372-2374.

Haskin, L.A., Wang, A., Rockow, K.M., Jolliff, B.L., Korotev, R.L., Viskupic, K.M., 1997. Raman spectroscopy for mineral identification and quantification for in situ planetary surface analysis: a point count method. Journal of Geophysical Research 102, 19293-19306.

Hofmann, B.A., Farmer, J.D., 2000. Filamentous fabrics in low-temperature mineral assemblages: are they fossil biomarkers? Implications for the search for a subsurface fossil record in the early Earth and Mars. Planetary Space and Science 48, 1077-1086.

Holland, H.D., 2002. Volcanic gases, black smokers, and the Great Oxidation event. Geochimica et Cosmochimica Acta 66, 3811-3826.

Horneck, G., 2000. The microbial world and the case for Mars. Planetary and Space Science 48, 1053-1063.

Huston, D.L., Logan, G.A., 2004. Barite, BIF's and bugs: evidence for the evolution of the Earth's early hydrosphere. Earth and Planetary Science Letters 220, 41-55.

Jones, B., Renaut, R.W., Rosen, M.R., 2001. Taphonomy of silicified filamentous microbes in modern geothermal sinters – implications for identification. Palaios 16, 580-592.

Kasting, J.F., 2005. Methane and climate during the Precambrian era. Precambrian Research 137, 119-129.

Kawaguchi, T., Decho, A.W., 2002. A laboratory investigation of cyanobacterial extracellular polymeric secretions (EPS) in influencing $CaCO_3$ polymorphism. Journal of Crystal Growth 240, 230-235.

Kazmierczak, J., Kremer, B., 2002. Thermal alteration of the Earth's oldest fossils. Nature 420, 477-478.

Konhauser, K.O., 1998. Diversity of bacterial iron mineralization. Earth-Science Reviews 43, 91-121.

Konhauser, K.O., Urrutia, M.M., 1999. Bacterial clay authigenesis: a common biogeochemical process. Chemical Geology 161, 399-413.

Lasaga, A.C., Ohmoto, H., 2002. The oxygen geochemical cycle: dynamics and stability. Geochimica et Cosmochimica Acta 66, 361-381.

Lawrence, J.R., Neu, T.R., Swerhone, G.D.W., 1998. Application of multiple parameter imaging for the quantification of algal, bacterial and exopolymer components of microbial biofilms. Journal of Microbiological Methods 32, 253-261.

Lawrence, J.R., Swerhone, G.D.W., Leppard, G.G., Araki, T., Zhang, X., West, M.M., Hitchcock, A.P., 2003. Scanning transmission x-ray, laser scanning, and transmission electron microscopy mapping of the exopolymeric matrix of microbial biofilms. Applied and Environmental Microbiology 69, 5543-5554.

Libes, S.M., 1992. An introduction to marine biogeochemistry. John Wiley & Sons, Inc., New York.

Lindsay, J.F., Brasier, M.D., 2002. A comment on tectonics and the future of terrestrial life-reply. Precambrian Research 118, 293-295.

Lindsley, D.H., 1991. Experimental studies of oxide minerals. In: Lindley, D.H. (Ed), Oxide minerals: petrologic and magnetic significance. Mineralogical Society of America, Chelsea.

Lippson, A.J., 1997. Life in the Chesapeake Bay. The Johns Hopkins University Press, Baltimore.

Lowe, D.R., 1992. Major events in the geologic development of the Precambrian Earth. In: Schopf, J.W., Klein, C. (Eds), The Proterozoic biosphere. Cambridge University Press, Cambridge.

Lundgren, P., Falkowski, P., 2003. Nitorgen fixation and photosynthetic oxygen evolution in cyanobacteria. Research in Microbiology 154, 157-164.

Malin, M.C., Edgett, K.S., 2000. Sedimentary rocks of early Mars. Science 290, 1927-1937.

Marshall, C.P., Javaux, E.J., Knoll, A.H., Walter, M.R., 2005. Combined micro-Fourier transform infrared (FTIR) spectroscopy and micro-Raman spectroscopy of Proterozoic acritarchs: a new approach to paleobiology. Precambrian Research 138, 208-224.

McKay, C.P., 1998. Life on Mars. In: Brack, A. (Ed.), The molecular origins of life. Cambridge University Press, Cambridge.

Menendez, B., David, C., Martinez Nistal, A., 2001. Confocal scanning laser microscopy applied to the study of pore and crack networks in rocks. Computers and Geosciences 27, 1101-1109.

Milliken, K.L., 2005. Late diagenesis and mass transfer in sandstone-shale sequences. In: Mackenzie, F.T. (Ed), Sediments, diagenesis, and sedimentary rocks. Elsevier, Amsterdam.

Morrison, D., 2001. The NASA Astrobiology program. Astrobiology 1, 3-13.

Nesse, W.D., 2000. Introduction to mineralogy. Oxford University Press, Oxford.

Nhleko, N., 2004. The Pongola Supergroup in Swaziland. PhD Thesis. Raand Afrikaans University, Johannesburg, South Africa.

Noffke, N., 1998. Multidirected ripple marks arising from bacterial stabilization counteracting physical rework in modern sandy deposits (Mellum Island, southern North Sea). Geology 26, 879-882.

Noffke, N., 1999. Erosional remnants and pockets evolving from biotic-physical interactions in a Recent lower supratidal environment. Sedimentary Geology 123, 175-181.

Noffke, N., 2000. Extensive microbial mats and their influences on the erosional and depositional dynamics of a siliciclastic cold water environment (Lower Arenigian, Montagne Noire, France). Sedimentary Geology 136, 207-215.

Noffke, N., 2003. Epibenthic cyanobacterial communities interacting with sedimentary processes in siliciclastic depositional systems (present and past). In: Krumbein, W, Paterson, D.M., Zavarin, G.A. (Eds), Fossil and Recent Biofilms. Kluwer Academic Publishers, Dordrecht.

Noffke, N., 2007. Microbially induced sedimentary structures in Archean sandstones: a new window into early life. Gondwana Research 11, 336-342.

Noffke, N., Krumbein, W.E., 1999. A quantitative approach to sedimentary surface structures contoured by the interplay of microbial colonization and physical dynamics. Sedimentology 46, 417-426.

Noffke, N., Gerdes, G., Klenke, T., Krumbein, W.E., 1997. A microscopic sedimentary succession of graded sand and microbial mats in modern siliciclastic tidal flats. Sedimentary Geology 110, 1-6.

Noffke, N., Gerdes, G., Klenke, T., Krumbein, W.E., 2001a. Microbially induced sedimentary structures- a new category within the classification of primary sedimentary structures. Journal of Sedimentary Research 71, 649-656.

Noffke, N., Gerdes, G., Klenke, T., Krumbein, W.E., 2001b. Microbially induced sedimentary structures indicating climatological, hydrological and depositional conditions within Recent and Pleistocene coastal facies zones (Southern Tunisia). Facies 44, 23-30.

Noffke, N., Knoll, A.H., Grotzinger, J.P., 2002. Sedimentary controls on the formation and preservation of microbial mats in siliciclastic deposits: a case study from the Upper Neoproterozoic Nama Group, Namibia. Palaios 17, 533-544.

Noffke, N., Gerdes, G., Klenke, T., 2003a. Benthic cyanobacteria and their influence on the sedimentary dynamics of peritidal depositional systems (siliciclastic, evaporitic salty, and evaporitic carbonatic). Earth Science Reviews 62, 163-176.

Noffke, N., Hazen, R., Nhleko, N., 2003b. Earth's earliest microbial mats in a siliciclastic marine environment (2.9 Ga Mozaan Group, South Africa). Geology 31, 673-676.

Noffke, N., Beukes, N., Gutzmer, J., Hazen, R., 2006a. Spatial and temporal distribution of microbially induced sedimentary structures: a case study from siliciclastic storm deposits of the 2.9 Ga Witwatersrand Supergroup, South Africa. Precambrian Research 146, 35-44.

Noffke, N., Eriksson, K.A., Hazen, R.M., Simpson, E.L., 2006b. A new window into Early Archean life: microbial mats in Earth's oldest siliciclastic tidal deposits (3.2 Ga Moodies Group, South Africa). Geology 34, 253-256.

Noffke, N., Beukes, N., Bower, D.M., Hazen, R.M., Swift, D.J.P., 2008. An actualistic perspective into Archean worlds – (cyano-)bacterially induced sedimentary structures in the siliciclastic Nhlazatse Section, 2.9 Ga Pongola Supergroup, South Africa. Geobiology 6, 5-20.

Ohmoto, H., 2004. The Archaean atmosphere, hydrosphere, and biosphere. In: Ericksson, P.G., Altermann, W., Nelson, D.R., Mueller, W.U., Catuneanu, O. (Eds), The Precambrian Earth: tempos and events. Elsevier, Netherlands.

Olson, J.M., 2006. Photosynthesis in the Archean era. Photosynthesis Research 88, 109-117.

Ormerod, J.G., 1992. Diversity, ecology, and taxonomy of the cyanobacteria. In: Mann, N.H., Carr, N.G. (Eds), Photosynthetic prokaryotes. Plenum Press, New York.

Parizot, M., Ericksson, P.G., Aifa, T., Sarkar, S., Banerjee, S., Catuneanu, O., Altermann, W., Bumby, A., Bordy, E.M., Van Rooy, J.L., Boschoff, A.J., 2005. Suspected microbial mat-related crack-like sedimentary structures in the Paleoproterozoic Magaliesberg Formation sandstones, South Africa. Precambrian Research 138, 274-296.

Pelletier, M.J., 1999. Analytical applications of Raman spectroscopy. Blackwell Science, Ltd, Cornwall.

Petford, N., Davidson, G., Miller, J.A., 1999. Pore structure determination using confocal scanning laser microscopy. Physical Chemistry of the Earth 24, 563-567.

Pettjohn, F.J., Potter, P.E., Siever, R., 1987. Sand and sandstone. Springer-Verlag, New York.

Pierson, B.K., Parenteau, M.N., 2000. Phototrophs in high iron microbial mats: microstructure of mats in iron-depositing hot springs. FEMS Microbiology Ecology 32, 181-196.

Popp, J., Tarcea, N., Kiefer, W., Hilchenbach, M., Thomas, N., Stuffler, T., Hofer, S., Stoffler, D., Greshake, A., 2002. The effect of surface texture on the mineralogical analysis of chondritic meteorites using Raman spectroscopy. Planetary and Space Science 50, 865-870.

Powers, M.C., 1953. A new roundness scale for sedimentary particles. Journal of Sedimentary Petrology 23, 117-119.

Purevdorj-Gage, L.B., Stoodley, P., 2004. Biofilm structure, behavior, and hydrodynamics. In: Ghannoum, M., O'Toole, G.A. (Eds), Microbial Biofilms. ASM Press, Washington, D.C.

Quesada, A., Vincent, W.F., Lean, D.R.S., 1999. Community and pigment structure of Arctic cyanobacterial assemblages: the occurrence and distribution of UV-absorbing compounds. FEMS Microbiology Ecology 28, 315-323.

Ransom, B., Bennett, R.H., Baerwald, R., Hulbert, M.H., Burkett, P., 1999. In situ conditions and interactions between microbes and minerals in fine-grained marine sediments. American Mineralogist 84, 183-192.

Reed, S.J.B., 2005. Electron microprobe analysis and scanning electron microscopy in geology. Cambridge University Press, Cambridge.

Reineck, H.E., 1970. Relief casts and thick sections suitable for projection. Senckenbergiana Maritima 2, 31-59.

Ronto, G., Berces, A., Lammer, H., Cockell, C.S., Molina-Cuberos, G.J., Patel, M.R., Selsis, F., 2003. Solar UV irradiation conditions on the surface of Mars. Photochemistry and Photobiology 77, 34-40.

Satish-Kumar, M., 2005. graphite-bearing CO2-fluid inclusions in granulites: insights on graphite precipitation and carbon isotope evolution. Geochimica et Cosmochimica Acta 69, 3841-3856.

Schieber, J., 1998. Possible indicators of microbial mat deposits in shales and sandstones: examples from the Mid-Proterozoic Belt Supergroup, Montana, U.S.A. Sedimentary Geology 120, 105-124.

Schieber, J., 2004. Microbial mats in the siliciclastic rock record: a summary of diagnostic features. In: Nelson, D.R., Mueller, W.U., Catuneanu, O. (Eds), The Precambrian earth: tempos and events. Elsevier, Amsterdam.

Schidlowski, M., 1988. A 3,800-million-year isotopic record of life from carbon in sedimentary rocks. Nature 333, 313-318.

Schidlowski, M., 2001. Carbon isotopes as biogeochemical recorders of life over 3.8 Ga of Earth history: evolution of a concept. Precambrian Research 106, 117-134.

Schopf, J.W., 2004. Earth's earliest biosphere: status of the hunt. In: Nelson, D.R., Mueller, W.U., Catuneanu, O. (Eds), The Precambrian Earth: tempos and events. Elsevier, Amsterdam.

Schopf, J.W., 2006. Fossil evidence of Archean life. Philosophical Transactions of the Royal Society, B 361, 869-885.

Schopf, J.W., Kudryavstev, A.B., Agresti, D.G., Wdowiak, T.J., Czaja, A.D., 2002. Laser-Raman imagery of Earth's earliest fossils. Nature 416, 73-76.

Schultze-Lam, S., Fortin, D., Davis, B.S., Beveridge, T.J., 1996. Mineralization of bacterial surfaces. Chemical Geology 132, 171-181.

Sharma, S.K., 2007. New trends in remote Raman spectroscopic instrumentation. Spectrochimica Acta Part A 68, 1008-1022.

Sharma, S.K., Lucey, P.G., Ghosh, M., Hubble, H.W., Horton, K.A., 2003. Stand-off Raman spectroscopic detection of minerals on planetary surfaces. Spectrochimica Acta Part A 59, 2391-2407.

Sharma, S.K., Misra, A.K., Ismail, S., Singh, U.N., 2006. Remote Raman spectroscopy of various mixed and composite mineral phases at 7.2m distance. 37th Lunar and Planetary Science Conference.

Sroga, G.E., 1997. Regulation of nitrogen fixation by different nitrogen sources in the filamentous non-heterocystous cyanobacterium Microcoleus sp. FEMS Microbiology Letters 153, 11-15.

Stal, L.J., 1994. Microbial mats in coastal environments. In: Stal, L.J. and Caumette, P. (Eds), Microbial mats- structure, development and environmental significance. Springer-Verlag, Berlin.

Stal, L.J., 2000. Cyanobacterial mats and stromatolites. In: Whitton, B.A. and Potts, M. (Eds), The ecology of cyanobacteria – their diversity in time and space. Kluwer Academic Publishers, Dordrecht.

Starkey, M., Gray, K.A., Chang, S., Parsek, M.R., 2004. A sticky business: the extracellular polymeric substance matrix of biofilms. In: Ghannoum, M., O'Toole, G.A. (Eds), Microbial biofilms. ASM Press, Washington, D.C.

Stolz, J.F., 2003. Structure of marine biofilms. In: Krumbein, W, Paterson, D.M., Zavarin, G.A. (Eds), Fossil and recent biofilms. Kluwer Academic Publishers, Dordrecht.

Stolz, J.F., 2000. Structure of microbial mats and biofilms. In: Riding, R.E., Awramik, S.M. (Eds), Microbial sediments. Springer-Verlag, Berlin.

Stone, A.T., 1997. Reactions of extracellular organic ligands with dissolved metal ions and mineral surfaces. In: Banfield, J.F., Nealson, K.H., (Eds), Geomicrobiology: interactions between minerals and microbes. Mineralogical Society of America, Washington, D.C.

Stopar, J. D., Lucey, P.G., Sharma, S.K., Misra, A.K., Taylor, G.J., Hubble, H.W., 2005. Raman efficiencies of natural rocks and minerals: performance of a remote Raman system for planetary exploration at a distance of 10 meters. Spectrochimica Acta Part A 61, 2315-2323.

Strauss, H., 2004. 4 Ga of seawater evolution: evidence from the sulfur isotopic composition of sulfate. Geological Society of America Special Paper 379.

Strevett, K.A., Chen, G., 2003. Microbial surface thermodynamics and applications. Research in Microbiology 154, 329-335.

Tice, M.M., Bostick, B.C., Lowe, D.R., 2004. Thermal history of the 3.5-3.2 Ga Onverwacht and Fig Tree Groups, Barberton greenstone belt, South Africa, inferred by Raman microscopy of carbonaceous material. Geology 32, 37-40.

Tucker, M.E., 1988. Techniques in sedimentology. Blackwell Scientific Publications, Oxford.

Ueno, Y., Yurimoto, H., Yoshioka, H., Komiya, T., Maruyama, S., 2002. Ion microprobe analysis of graphite from ca. 3.8 Ga metasediments, Isua supracrustal belt, West Greenland: relationship between metamorphism and carbon isotopic composition. Geochimica et Cosmochimica Acta 66, 1257-1268.

Van Zuilen, M.A., Lepland, A., Arrhenius, G., 2002. Reassessing the evidence for the earliest traces of life. Nature 418, 627 -630.

Wang, A., Haskin, L.A., Jolliff, B.L., 1998. Characterization of mineral products of oxidation and hydration by laser raman spectroscopy- implications for *in situ* petrologic investigation on the surface of Mars. Lunar and Planetary Science XXIX 1819.

Watanabe, Y., Stewart, B.W., Ohmoto, H., 2004. Organic- and carbonate-rich soil formation ~ 2.6 billion years ago at Schagen, East Transvaal district, South Africa. Geochimica et Cosmochimica Acta 68, 2129-2151.

Westall, F., De Wit, M.J., Dann, J., Van der Gaast, S., De Ronde, C.E.J., Gernecke, D., 2001. Early Archean fossil bacteria and biofilms in hydrothermally-influenced sediments from the Barberton greenstone belt, South Africa. Precambrian Research 106, 93-116.

Whitfield, J., 2004. It's life, isn't it? Nature 430, 288-290.

Whitton, B.A., 1992. Diversity, ecology, and taxonomy of the cyanobacteria. In: Mann, N.H., Carr, N.G. (Eds), Photosynthetic prokaryotes. Plenum Press, New York.

Whitton, B.A., Potts, M., 2000. Introduction to the cyanobacteria. In: Whitton, B.A., Potts, M. (Eds), The ecology of cyanobacteria – their diversity in time and space. Kluwer Academic Publishers, Dordrecht.

Wimpenny, J., Manz, W., Szewzyk, U., 2000. Heterogeneity in biofilms. FEMS Microbiology Reviews 24, 661-671.

Wynn-Williams, D.D., Edwards, H.G.M., Garcia-Pichel, F., 1999. Functional biomolecules of Antarctic stromatolitic and endolithic cyanobacterial communities. European Journal of Phycology 34, 381-391.

Wynn-Williams, D.D., Edwards, H.G.M., 2000. Proximal analysis of regolith habitats and protective biomolecules *in situ* by laser Raman spectroscopy: and overview of terrestrial Antarctic habitats and Mars analogs. Icarus 144, 486-503.

Wynn-Williams, D.D., Edwards, H.G.M., Newton, E.M., Holder, J.M., 2002. Pigmentation as a survival strategy for ancient and modern photosynthetic microbes under high ultraviolet stress on planetary surfaces. International Journal of Astrobiology 1, 39-49.

VITA

Dina M. Bower
Old Dominion University, Ocean, Earth & Atmospheric Sciences
Norfolk, VA 23529
E-Mail: dbower@odu.edu

Education

PhD, Ocean, Earth, and Atmospheric Science — August 2008
Old Dominion University, Norfolk, Virginia
Dissertation: Microtextures of cyanobacterial mats in siliciclastic sedimentary environments (modern and ancient): applications to NASA's search for life on Mars
Advisor: Nora Noffke

Bachelor of Science, Oceanography — May 2003
Bachelor of Arts, Geology — May 2003
Richard Stockton College of New Jersey, Pomona, New Jersey

Research Experience

-Investigation of macro- and microstructures in Archean siciliclastic rocks using optical and petrographic microscopy, CSLM, electron microprobe, C-isotopes, and micro Raman spectroscopy funded under the NASA Mars Fundamental Research Program and work done in conjunction with the Geophysical Laboratory, Carnegie Institution, Washington, D.C. — 2003- present
-Field work in the Archean Pongola Supergroup, South Africa — 2005
-Analysis of low-level phosphates in sea water onboard a research vessel in the Sargasso Sea using MAGIC method — 2003
-Summer internship at Shannon Point Marine Center, Anacortes, WA investigating the effects of grazing on marine phytoplankton populations — 2002
-Internship in the aquatic chemistry laboratory of the New Jersey State Aquarium to refine denitrification methods — 2001-2002
-Paleomagnetic research on core samples from the Hurricane fault, Utah to determine slip motion — 2001
-Principal undergraduate marine chemistry research assistant with collection of samples, development of experimental methods, and analysis of data — 1999-2003

Publications

Noffke, N., Schiffbauer, J.D., Hazen, R.M., Bower, D.M., Simpson, C., Swift, D.J.P. (Submitted) Earth's oldest fossils – evidence for Eaoarchean biofilms in >3.7 Ga sediments, Isua Greenstone Belt, Greenland. Nature.

Noffke, N., Beukes, N., Bower, D.M., Hazen, R.M., Swift, D.J.P. (2008) An actualistic perspective into Archean worlds – (cyano-)bacterially induced sedimentary structures in the siliciclastic Nhlazatse Section, 2.9 Ga Pongola Supergroup, South Africa. Geobiology, 6 : 5-20.

Bower, D.M., Noffke, N. (2008) Analysis of microtextures in MISS in siliciclastic sedimentary rocks of the 2.9 Ga Pongola Supergroup, South Africa. Astrobiology, 8 (2) Abstract No. 8-05-O.

Bower, D.M., Noffke, N. (2008) Raman Analysis of microfossils in Archean siliciclastic sedimentary rocks of the Pongola Supergroup, South Africa. Gordon Research Conference, Origins of Life, Ventura, CA.

Noffke, N., Bower, D. M. (2007) Microbially induced sedimentary structures (MISS) – biosignatures in sands and sandstones. Geological Society of America Annual Meeting, Paper No. 47-9.

Bower, D.M. (2007) Raman analysis of microtextures in Archean siliciclastic sedimentary rocks of the Pongola Supergroup, South Africa. Biosignatures in Archean Rocks Workshop, Sudbury, Canada.

Bower, D.M., Noffke, N. (2004) Investigations by confocal scanning laser microscopy on modern microbial mats and comparison with 2.9 Ga old bacterial textures from the Pongola Supergroup, South Africa. Geological Society of America, Annual Meeting, Abstract #80310.